DELINEATION OF THE SUBSURFACE STRUCTURAL FEATURES FAVOURABLE FOR URANIUM MINERALISATION USING IP/RESISTIVITY AND MAGNETIC TECHNIQUES ALONG HULKAL-HALBHAVI TRACT, BHIMA BASIN, YADGIR DISTRICT, KARNATAKA.

by

AYUSH SRIVASTAVA

ENGG1G201801004

Bhabha Atomic Research Centre, Mumbai

A thesis submitted to the
Board of Studies in Engineering Sciences

In partial fulfillment of requirements

for the Degree of

MASTER OF TECHNOLOGY

of

HOMI BHABHA NATIONAL INSTITUTE

February, 2021

HOMI BHABHA NATIONAL INSTITUTE

Recommendations of the Thesis Examining Committee

As members of the Thesis examining Committee, we recommend that the dissertation prepared by **Ayush Srivastava** entitled "Delineation of the subsurface structural features favourable for uranium mineralisation using IP/Resistivity and magnetic techniques along Hulkal-Halbhavi tract, Bhima basin, Yadgir district, Karnataka" be accepted as fulfilling the dissertation requirement for the Degree of Master of Technology.

Designation	Name	Signature
Member-1	Dr. D. K. Sinha	DKSinha
Member-2	Dr. T. S. Sunil kumar	[illegible]
Member-3	Dr. V. Ramesh Babu	[illegible]
Member-4	Dr. A. Rama Raju	A. R. R.
Technical advisor	Shri Satyam	Satyam
Examiner	Prof. V. Chakravarthi	[illegible]
Guide/Convenor	Dr. M Narsimha Chary	[illegible]
Chairman	Prof. Vivekanand Kain	[illegible]

Final approval and acceptance of this thesis is contingent upon the candidate's submission of the final copies of the thesis to HBNI.

I hereby certify that I/we have read this thesis prepared under my/our direction and recommend that it may be accepted as fulfilling the thesis requirement.

Date: 15-02-2021

Place: Hyderabad

Signature of the Guide

Name of the Guide:

DECLARATION

I, hereby declare that the investigation presented in the thesis has been carried out by me. The work is original and has not been submitted earlier as a whole or in part for a degree / diploma at this or any other Institution / University.

Ayush

AYUSH SRIVASTAVA
Scientific Officer-C
EGPG, AMD,
Bangalore

ACKNOWLEDGEMENTS

I am grateful to Dr. D.K.Sinha, Director of Atomic Minerals Directorate for Exploration & Research (AMD), Department of Atomic Energy (DAE) for giving me the opportunity to do M.Tech. degree course from HBNI through BARC training School.

I would like to thank the Additional Director OP-I, Additional Director OP-II, Additional Director OP-III and Additional Director R & D for their guidance and support. I am grateful to Dr. S.K. Srivastava, Ex-Incharge, BARC training school, AMD complex, Hyderabad, and Dr. A. Rama Raju, Incharge, BARC training school.

I would also like to thank Shri D.K. Choudhury, Regional Director, AMD, SR and Shri Mayank Agarwal, Deputy Regional Director AMD, SR for their continuous support and discussions at various steps during this thesis work.

I wish to express gratitude to my guide Dr. M. Narsimha Chary and technical adviser Shri Satyam for their supervision and generous giving of time and guidance whenever needed.

I am grateful to Shri A Markandeyulu, Incharge, EGPG, Hyderabad and Shri S. K. Varughese, Incharge, Bhima basin investigation for their support and helpful discussions.

I also thankful to my colleagues, all technical and nontechnical staff who have supported me directly or indirectly in the completion of my project work.

CONTENTS

SYNOPSIS

This thesis is for the M.Tech project through HBNI, deals with the geophysical data acquisition in Hulkal area, Yadgir district, Karnataka using magnetic, IP (Induced Polarisation) & Resistivity methods and their results. The main objective of the study was to demarcate subsurface geological structures such as fracture, fault and altered/ deformed zones associated with low resistivity and high chargeability, favourable for uranium mineralization. The magnetic and IP/resistivity data have been acquired over an area of 4.5 sq.km and 3.5 sq.km respectively. Data processing was carried out by applying different data enhancement techniques; interpreted qualitatively as well as quantitatively.

The study area is located around 12 km to the east of well-known Gogi uranium deposit in Bhima basin. In the eastern part of the basin, Bhima Group unconformably overlies the basement crystalline rocks comprising enclaves of greenstone belt within the Peninsular gneisses, younger intrusive pink and grey granitoids belonging to Neoarchean-Paleoproterozoic (~2.5-2.0 Ga) Closepet Granite and its equivalent. A number of basic dykes traverse the crystalline terrain. The basin is transected by prominent E-W and NW–SE trending faults beside a number of smaller N-S and NE-SW trending faults.

The qualitative interpretation of magnetic data shows that the fracture zone F1 related to Gogi-Kurlagere fault, trending in NE-SW direction. Different lithologies are also mapped based on their magnetic response. The magnetic data is further interpreted quantitatively for obtaining the depth to causative geological bodies using spectral analysis and advance processing technique known as Continuous Wavelet Transform and thereby compared with the results of geophysical modelling. It is found that the basement depth is approximately 380 m which is obtained by using both depth estimation techniques. A forward two dimensional modelling was also done to understand subsurface geology.

Chargeability and resistivity depth sections has brought out the subsurface information up to the depth of 312m. Low resistivity signatures revealed fracture within the high resistive massive limestone trending in E-W direction. Faulted basement-sediment contact has been delineated and showing directional change from NE-SW to E-W as move from west to east. Resistivity values within the K-G fault zone is of the order of 100-300 ohm-m and within the sediment, order is 300-600 ohm-m. In the western part along the line numbers 690050, 690200 and 690400 chargeability is of the order (8mV/V - 16mV/V) within the sediments and lower order (<3mV/V) along the K-G fault zone. In the eastern part, along the line number 691200, 691400 and 691600 chargeability is of the order (8mV/V- 15mV/V) along K-G fault zone. When we compare the chargeability (4.5mV/V-5.5mV/V) values in mineralised zone of Kanchankayi with the present study area which is adjacent to Kanchankayi, it is found that chargeability is of very higher order. Additionally, Limestone-Arenite and Limestone-Shale contacts are also delineated.

Fracture zone within the sediment is characterized by the strike length of 400 m and width of 100-150 m, which extends up to the depth of 300m. The width of K-G fault zone is approximately 300 m. The high chargeability value is attributed to the presence of sulphide in fractures. This zone might be the potential target for Uranium exploration and could be considered for formulating the further exploration program in the area.

LIST OF FIGURES

LIST OF TABLES

CHAPTER 1

INTRODUCTION

1.1 General

Geophysical surveying methods have been extensively used on land, air and sea in mineral exploration. Various methods are based on the measurement of physical properties of rocks and minerals which vary systematically. The role of geophysics continues to play in earth system exploration when the surface manifestation of the structural features and lithology are poor.

Ground geophysical surveys are mainly used in an exploration program to delineate favourable target zones. Geophysical techniques are indirect tools as for as uranium exploration is concerned, whereas the radioactive method is the direct technique for near surface deposits. Most of the techniques are used to map geology and structural features in the exploration programs. Induced polarization (IP) is used to find disseminated sulphides, magnetics to delineate magnetite hosting rocks, and gravity and electrical techniques for massive sulphides. Examples of indirect detection of targets include using IP to detect pyrite in association with sphalerite and gold (both non-responders to IP geophysical techniques), and copper and molybdenum in porphyry systems. Magnetics are routinely used to search for hydrothermal alteration in association with porphyry coppers, and can be used to map buried stream channels (magnetite sands) that might host placer gold. Geologic mapping applications include gravity and seismic to map faults and thickness of alluvial fill; magnetics and seismic for mapping structure, and possible signatures associated with different rock types; radiometric for mapping alteration and geology; and electrical techniques for mapping depth to bedrock, layered structure, and different rock units.

Success of any particular geophysical method in exploration for any mineral depends on physical property contrast of the mineral as well as its host rocks exists. Although the non-radiometric geophysical techniques are the indirect methods for Uranium exploration, the study of its origin and mode of occurrence, geological setup of study area and physical properties of host environment warrants the suitable geophysical tools.

1.1.1 Uranium and its properties.

Uranium is a high density (19.1gm/cc) silvery-white metallic chemical element in the actinide series of the periodic table, with symbol U and atomic number 92 and atomic weight of 238. A Uranium atom has 92 electrons and 92 protons with six valence electrons and it has six isotopes, U-233, U-234, U-235, U-236, U-237 and U-238. The most common isotopes of uranium are uranium-238 and uranium-235. All the isotopes are unstable and uranium is weakly radioactive and it decays slowly by emitting alpha particle. The half life period of Uranium is 4500 million years. Uranium was discovered in 1789 by Martin Klaproth, a German chemist, in the mineral called pitchblende. It was named after the planet Uranus, which had been discovered eight years earlier. Uranium was apparently formed in supernova about 6.6 billion years ago. Presence of U forms the main source of heat inside the Earth, causing convection and continental drift. Uranium occurs naturally in low concentration of few ppm (2-4ppm) in soil and in water. It is commercially extracted from uranium bearing minerals such as uraninite. In nature, uranium is found as U-238 (99.247%), U-235(0.7204%). Uranium is extracted from ore chemically and converted into uranium oxide and tri uranium octaoxide. Both are solids that have low solubility in water and relatively stable over a wide range of environment conditions. UO_2 is form in which uranium is used as nuclear reactor fuel. At ambient temperature UO_2 will gradually convert to U_3O_8. Because of their stability, these uranium oxides are generally considered as the preferred chemical form for storage and dispose. The most common uranium mineral is uraninite. The other uranium minerals are Carnotite($K_2(UO_2)_2(VO_4)_2 \cdot 3H_2O$), Autunite ($Ca(UO_2)_2(PO_4)_2 \cdot 10\text{-}12H_2O$), Coffinite($U(SiO_4)_{1-x}(OH)_{4x}$), Torbernite ($Cu(UO_2)_2(PO_4)_2 \cdot 8 - 12\ H_2O$).

Many contemporary uses of uranium exploit its unique nuclear properties. Uranium-235 has the distinction of being the only naturally occurring fissile isotope. Uranium-238 is fissionable by fast neutrons, and is fertile, meaning it can be transmuted to fissile plutonium-239 in a nuclear reactor. Another fissile isotope, uranium-233, can be produced from natural thorium and is also important in nuclear technology. While uranium-238 has a small probability for spontaneous fission or even induced fission with fast neutrons, uranium-235 and to a lesser degree uranium-233 have a much higher fission cross-section for slow neutrons. In sufficient concentration, these isotopes maintain a sustained nuclear chain reaction. This generates the heat in nuclear power reactors, and produces the fissile material for nuclear weapons. Depleted uranium (U238) is used in kinetic energy penetrators and armor plating.

Uranium is the main source of fuel for nuclear reactors which are used for generating 14% of world electricity. There are 440 nuclear reactors all over the world with a total output capacity of about 377 000 megawatts (MW) operating in 30 countries. Over 60 more reactors are under construction and another 150 are planned. One kg of Uranium produces 80 terrajoules of energy assuming completely fission as much as 3000 metric tonns of coal.

1.1.2 Types of uranium deposit

a. Unconformity type deposits

Many types of uranium deposits in the world have been discovered and mined. There are different types of uranium deposits out of which unconformity-type and vein type deposits are important. More than one third of the uranium resources are unconformity related deposits and have grades 3-100 times higher than any other types of deposit (Jefferson et al., 2007). The

Athabasca and Thelon Basins of Canada, and the Kombolgie Basin, sub-basin of the McArthur Basin, Australia, host this type of uranium deposit.

b. Uranium deposits in sedimentary rock

Sandstone uranium deposits are generally of two types. **Roll-front** type deposits occur at the boundary between the up dip and oxidized part of a sandstone body and the deeper down dip reduced part of a sandstone body. **Peneconcordant** sandstone uranium deposits, also called **Colorado Plateau**-type deposits, most often occur within generally oxidized sandstone bodies, often in localized reduced zones, such as in association with carbonized wood in the sandstone.

Precambrian quartz-pebble conglomerate-type uranium deposits occur only in rocks older than two billion years old. The conglomerates also contain pyrite. These deposits have been mined in the Blind River-Elliot Lake district of Ontario, Canada, and from the gold-bearing Witwatersrand conglomerates of South Africa.

c. Igneous or hydrothermal uranium deposits

Hydrothermal uranium deposits encompass the vein-type uranium ores. Igneous deposits include nepheline syenite intrusives at Ilimaussaq, Greenland; the disseminated uranium deposit at Rossing, Namibia; and uranium-bearing pegmatites. Disseminated deposits are also found in the states of Washington and Alaska in the US.

d. Hematite Breccia Complex deposits

Deposits of this group occur in hematite-rich breccias and contain uranium in association with copper, gold, silver and rare earths. The main representative of this deposit type, Olympic Dam, has been assigned to a broad suite of loosely related iron oxide–copper–gold deposits ranging in age from ~2570 to 1000 Ma that include Prominent Hill, Ernest Henry (~1480 Ma), Starra (~1500 Ma), Osborne (1540 Ma) in Australia; Candelaria (~1100 Ma), Salobo (2570–1880 Ma) and Sossego in South America, Michelin and Sue-Dianne in Canada.

e. Metasomatic deposits

Uranium deposits of this type are related to alkaline metasomatites of sodium or potassium series. The metasomatites are developed in ancient shields and median masses, where they form stockworks controlled by long-lived ancient faults. Sodium metasomatites are predominantly albite in composition, usually with minor carbonate and alkaline amphiboles and pyroxenes — albitites and eisites. The largest uranium deposits in sodium metasomatites occur in the Kirovograd Ore District, Ukraine. Other regions with similar deposits are Beaverlodge (Canada), Itatiaia (Brazil), Jaduguda (India), and Kokchetav Massif (Kazakhstan).

f. Phosphorite deposits

Uraniferous phosphorite deposits consist of syn-sedimentary, stratiform, disseminated uranium in marine phosphate-rich rocks or phosphorite deposits that formed in continental shelf environments. The uranium mineralization is substituted for Ca in cryptocrystalline fluor-carbonate apatite grains. Phosphorite deposits constitute large uranium resources, but are very low grade (25–150 ppm). Phosphate rock is a key raw material for the world's chemical fertilizer industry. Therefore, uranium can only be recovered as a by-product of phosphoric acid production.

g. Metamorphic deposits

Metamorphic uranium deposits result from regional metamorphism of uraniferous sediments or volcanics. Accordingly, they occur in metasediments and/or metavolcanics in which the uranium mineralization resulted directly from metamorphic processes. Examples include the Mary Kathleen deposit, Australia and the Forstau deposit, Austria.

1.1.3 Uranium provinces of India

Among the major Uranium provinces of India (Figure1.1), Jaduguda in Singhbhum Thrust Belt (in the state of Jharkhand, formerly part of Bihar) is the first uranium deposit discovered in the country in 1951. The Singhbhum Thrust Belt (also known as Singhbhum Copper belt or Singhbhum Shear Zone) is a zone of intense shearing and deep tectonization with less than 1km width and known for a number of copper deposits with associated nickel, molybdenum, bismuth, gold, silver etc. It extends in the shape of an arc for a length of about 160 km. This discovery of uranium at Jaduguda in this belt paved the way for intensive exploration work and soon a few more deposits were brought to light in this area. Some of these deposits like Bhatin, Narwapahar and Turamdih are well known uranium mines of the country. Other deposits like Bagjata, Banduhurang and Mohuldih are being taken up for commercial mining operations. Some of the other areas like Garadih, Kanyaluka, Nimdih and Nandup in this belt are also known to contain limited reserves with poor grades.

Apart from discoveries in the Singhbhum Thrust Belt, several other uranium occurrences have also been found in Cuddapah basin of Andhra Pradesh. These include Lambapur-Peddagattu, Chitrial, Kuppunuru, Tumallapalle, Rachakuntapalle, which have significantly contributed towards the uranium reserves of India. In the Mahadek basin of Meghalaya in North-Eastern part of the country, sandstone type uranium deposits like Domiasiat, Wahkhyn, Mawsynram provide near-surface flat ore bodies amenable to commercial operations. Other areas in Rajasthan, Karnataka and Chhattisgarh hold promise for developing into some major deposits. India's identified conventional uranium resources are hosted by the following types of deposits.

Table1: Different type of Uranium deposits discovered in India

S. No.	Category	Resources
1	Vein Type	49.06%
2	Sandstone type	14.57%
3	Unconformity type	12.92%
4	Metasomatic	0.63%
5	QPC	0.33%
6	Others	22.49%

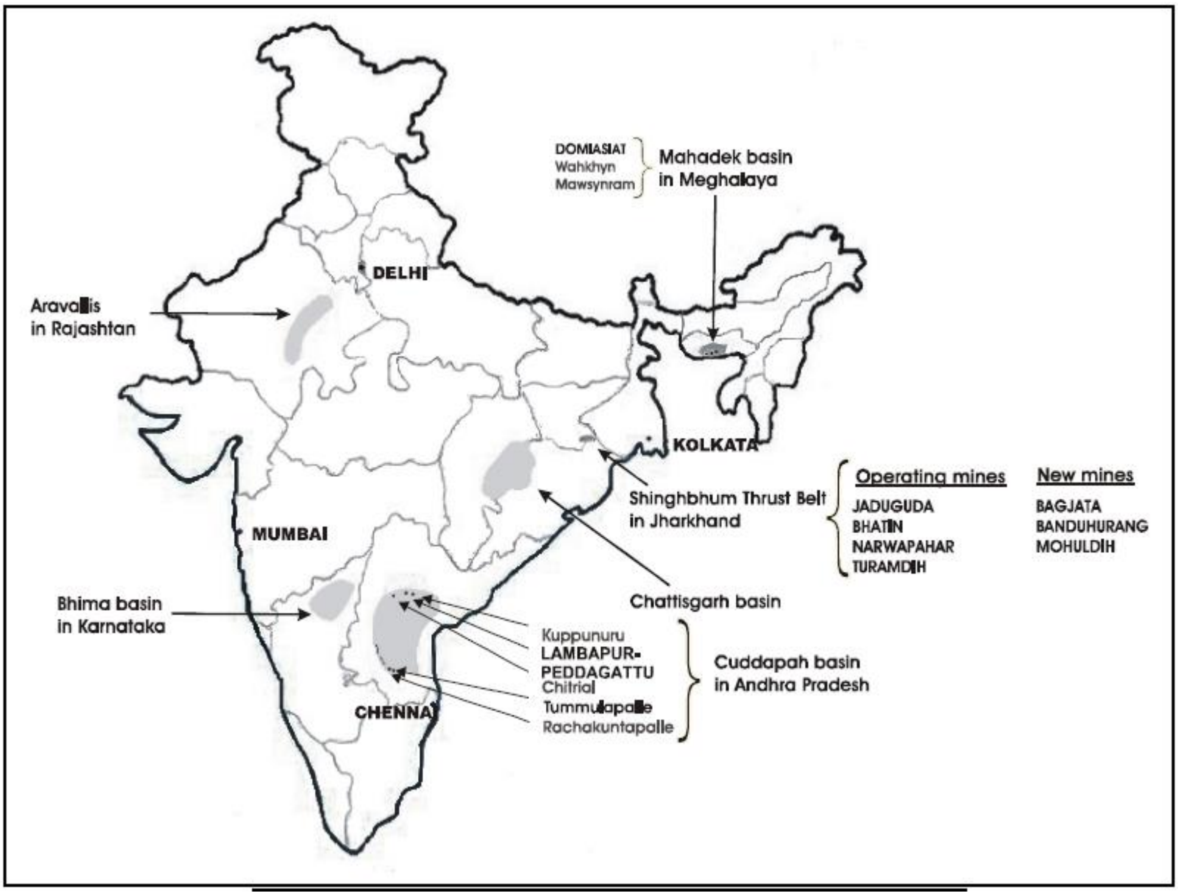

Figure1.1 Major Uranium provinces of India

1.1.4 Role of geophysics in uranium exploration

Geophysics is one of the important branch of earth science that applies the principles and laws of physics to the study of internal structure of the earth. Geophysical investigation of the interior of the earth involves taking measurements at or near the earth's surface that are influenced by internal distribution of physical properties. Analysis of these measurements can reveal how the physical properties of the earth's interior vary vertically and laterally. By working at different scales, geophysical methods may be applied to a wide range of geological problems from deep crustal studies of earth to exploration of localized targets in upper crust for mineral exploration or other purposes like groundwater exploration archaeological investigations and environmental issues.

A wide range of geophysical surveying methods exists, for each of which there is an specific physical property to which the method is sensitive. Geophysical surveys measure the variation of certain physical quantity, with respect to either position or time. A local variation of this type is known as a geophysical anomaly. The quantity, for example, may be the strength of the Earth's magnetic field along a profile across an igneous intrusion. It may also be the motion of the ground surface as a function of time associated with the passage of seismic waves. Electrical and EM methods are useful for delineating subsurface conductors.

In various geophysical survey methods, it is the local variation, which is measured parameter as primary interest, relative to some normal background value. Geophysical anomaly is the vertical component of the anomalous field alone, which can be attributed to a localized sub surface zone of distinctive physical property and possible geological importance (Philip Keary, 2002). Geophysical methods are often used in combination of different methods because the ambiguities arising from single method at the interpretation stage; from the results of one survey method may often be removed by consideration of results from a second survey method. For example, the initial search for metalliferous mineral deposits often utilizes airborne magnetic and electromagnetic surveying followed by ground geophysical survey.

The methods applied for the Uranium exploration can be of direct or indirect nature. Direct methods Geological mapping, radiometric survey are applicable when area contains exposed rocks. The indirect methods of Geophysical survey will aid to find the presence of favourable locales for such mineralization in areas where exposure is scanty. Application of non-radiometric geophysical methods for mineral exploration is one such indirect approach that helps to locate the subsurface mineralization or to find the associated structure controlling the mineralisation .i.e. favourable geological setup. This is done by mapping the distributions of physical properties reflecting the subsurface geology. The map is interpreted in terms of geophysical parameters and finally arrived at the probable subsurface geological attributes. More than one geophysical method is, generally, applied over an area and the results are analyzed in conjunction to strengthen the inference regarding the subsurface geology of the area to improve the confidence level of the interpretation of the data.

Geophysical survey for uranium starts with the reconnaissance survey followed by the detailed survey. The initial phase of survey includes profiling (lateral scanning) along pre-planned lines over an area depending upon the phase of exploration. The reconnaissance phase can be done by heliborne/ airborne mode or ground geophysical survey with larger line spacing and wider station interval. The results are interpreted with what is already known of the geology.

Uranium emits gamma rays at specific energy level that can be detected with the appropriate equipment from the air, on the ground or in borehole.

Uranium despite its high density is not detectable by gravity technique due to low concentration. But gravity is one of the most useful geophysical techniques applicable for detecting lateral, and to a certain extent, vertical differences in the densities of subsurface rocks. Gravity survey is applicable to delineate lithological boundaries and structural features such as paleo-channels, fault structures, basement configuration etc. Magnetic survey is useful for mapping geological boundaries, structures, magnetic basement and finding some types of ores. Both gravity and magnetic surveying can be applied in geological mapping during the early stages of uranium exploration.

Electromagnetic methods measures conductivity and are thus capable of constructing picture of the subsurface in terms of conductivity variation in subsurface. It is utilized to detect subsurface geological targets often associated with uranium mineralization. Such geological targets include large graphitic conductors or other similar stratigraphic units with strong carbonaceous affinities. Other applications of EM method include the mapping of subsurface structures, faults, fractured zones and paleochannels in sedimentary basins on the basis of conductivity variation.

Resistivity survey techniques have been used to determine the vertical and lateral changes in resistivity. Resistivity profiling delineates lateral resistivity changes such as the presence of geological boundary. The induced polarization (IP) method is the most useful technique for detecting conductive mineralization, such as disseminated sulphides that typically shows chargeability characteristic of the geological formations.

Seismic method in general is a method suitable for investigation of subsurface geological structures and lithological boundaries and in specific to determine an unconformity contact. It is based on the study of velocities of artificially excited elastic waves passing through different formations. A geological boundary with a velocity contrast can reflect and refract the wave, returning it to the Earth’s surface where it is recorded.

1.2 Location of the study area

The study area, Hulkal is geographically located at 11km east to the Gogi village, Yadgir district, Karnataka, where significant uranium deposit has been established by the Atomic Minerals Directorate for Exploration and Research, Department of Atomic Energy. The area is located 31 km west to Yadgir district and 80km east to Gulbarga district (Figure 1.2). The geographical latitude and longitude of the study block are 76°46’50’’E to 76°48’25”E and 16°44’35”N to 16°45’27.6”N.

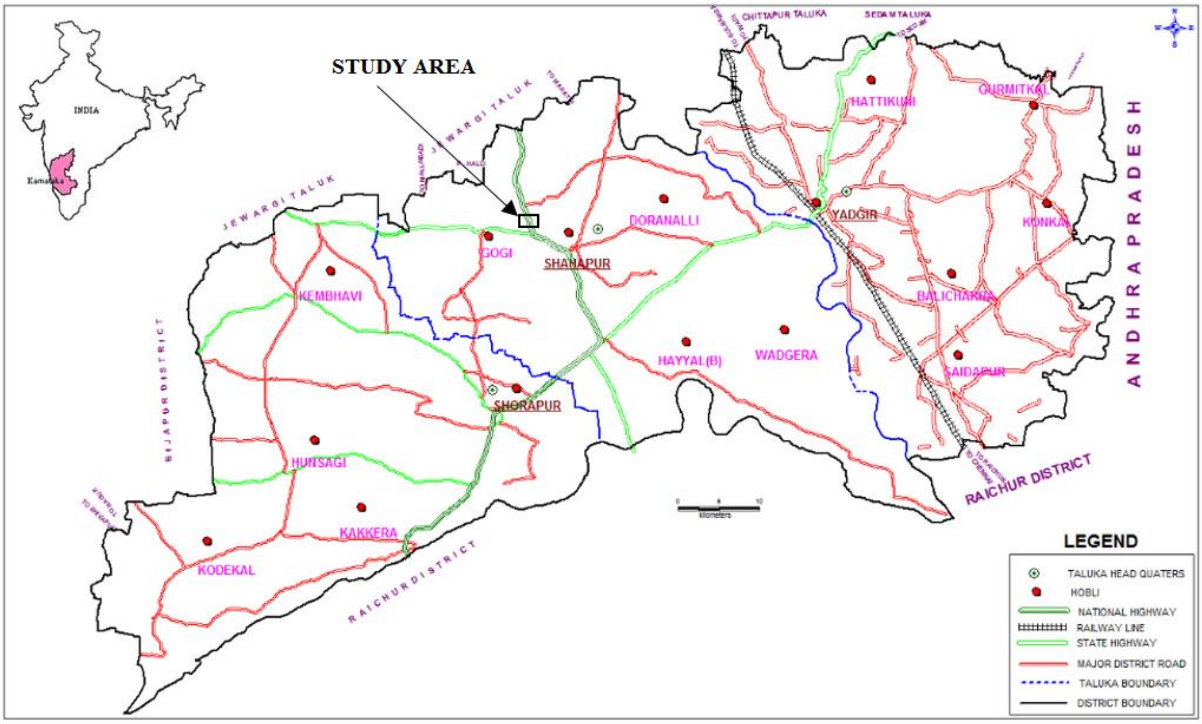

Figure 1.2 Location map of study area

1.3 Geology and structure

1.3.1 Geology and structure of the Bhima basin

The Bhima Basin occurs on the north western fringe of Eastern Dharwar Craton and is bounded by latitude 16° 20’ 00”N –17° 05’ 00”N and longitude 76° 15’ 00”E – 77° 44’ 00”E. The basin has reverse sigmoid array of outcrops arranged in an *en echelon* pattern over a stretch of 160 km with a maximum width of 40 km across Sedam between Tandur in the northeast to

Muddebihal in the southwest. The exposed area of the basin is around 5200 sq kms. These exposures are sandwiched between the Archean granite-greenstone terrain of Eastern Dharwar Craton in the south and east and the late Cretaceous-Palaeocene Deccan Trap Volcanic Province in the north and northwest.

The major stratigraphic supracrustal belts that are exposed in the region of Bhima basin include Archean Basement complex overlain by the Proterozoic Clastic and limestone sediments of Bhima basin with an erosional unconformity, which in turn, is followed above by a few outcrops of late Cretaceous Gulbarga Infratrappean Formation with another erosional unconformity in between. These sedimentary belts are overlain by the late Cretaceous-Early Tertiary Deccan Trap volcanism that partially covered the rocks of all the supracrustal belts, older to it. The youngest stratigraphic unit in the area is alluviums and laterites of Quaternary to Holocene age (Figure 1.3).

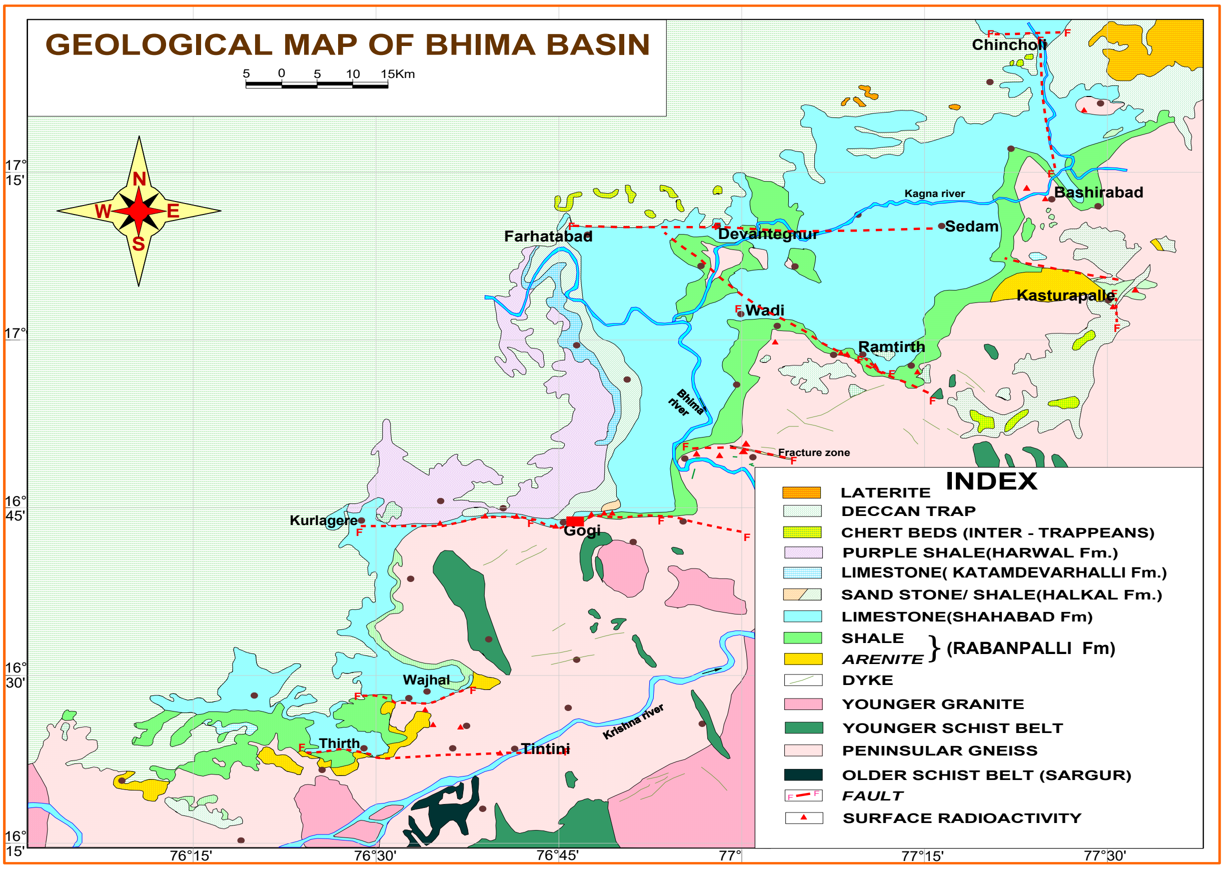

Figure 1.3 Geological map of Bhima Basin

The crystalline, metamorphic and granitoid rocks comprise the basement to the Bhima sediments. The basement rocks are mainly older schistose rocks comprising amphibolites, metasedimentary and metabasic schists of Hutti Group and Raichur Group (Equivalent of Bababudan Group) followed by Peninsular gneisses. The gneissic rocks include a variety of tonalitic and granodioritic gneisses belonging to Peninsular Gneissic Complex, which is intruded by the younger granites equivalent of Closepet Granite. The basement terrain is intruded by a number of basic dykes exposed in the southeast of Bhima Basin, which marks the youngest basic igneous activity followed by the initiation of sedimentation in the Bhima basin.

The Bhima Group is divisible into two major sedimentological facies associations with a gradational contact between them, namely the siliciclastic facies association and the carbonate facies association, belonging to the Rabanpalli and Shahabad Formations respectively (Kale, 1995). The coarse clastics comprising conglomerate, pebbly arenites and massive to cross stratified arenites of Rabanpalli Formation which are believed to be the products of shallow marginal marine environment. These clastics are overlain by glauconitic shales deposited in a mudflat environment. The overlying Shahabad Formation comprises the low-magnesium limestones deposited in a carbonate flat platformal environment.

1.3.2 Geology of the Hulkal area

Hulkal is located about 5 km east of Gogi Uranium deposit and lies in the close vicinity of the Gogi–Kurlagere fault zone. The study area comprises an alternating sequence of clastic and carbonate sediments with the carbonates dominating over the clastics.

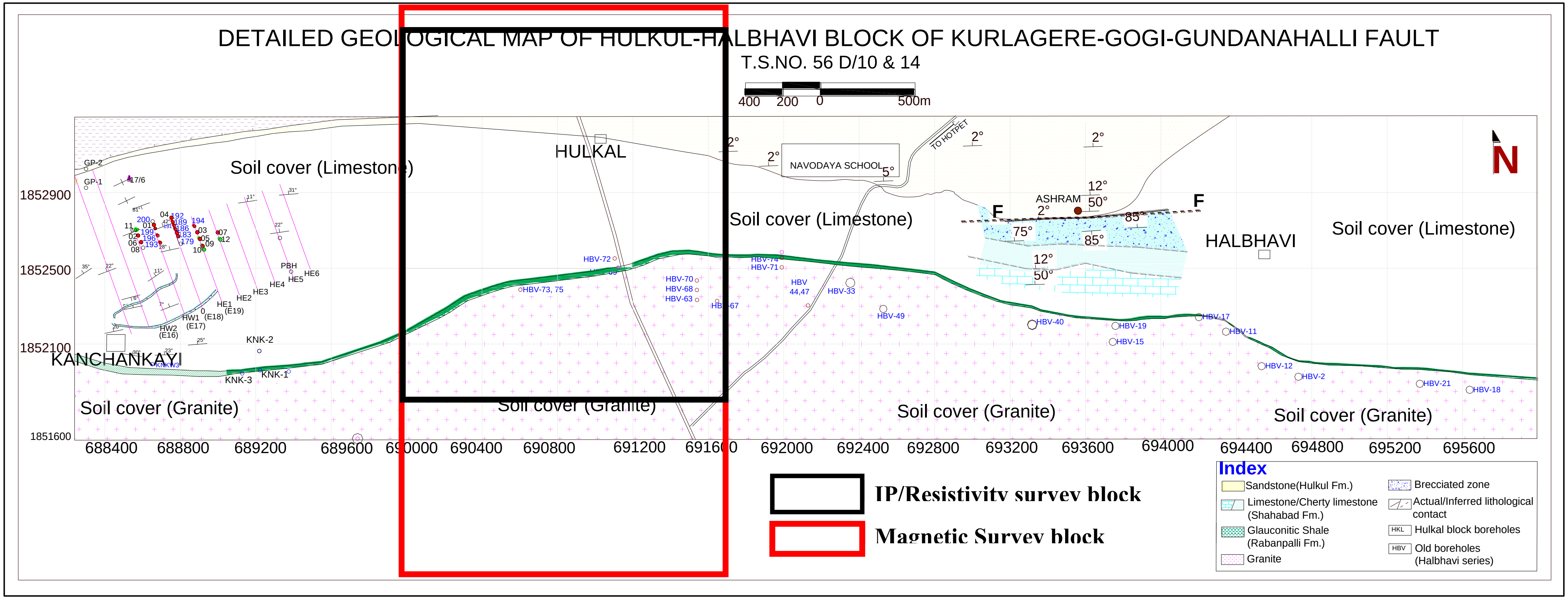

Figure 1.4 Geological map of Hulkal-Halbhavi tract

In the southern part of Hulkal area basement granitoids are exposed which are unconformably overlain by the Mesoproterozoic carbonate-siliciclastic dominated sediments of Bhima Group in the north.

1.3.3 Previous work on uranium exploration in Bhima basin

The uranium mineralisation in Halbhavi and Hulkal was first reported in 1997-98 by AMD. This study has opened up a new target area for uranium exploration along Gogi-Kurlagere fault. However, gamma ray logging of 37 borewells in the area during same field season did not record any significant mineralisation. In 1998-99, detailed geological mapping (1:5000 scale) and SSNTD /Radon survey along Kanchankayi to Madnal tract was carried out and observed two more uranium anomalies east and west of Halbhavi. The analysing of the samples revealed 0.175% eU_3O_8 and 0.279% U_3O_8 with low P_2O_5 (0.3%). In order to explore the deeper level sub-surface continuity of the surface uranium mineralisation reconnoitory drilling at Halbhavi was initiated. Few boreholes drilled in this area brought out a wealth of subsurface geology. It has been established by limited drilling input that the litho-structural set up is very similar to Gogi area. To understand the sub-surface geology and structure of the Gogi deposit, geophysical survey was carried out. The integrated geophysical study of the airborne magnetic (Figure 1.5) and TEM (Figure 1.6) maps reveal that the study area lies within low magnetic zone, which is considered as the part of the main Gogi- Kurlagere fault and also reflect the presence of conductive body. High resistivity zone in the area attributed to limestone. High chargeability associated with high resistivity zone was also observed, that may be due to the carbonaceous or pyrite minerals present there, which was interpreted from the borehole data present in the adjoining the area. So, further subsurface exploration in this area will confirm the causative minerals.

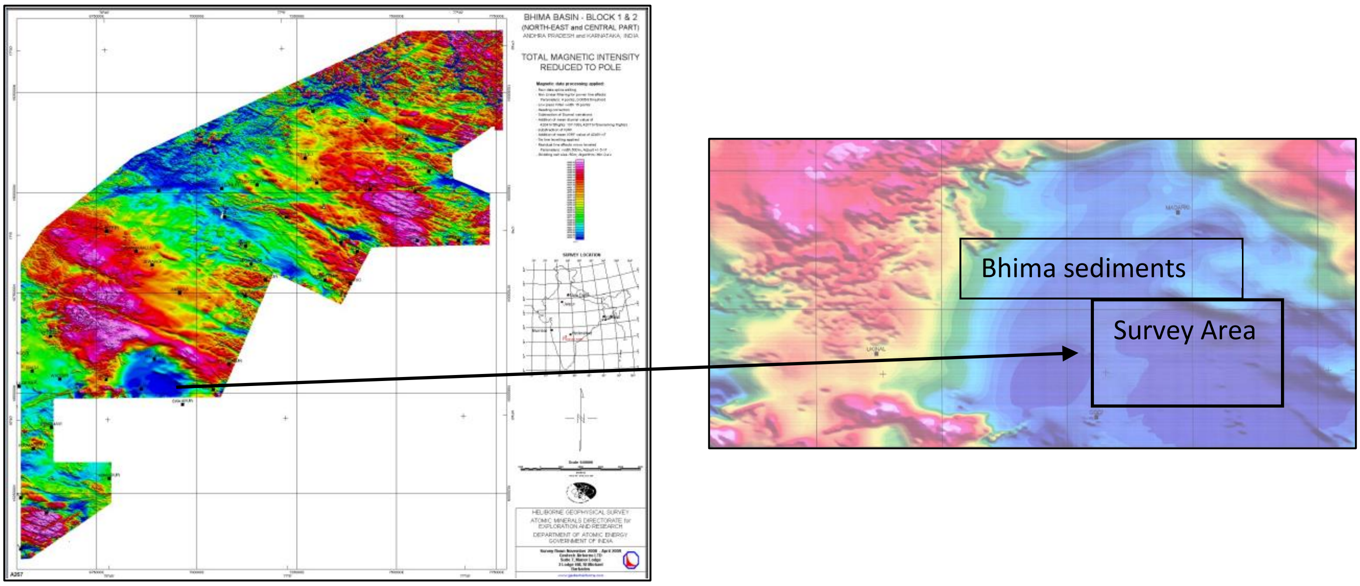

Figure 1.5 Heliborne magnetic map of the Bhima basin

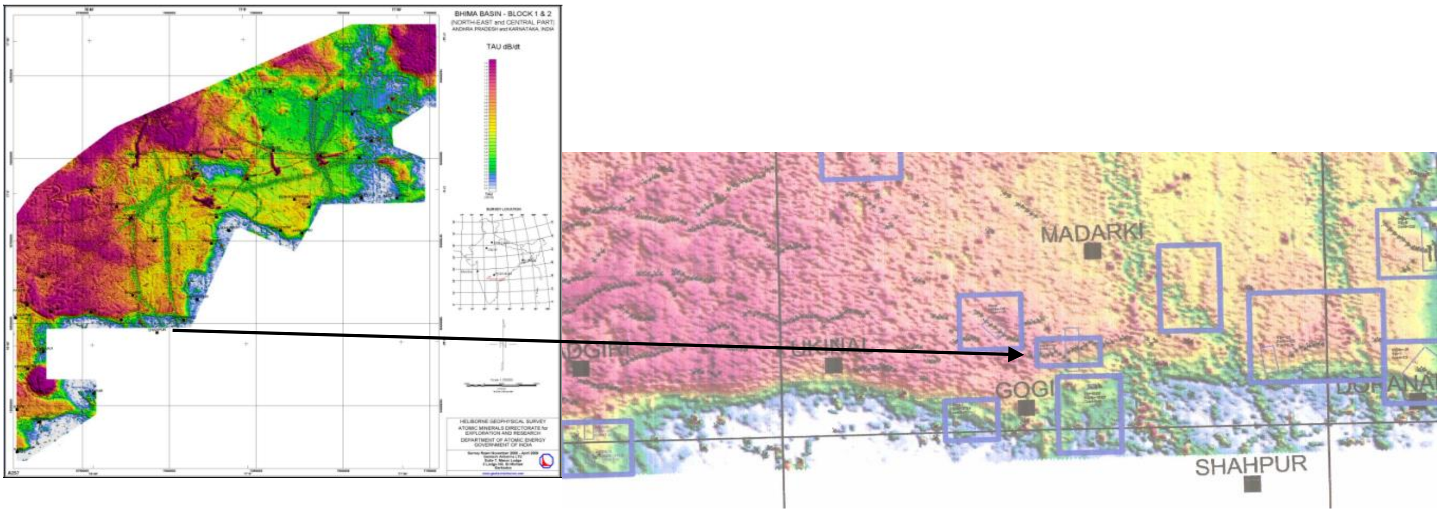

Figure 1.6 Heliborne TEM map of the Bhima basin

1.4 Aim and scope of the present work

The uranium mineralisation in Gogi is intimately associated with the sulphides, which are conductive in nature. Results from airborne geophysical data revels the presence of shale in the area which produces the screening effect over the EM data and it becomes difficult to interpret that the EM conductors are mainly due to shale or sulphide. One project was carried out to separate the responses due to sulphide body with the shale by using induced polarization method with the help of Scintrex instrument but depth persistency of that survey was not enough to get the clear results. Therefore, main objective of the present project is to gather the data from larger depths to demarcate the subsurface deeper fracture zones in sediments and underlying basement by using IRIS instrument of higher capacity generating power.

1.5 Work strategy of the project work

Based on the objective stated above, IP/Resistivity and magnetic survey has been carried out covering an area of approximately 3.5 sq. km and 4.5 sq. km respectively near Hulkal, Yadgir district, Karnataka to decipher the structural features within the Bhima sediments and basement. The results obtained from the IP/Resistivity and magnetic data has revealed the structural features which may be the favourable zones of uranium.

The entire work has been organised into five chapters. Chapter-I, gives the general properties of uranium, role of geophysics in uranium exploration, regional and local geology of the study area. Objectives and scope of the work are also incorporated in this chapter.

Chapter-II, deals with the theory of the Ground magnetic, data acquisition, processing, modelling and interpretation.

Chapter –III, deals with the theory of Induced polarisation/ Resistivity, data acquisition, processing and interpretation.

Chapter-IV, correlation between the results of IP/Resistivity and Magnetic methods are described in this chapter.

In chapter-V, summary and conclusions of the investigation and the salient features of the results are presented.

CHAPTER -2

INVESTIGATION BY MAGNETIC METHOD

2.1 Introduction

The magnetic method of prospecting is based on the study of the local geomagnetic field produced by the variations in the intensity of magnetization of rock formations. It is a versatile geophysical tool and responds to most of the geological conditions. The magnetization of rocks is partly due to induction in the earth's magnetic field and to some extent due to the remnant magnetization. The induction component depends on magnetic susceptibility (k) of rocks and on the intensity of the magnetic field. The susceptibility varies with the variation of rock types. While the magnetizing field remains constant over a small area, the remnant magnetic intensity and its variation for a given rock type also remain the same. In turn, the variation in the measured magnetic field can be attributed to the presence of various rock types with different susceptibilities. Therefore, the magnetic method can be used effectively for geological mapping and structural studies. The theory and practice of magnetic method are well documented in Telford et al., (1990).

2.1.1 Application of magnetic method in uranium exploration

Magnetic surveys are much useful for mapping of geological formations and associated bedrock. Depending upon the susceptibility contrast this methods identifies the geological structural features such as fracture, shear zones. In addition, the magnetic methods are useful for mapping basement faults and related tectonic features and also to locate intrusive bodies of acidic, mafic and ultramafic rocks. These geological structures and tectonic features act as a control for the uranium mineralization.

2.1.2 Magnetic Susceptibility of Rocks

For geological mapping by geophysical prospecting, knowledge of physical properties of rocks is of considerable importance for a plausible interpretation. The ultimate result of any geophysical survey is to convert the inferred anomaly into geology. In view of this, the knowledge of magnetic susceptibility of rocks is relevant to the interpretation of magnetic data which otherwise may lead to erroneous conclusions about the position (spatial location) and nature of the causative geological features favourable for mineralization. Magnetic susceptibilities of various rocks and minerals are given in **Table 2.1.** Magnetic susceptibility of rocks is primarily dependent on the presence of ferromagnetic minerals chief among them being magnetite and members of the titanomagnetite series. These ferromagnetic minerals are common accessory minerals in igneous and metamorphic rocks and occur in the trace in sedimentary rocks.

Table2.1 Common minerals and rocks with their magnetic susceptibility values (Telford et al., 1990)

Minerals	Average susceptibility * 10^{-3} (SI)	Some common rocks	Average susceptibility * 10^{-3} (SI)
Quartz	-0.01	Sandstones	0.4
Clays	0.2	Shales	0.6
Rocks Salt	-0.01	Amphibolite	0.7
Pyrrhotite	1500	Schist	1.4
Calcite	-0.001- -0.01	Limestones	0.3
Sphalerite	0.7	Quartzite	4
Pyrite	1.5	Phyllite	1.5
Magnetite	6000	Gabbro	70
Ilmenite	1800	Basalts	70
Hematite	6.5	Peridotite	150

2.1.3 Instrumentation

The instrument used for magnetic survey was the GEM system, GSM 19T Proton

Figure 2.1 GEM Systems, GSM 19T Proton Precision Magnetometer used for Data acquisition.

Precision Magnetometer with a dynamic range of 20,000nT - 1,20,000 nT. It measures the absolute value of total magnetic field to a resolution of 0.01 nT and with an accuracy of +/- 0.2 nT. Data can be recorded in three modes (Walking, Mobile, and Base). In walking mode data is recorded continuously with the different sampling but in this mode noise is too high, so mobile mode is preferable in which data collection is not continuous and noise is less. In this survey, mobile mode is used for data acquisition. This instrument has a large volume on-board storage and memory and comes with a high resolution (0.6m) integrated GPS. It is used in various field applications such as fault and geological mapping, mining and location of magnetic minerals.

2.1.4 The principle of proton precision magnetometer

The proton-precession magnetometer depends on the nucleus of the hydrogen atom, a proton, has a magnetic moment proportional to the angular momentum of its spin. Because the angular momentum is quantized, the proton magnetic moment can only have specified values, which are multiples of a fundamental unit called the nuclear magneton. Proton magnetometer is simple and robust in design. The sensing device of the proton magnetometer is filled with a liquid rich in hydrogen atoms for example kerosene or water which is surrounded by a coil. The hydrogen nuclei (protons) act as small dipoles and normally align parallel to the ambient geomagnetic field B_e.

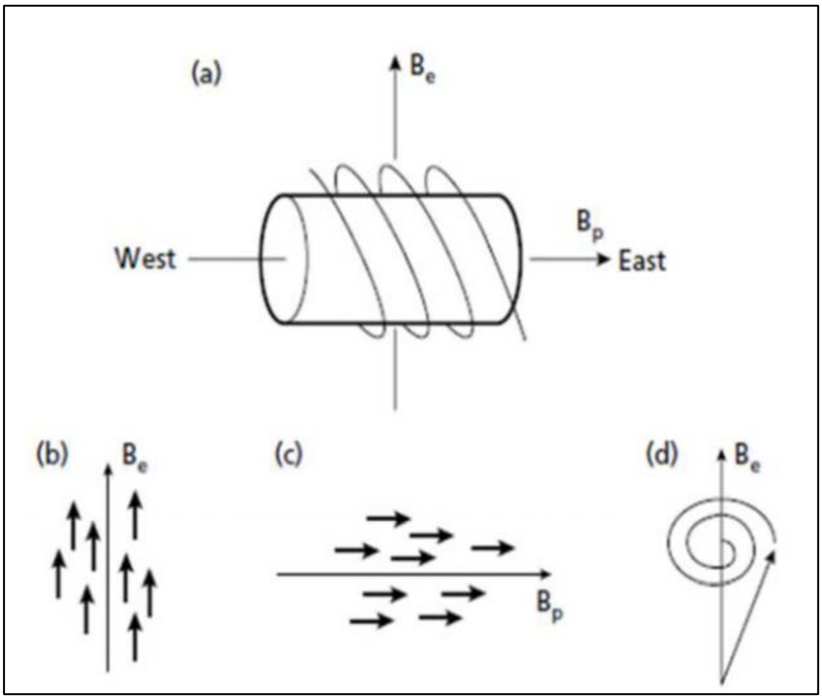

Figure 2.2 Principle of working of PPM (William Lowrie, 2007)

2.2 Magnetic Data Acquisition

Data acquisition depends upon the nature of the problem to be solved, the accuracy of the survey needed and the characteristics of instruments, corrections to be applied etc. GEM's advanced Proton Precession magnetometer (GSM-19T) was employed for the entire magnetic survey. The magnetic data were collected in S-N direction perpendicular to the strike of the geology of the formation in the study area with station spacing of 25 m and profile spacing of 100 m as shown in (Figure2.3). Before any measurement, a fixed base station for all profiles was established at a place which is less noisy and the instrument was checked for batteries, then two or three test measurements to check if there was a magnetic storm in that day. In this survey, one magnetometer was used as a rover and another for base station reading. Purpose of rover magnetometer is to record the magnetic field along the line and base magnetometer is to monitor diurnal variation of earth magnetic field at a particular location in the study area. The accurate positions of the magnetic data points were determined by fully integrate GPS (Global Positioning System) with the magnetometer.

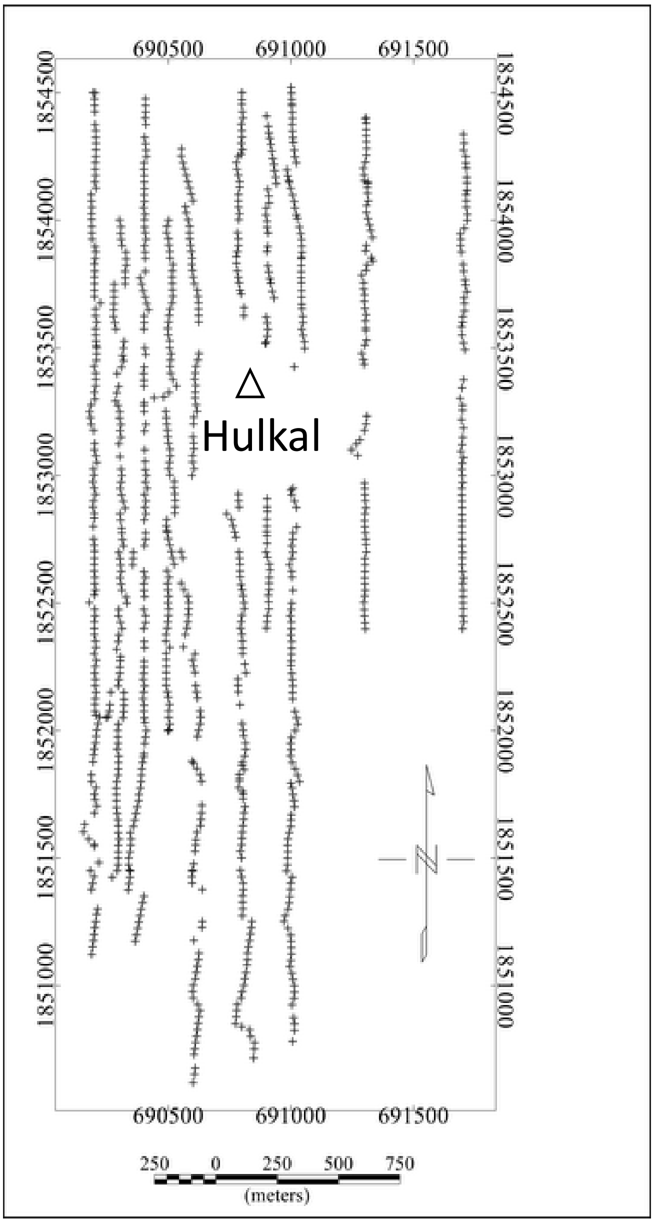

Figure 2.3 Profile layout of the survey area

This GPS can locate the coordinate of the data points along with the elevation, which is essentially needed in the magnetic data reductions. The collected data is processed for effective interpretation of the subsurface mineralized zones (faults/fractures) geometry. Thus, the raw total magnetic field data collected in the instrument were transferred to the system by using Gem-Link software and diurnal correction was also performed by using same software.

2.3 Measurement of Physical Properties

In situ magnetic susceptibility of exposed rocks and grab samples have been measured to get an aid in the interpretation of the magnetic map. Based on these measurement of rock unit present in the area, susceptibility of different rock are listed in (Table 2.2).

Table 2.2 Susceptibility values of rock samples, Hulkal area

Rock types	No. of Samples	Magnetic Susceptibility $\times 10^{-3}$ SI
Weathered granite	6	0.007-0.01
Granite	8	0.02-0.03
Limestone	15	0.02-0.04
Shale	8	0.17-0.23
Brecciated Limestone	4	0.02-0.04

Magnetic susceptibility is measured using the portable handheld susceptibility meter KT-10 of Terraplus make, Canada. The principle of working of this instrument is based on the fact that the alternating magnetic field produced by Helmholtz coil induces a magnetic field in the specimen which is proportional to the rate of change of its magnetic moment. Knowing the magnetic field and the volume of the specimen, its susceptibility is calculated. It is conspicuous from the above table the susceptibility for shale is highest and lowest for the weathered granite but the variation is not large enough. Magnetic susceptibility contrast between rocks is less, therefore it is difficult to discriminate the lithology on the basis of magnetic susceptibility alone. That is why, in the survey, it is difficult to discriminate fracture within granites and sediments.

Figure 2.4 Hand held susceptibility meter (KT-10)

2.4 Reductions and processing of Magnetic Data

Geophysical data processing is an intermediate stage between data acquisition and interpretation of the observed data. During processing, the observed data is corrected for natural and instrumental variations.

2.4.1 Diurnal variation correction

After the data collection from a fixed base station its variation with time is checked to know the effect of the solar magnetic storm, if the base data is disturbing then complete data is discarded. After checking the base data the complete data is corrected for diurnal effect and this is done by GEM link software. This software yields a corrected magnetic anomaly with respect to the base station. Noise due to secular change or epoch was considered negligible because it does not change much in short duration. Normal corrections (which accounts for the variation of magnetic intensities with latitude) were not considered here due to the limited survey area.

2.4.2 Representation of magnetic data

Magnetic data may be represented in form of profiles, contour map, image map, greyscale raster image map, shaded relief map, and colour raster map. Most frequently used are profiles, contour map and image map. For better representation, any of the combinations of these also can be used.

2.4.3 Preliminary processing of the data

2.4.3.1 Gridding

Diurnal corrected data was subjected to gridding by using minimum curvature statistical method. It takes into account the surface of minimum curvature. According to Briggs (1974), the minimum curvature gridding method is a very popular gridding algorithm.

Different mathematical filtering techniques have been applied to the diurnal corrected data to enhance the geological features of interest. In general to apply different mathematical filters data is subjected to Fourier transform to transform into wavenumber domain. Geosoft, Oasis Montaj, inbuilt MAGMAP fulfilled this purpose which facilitates application of most of the useful filters in different ways. Some of the filters applied to the data are given here with their description. Total magnetic field intensity data were gridded using minimum curvature gridding method with 13m cell size.

2.4.3.2 Reduced to pole (RTP)

The magnetic field is a dipolar field and anomalies depend upon the geomagnetic inclination and declination of the area. Along with this, magnetic anomalies are also affected by the orientation of the magnetic body with respect to the present day magnetic field direction. Hence, it is relatively difficult to interpret magnetic anomalies compared to gravity anomalies. Therefore, to make interpretation easier, we have to remove the dipolar nature of the anomalies. Reduced to magnetic pole filter transforms an observed magnetic anomaly at any given location into the anomaly that would appear if the data have been acquired over the magnetic pole. The algorithm for RTP was proposed by Baranov (1957) and Baranov and Naudy (1964) and was primarily meant to simplify the shape of the anomaly.

2.4.3.3 Analytical signal

The concept of the analytic signal applied to magnetic anomalies was developed in two dimensions by Nabighian (1972) based on a concept initially proposed by the French Ville in 1948. In two dimensions, the complex analytic signal of the magnetic signal $M(x, y, z)$ can be expressed as (Thurston and Smith 1997):

$$A(x,y) = |A(x,y)|.\exp(j\varphi)$$

with,

$$|A(x,y)| = \sqrt{\left(\frac{\partial M}{\partial x}\right)^2 + \left(\frac{\partial M}{\partial y}\right)^2}$$

and

$$\varphi = \tan^{-1}\left(\frac{\partial M}{\partial z}\middle|\frac{\partial M}{\partial x}\right)$$

|A| is the 2D analytic signal amplitude, φ the local phase. A common theme of the normalized derivatives is the concept of mapping angles (or functions of angles) derived from the gradients of the magnetic intensity.

Using the 3-dimensional grid, the amplitude of the analytic signal A of $M(x, y, z)$ is calculated by taking the square root of the sum of the squares of each of the directional first derivatives of the magnetic field.

$$|A(x,y)| = \sqrt{\left(\frac{\partial M}{\partial x}\right)^2 + \left(\frac{\partial M}{\partial y}\right)^2 + \left(\frac{\partial M}{\partial z}\right)^2}$$

The analytic signal is useful for locating the edge of magnetized bodies in areas of low magnetic latitude. The analytic signal generates a maximum directly over discrete bodies as well as their edges. An important characteristic of the analytic signal is that it is independent of the direction of the magnetization of the source. (Macleod et al., 1993).

2.5 Interpretation of magnetic data

Interpretation of total magnetic field data of the area of investigation was based on qualitative as well as quantitative approaches. Data has been subjected to various filtering techniques to enhance the magnetic signal and to resolve the structural features. Then the data was interpreted qualitatively to bring out the structural features of the region.

2.5.1 Qualitative interpretation

A). Total magnetic intensity (TMI) anomaly map

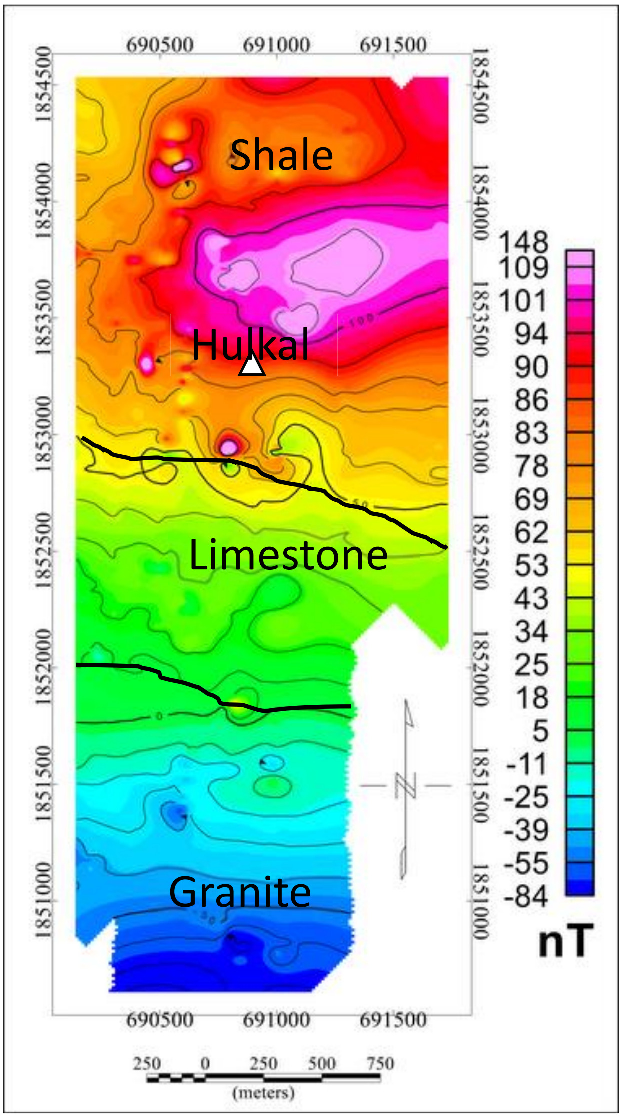

Figure 2.5 Total magnetic intensity anomaly map of study area.

Magnetic anomaly values are ranging from -64 to 109nT. In the southern part low magnetic anomaly is attributed to granite/ fractured granite, which is part of the basement. As moving from south to north, basement-sediment contact is demarcated in (Figure 2.5). Further north, limestone is persisted and in the northern most part shale is dominated with highest magnetic anomaly. In order to demarcate the features, the pattern of contours and amplitude of the anomalies are analysed. Some data filtering techniques have also been used to make the structures visible over the map. The technique applied have been discussed as follows.

B) Reduction To Pole (RTP) map

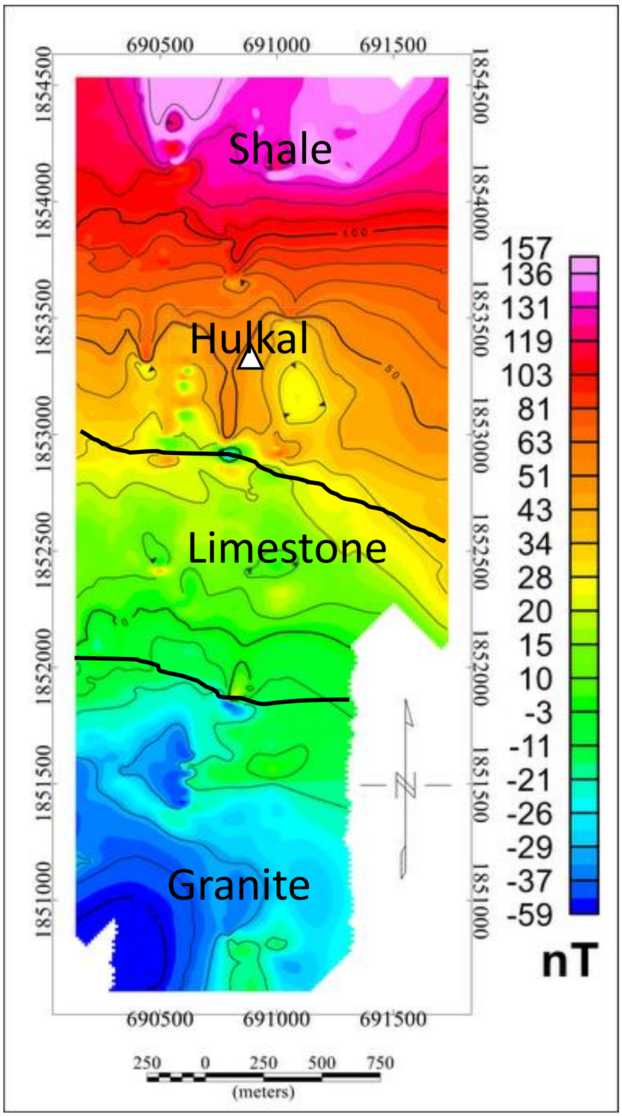

Figure 2.6 Reduction to pole anomaly map, Hulkal area

Reduction to pole technique removes asymetricity in anomaly and shift the anomaly just above the body. In this technique magnetic inclination (22.783^0) and declination (-0.5^0) is used. RTP map of the area shown in (Figure 2.6), anomaly varies from -45 nT to 137 nT. Low magnetic anomalies in the southern part is attributed to basement granite. Very low magnetic anomaly

(-45nT to -30nT) within the granite is due to the fractures in basement. In the central part of the area moderate magnetic anomalies (-10nT to -20nT) are associated with the limestone. Whereas very high magnetic anomaly (60nT -137nT) in the extreme north is due to presence of shale. Here limestone is contributing high magnetic anomaly compared to granite. On the basis of magnetic anomaly contrast basement-sediment contact towards southern side and shale-limestone contact in the northern part are delineated.

C) Analytical signal anomaly map

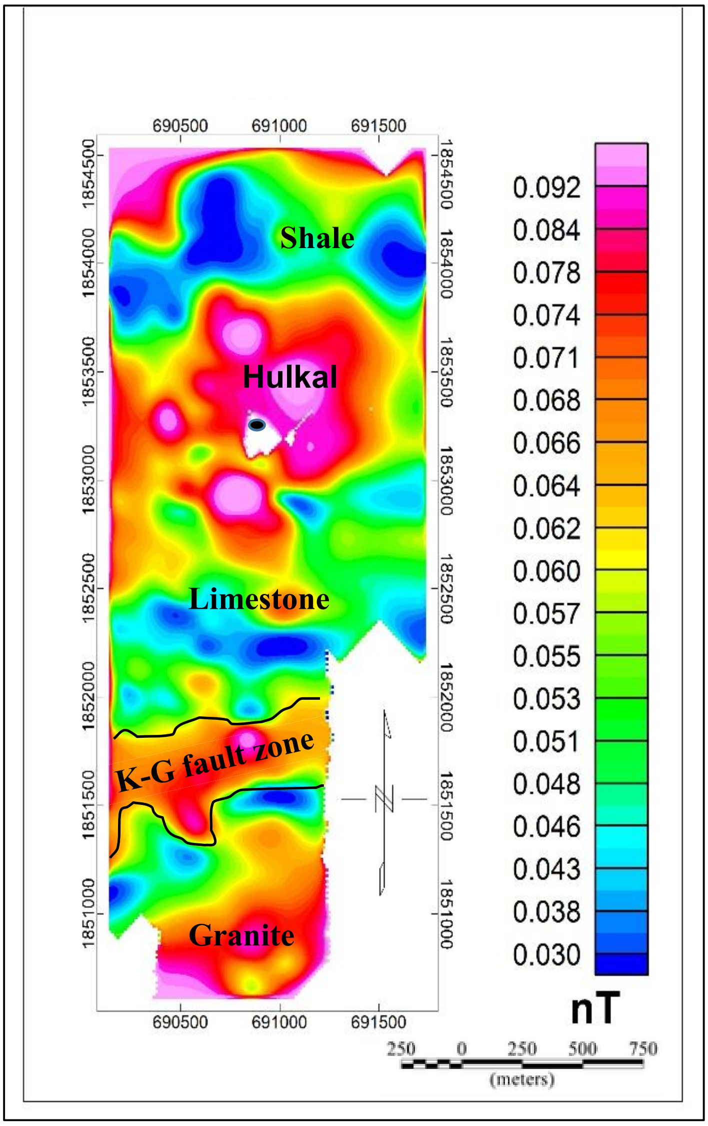

Figure 2.7 Analytical Signal map, Hulkal area

Analytical signal of magnetic data is useful for locating the edges of the body and this method is independent of direction of magnetisation so it discriminate the sources very precisely. In the above map Gogi-Kurlagere (K-G) fault zone is very well demarcated with trend of ENE-WSW. Southern most part is dominated by granite whereas limestone is present in the middle part and in the northern part shale is observed. There is no evidence of disturbance within the sediments, hence another method like electrical survey is needed to delineate this zone.

2.5.2 Quantitative interpretation

Interpretation done so far is only qualitative any feature is identified based on the visual analysis. Qualitative interpretation includes providing numerical information about the source bodies, such as depth to the top, dip, thickness etc. In the following section, different methods have been used as an aid in quantitative interpretation.

2.5.2.1 Depth estimation of source bodies using the spectral analysis

Processed magnetic data were further subjected to Fourier transformation which transforms/convert the magnetic data from the spatial domain (equivalent to time domain) to wave number domain (equivalent to frequency domain). Analysis of the data in the wavenumber domain is called spectral analysis.

When a statistical population of magnetic or gravity sources exists at a specific source depth, then the expression of those sources on a plot of the natural logarithm of energy against frequency is a straight line having a slope of $-4\pi h$ (Spector and Grant, 1970; 1974). It follows that where a spectrum shows a number of straight-line branches, statistical populations of sources exist at a number of depths. Radially averaged power spectrum is a plot between the natural log of power and wavenumber. This plot shows the variation of the power of a signal by increasing the signal wavenumber. The relation between power, wavenumber and source-body depth is expressed in the following equation (Hinze et al., 2013).

$$Power = e^{-4\pi hk}$$

$$h = -\frac{\ln(power)}{4\pi k}$$

$$depth\ to\ the\ source\ body\ h = \frac{slope\ of\ best\ fitted\ line\ of\ \ln(power)\ vs\ k\ plot}{4\pi}$$

Here, 'k' is wavenumber, 'h' is source body depth and a negative sign indicates downward direction.

In radially averaged power spectrum, slopes of the different tangents to the spectrum are used to calculate the depths to the source body. This method gives the average depths of the source body in the study area rather than absolute depths.

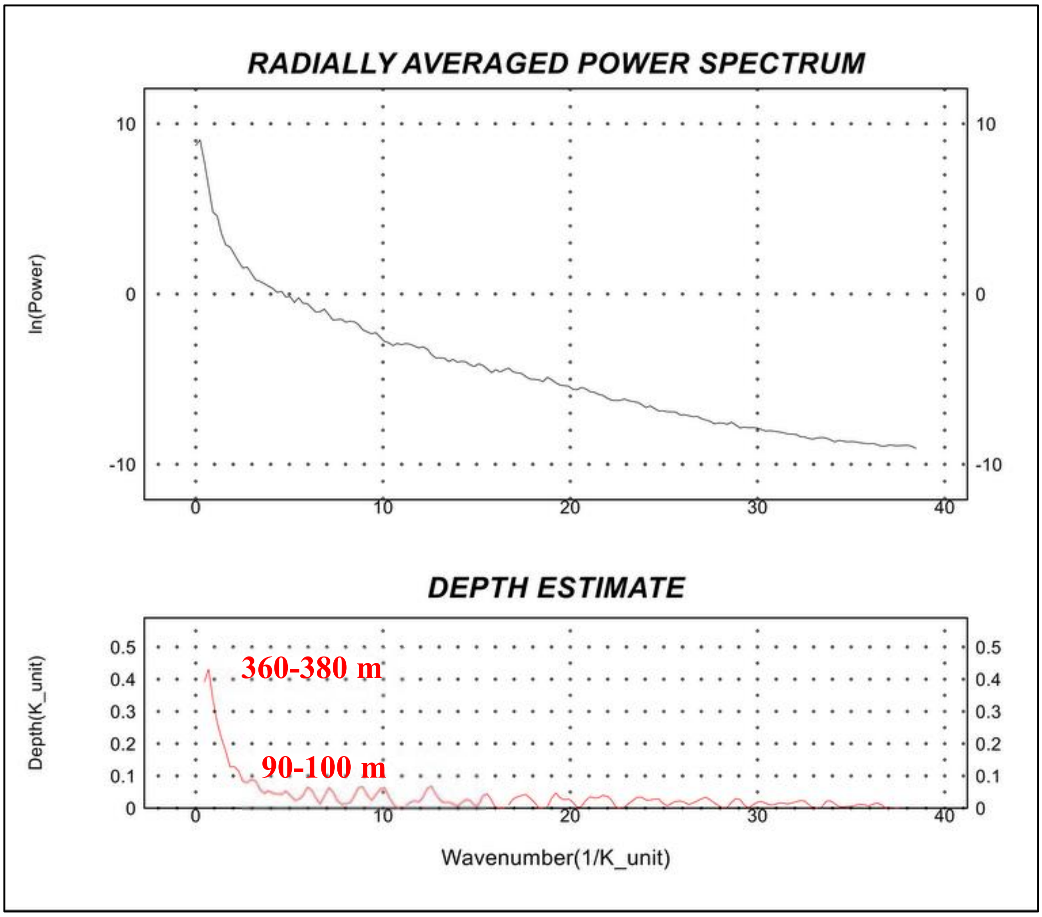

Figure 2.8 Spectral depth analysis of magnetic data observed in study area

As we know deep seated features gives low wavenumber response so the depth aproximatly 360-380 m is of deepest feature which may be attributed to basement depth. As depth of the source decreases wavenumber increases so the dept approximatly 90-100 m corresponds to response due to limestone expected bellow shale. Further shallow depth features give very high wavenumber and attributed to noise. This method revealed depth ranges (Table 2.3)

Table 2.3 Result of spectral analysis of magnetic data

Source depth range(m)	Causative source
360-380	Basement
90-100	Limestone

2.5.2.2 Depth estimate using Continuous Wavelet transform

Mathematical transformations are applied to signals to obtain further information from that signal which is not readily available in the raw signal. There are a number of transformations that can be applied, among which the Fourier transforms are probably by far the most popular. In many cases, the most distinguished information is hidden in the frequency content of the signal. The frequency spectrum of a signal shows what frequencies exist in the signal and that is calculated by Fourier transform (FT).

There are many transforms that are used quite often like, Hilbert transform, short-time Fourier transform, Wigner distributions, the Radon Transform and wavelet transform. Every transformation technique has its own area of application, with advantages and disadvantages. FT (as well as WT) is a reversible transform, that is, it allows to go back and forward between the raw and processed (transformed) signals. However, only either of them is available at any given time. That is, no frequency information is available in the time-domain signal, and no time information is available in the Fourier transformed signal. The FT gives the frequency information of the signal, which means that it tells us how much of each frequency exists in the signal, but it does not tell us when in time these frequency components exist. This information is not required when the signal is so called stationary. Signals whose frequency content do not change in time are called stationary signals. FT decomposes any signal to complex exponential functions of different frequencies. Following the two equations.

$$\boldsymbol{X(f) = \int_{-\infty}^{\infty} x(t).\, e^{-i\omega t}\, dt}$$

$$\boldsymbol{x(t) = \int_{-\infty}^{\infty} X(f).\, e^{i\omega t} df}$$

The signal, which has different frequencies at different time, known as non- stationary signal.

Fourier spectrums of stationary and nonstationary signals are almost identical, although the corresponding time-domain signals are not even close to each other. This is because, FT gives the spectral content of the signal, but it gives no information regarding where in time those spectral components appear. Therefore, FT is not a suitable technique for non-stationary signal. When the time localization of the spectral components are needed, a transform giving the TIME-FREQUENCY REPRESENTATION of the signal is needed.

The wavelet transform (WT) is a transform of this type. It provides the time-frequency representation. According to heisenberg uncertainty principle, the frequency and time information of a signal at some certain point in the time-frequency plane cannot be known. The best we can do is to investigate what spectral components exist at any given interval of time. This is a problem of resolution, and it is the main reason why we use WT. STFT gives fixed resolution whereas WT gives a variable resolution as follows: Higher frequencies are better resolved in time, and lower frequencies are better resolved in frequency. This means that, a certain high frequency component can be located better in time (with less relative error) than a low frequency component. On the contrary, a low frequency component can be located better in frequency compared to high frequency component.

However, there are two main differences between the STFT and the CWT:

1. The Fourier transforms of the windowed signals are not taken, and therefore single peak will be seen corresponding to a sinusoid, i.e., negative frequencies are not computed.

2. The width of the window is changed as the transform is computed for every single spectral component, which is probably the most significant characteristic of the wavelet transform.

The continuous wavelet transform is given by the following equation,

$$CWT_x^{\psi}(b,a) = W_{\psi}|_{\phi 0} = \int_{-\infty}^{\infty} \frac{dx}{a} \psi\left(\frac{b-x}{a}\right) \phi_0(x)$$

As seen in the above equation, the transformed signal is a function of two variables, **"b"** and **"a"**, the translation and scale parameters, respectively. $\psi(x)$ is the transforming function, and it is called the mother wavelet . The term mother wavelet gets its name due to two important properties of the wavelet analysis as explained below:

The term wavelet means a small wave. The smallness refers to the condition that this (window) function is of finite length (compactly supported). The wave refers to the condition that this function is oscillatory. The term mother implies that the functions with different region of support that are used in the transformation process are derived from one main function, or the mother wavelet. In other words, the mother wavelet is a prototype for generating the other window functions. The term translation is related to the location of the wavelet, as the wavelet is shifted through the signal. The selected type of wavelet is dilated at different scales and translated on the signal, with each scale convolution between wavelet and signal is performed and calculated CWT coefficients given by above equation are stored until the last scale is used.

THE SCALE

The parameter **scale** in the wavelet analysis is similar to the scale used in maps. As in the case of maps, high scales correspond to a non-detailed global view (of the signal), and low scales correspond to a detailed view. Similarly, in terms of frequency, low frequencies (high scales) correspond to a global information of a signal (that usually spans the entire signal), whereas high frequencies (low scales) correspond to a detailed information of a hidden pattern in the signal (that usually lasts a relatively short time). Scale parameter is defined as 1/frequency.

Time Frequency analysis:

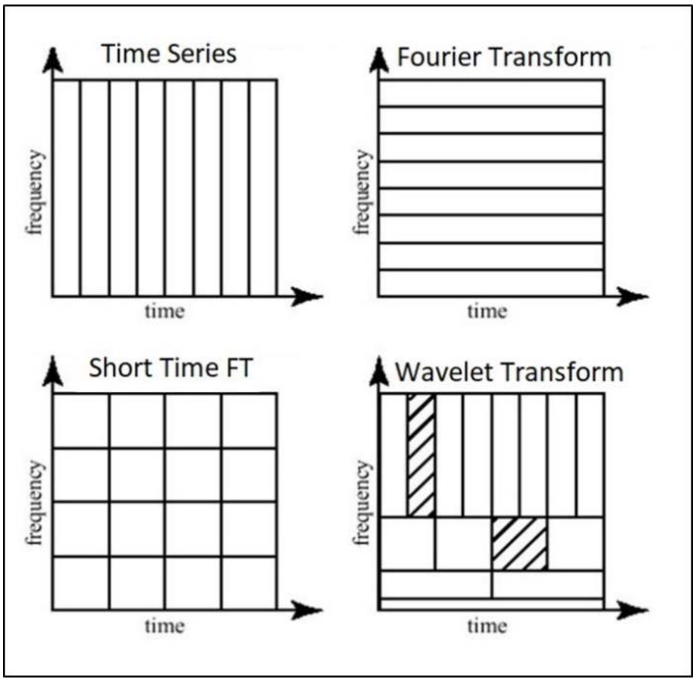

Figure 2.9 Time frequency plot

Here resolution property of transforms are explained. In Fourier transform we have very good frequency resolution as frequency contain can be clearly visible but not any time resolution. Hence this analysis shows, limitation of Fourier transform that gives only frequency content in the signal but these frequencies are not localised in time or space means it does not have space resolution. Every box in the Figure 2.9 corresponds to a value of the wavelet transform in the time-frequency plane. Each boxes have a certain non-zero area, which implies that the value of a particular point in the time-frequency plane cannot be known. All the points in the Time-frequency plane that falls into a box are represented by one value of the WT. Here widths and heights of the boxes change, the area is constant. That is each box represents an equal portion of the time-frequency plane, but giving different proportions to time and frequency.

Note, at low frequencies, the height of the boxes are shorter (which corresponds to better frequency resolutions, since there is less ambiguity regarding the value of the exact frequency), but their widths are longer (which correspond to poor time resolution, since there is more ambiguity regarding the value of the exact time). At higher frequencies the width of the boxes decreases, i.e., the time resolution gets better, and the heights of the boxes increase, i.e., the frequency resolution gets poorer. So we can collectively say that WT gives multi resolution results. Obtained resolution is varying based on the selected wavelets and scaling parameter. The choice for the scale and the translation parameter can be arbitrary.

Application of CWT on potential data

Potential data is interpreted in two ways first is modelling and second is processing. There are so many techniques developed to interpret potential field data by Forward and Inverse modelling (Blakely, 1995). For Identification and characterisation of the sources initial model is used in forward modelling and in inverse modelling so many constrains such as ill posed problem, non-uniqueness and need of some priori information (Dimri, 1992) are present.

Processing is next option to resolve these issues and give less ambiguous results. Wavelet Transform technique is efficient to use and show good resolution. The magnetic anomaly is transformed to wavelet domain and modulus maxima lines are interpreted as mean depth and location of causative sources.

Methodology:

Interpretation of potential field data in wavelet domain (CWT) is developed by Moreau et al. (1997, 1999). In the wavelet domain, a signal is convolved by some specific object oriented orthogonal mother wavelets. The continuous wavelet transform (W) of function $\phi_0(x)$ can be viewed as convolution product with the mother wavelet (Moreau et al., 1997, 1999) given by equation 1, Where (ψ) is analysing wavelet x is abscissa along the profile, a is dilation (scale), b is a position (translation) parameter and the dilation parameter D_a can be defined as

$$D_a\psi(x) = \frac{1}{a}\psi\left(\frac{x}{a}\right) \qquad (1)$$

If the signal has a spectral component that corresponds to the value of scale, which is arbitrarily chosen, the product of the wavelet with the signal at the location where this spectral component exists gives a relatively large value in other words wavelet transform coefficient is maxima at that point.

According to Moreau *et al*. (1997), modulus maxima of wavelet transform that is set of points where $\partial\ W[\psi,\phi](b,a) = 0$, form cone like structure and pointing toward source of homogeneity. For homogenous sources, Moreau (1995) has given the relationship between wavelet coefficients at two altitudes (scales) and for any wavelets.

$$W^{\gamma}(x,a') = \left(\frac{a'}{a"}\right)^{\gamma}\left(\frac{a"+z_0}{a'+z_0}\right)^{-\beta} W^{\gamma}\left(x\ \frac{a"+z_0}{a'+z_0}, a"\right) \qquad (2)$$

Where β represents the holder exponent related to shape of the source (homogeneity degree), γ is order of wavelet, a' and a'' represents different altitudes (scales), z_0 represents the depth of the causative body. The choice of mother wavelet is very crucial for wavelet transform. For Example: In case of time-frequency analysis of a function, complex Morlet Wavelet is used as a mother wavelet while for analysing the potential field data Poisson-kernel function or green's function is used as a mother wavelet. The linear regressions (slope) of log-log plots of normalized modulus $\left|\frac{W}{a^{\gamma}}\right|$ versus apparent depth $(a + z_0)$ (Moreau *et al.* 1999; Sailhac *et al.* 2000; Boukerbout, Gibert and Sailhac 2003, etc.) are easy to obtain and will provide β. the homogeneity degree of field (β) is given by the following expressions for magnetic field

$$\beta = \alpha - \gamma \qquad (3)$$

Application of Continuous Wavelet Transform

A) Continuous wavelet transform is applied on gravity data which is synthetically generated due to two horizontal cylinder at the depth of 15 m each.

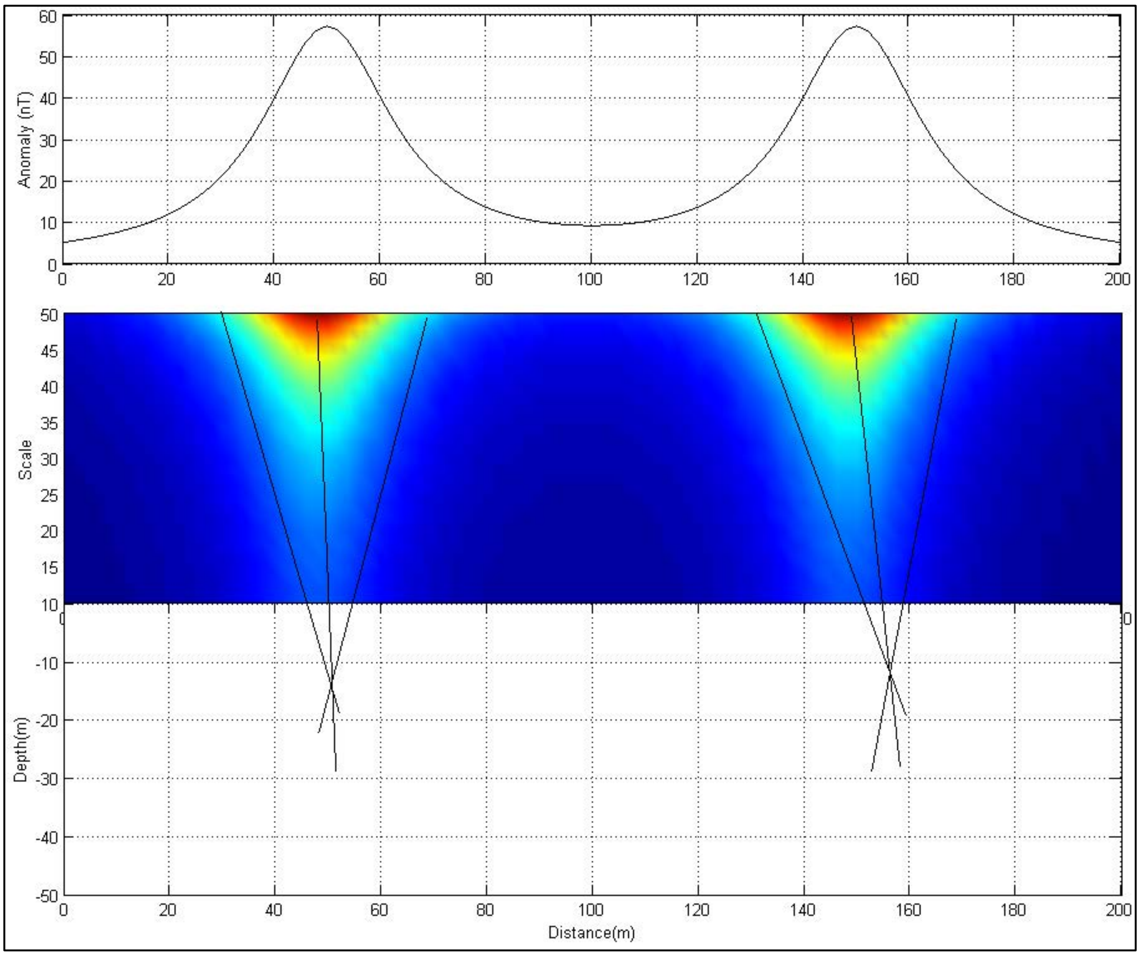

Figure 2.10 Wavelet transform of gravity anomaly.

Result after CWT of synthetic data is in good agreement. Modulus maxima is concentrated just over the location of cylinders and the depth derived from the method is 15 m.

B) Continuous wavelet transform is applied on magnetic data of Hulkal area

Continuous wavelet transform is applied on magnetic data along the line AA' shown in (figure 2.11) and result is shown in (figure 2.12) with three different sections.

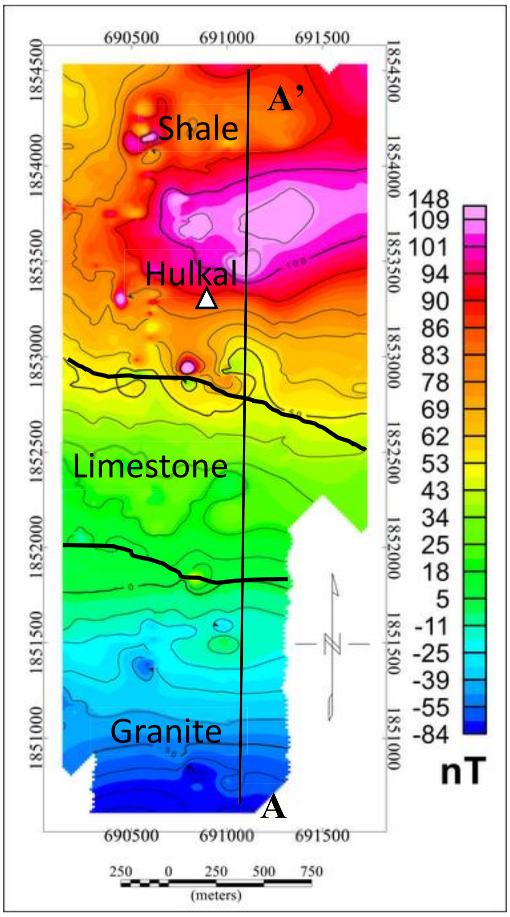

Figure 2.11Total magnetic intensity anomaly map showing profile AA'

First section is showing anomaly variation with distance. Second section is showing variation of CWT coefficients with scale and horizontal distance, here the zone of influence shown in, yellow colour, of continuous wavelet transform is conical in shape comprising maxima of wavelet coefficients (red colour) in the centre and third section is showing depth of the source. After applying it on magnetic data, maxima is located at horizontal distance of 700-750 m from the starting point of the survey. This zone can be consider as disturbed zone where coefficients are concentrated and shows maxima and geologically this can be basement-sediment contact. As described in the theory of CWT, tangents from envelope of maxima of coefficients intersect each other at the source of disturbance. Tangents from this envelope intersect each other at depth of approximately 340-370 m, this may be attributed to basement depth in the study area. This depth is also verified by radial average power spectral analysis of the data .As we move further north there are shallow feature also presents in study area.

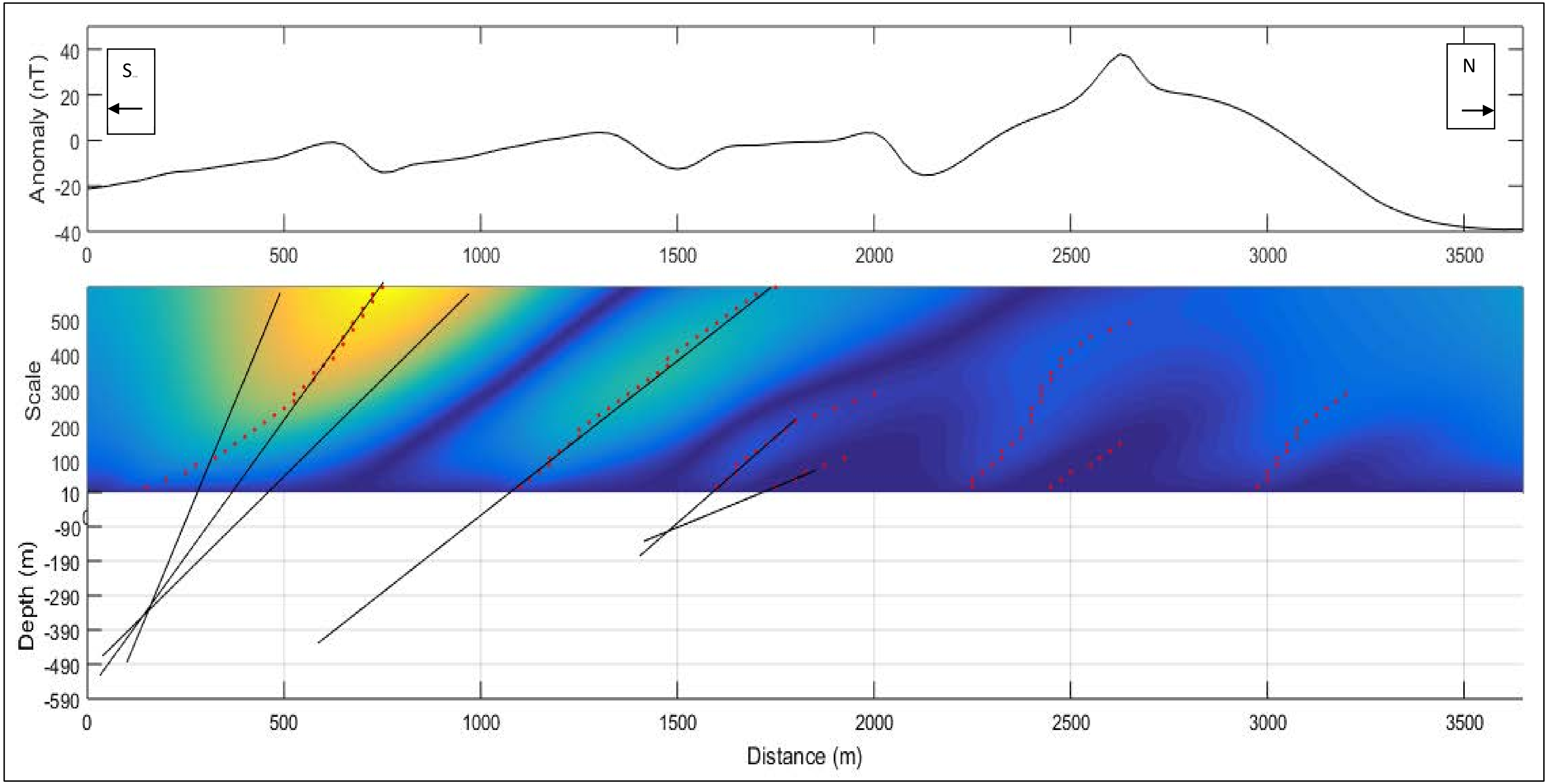

Figure 2.12 Results of WT of magnetic data

2.6 2D Magnetic modelling

Two dimension forward depth model along profile AA' is prepared using GMSYS 2D forward model software (Figure no. 2.13). In this model best fit between observed and calculated data is shown with the error of 3.8, so the depth model after matching can be accepted.

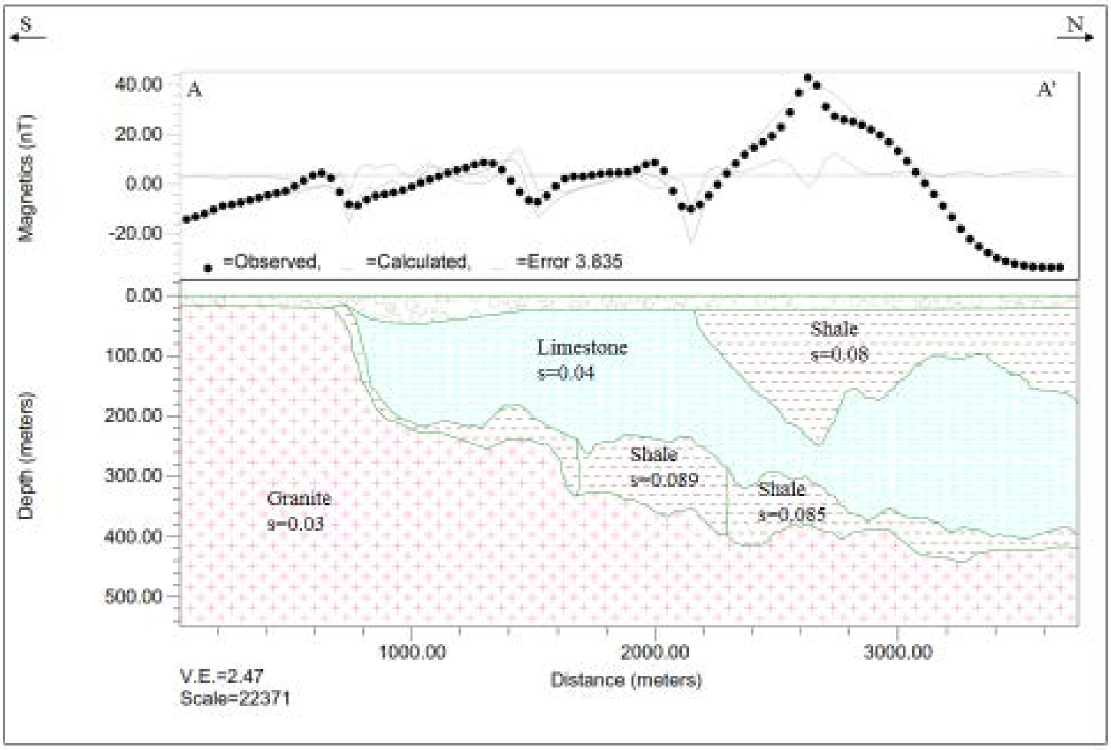

Figure 2.13 Two dimensional modelling of magnetic data

It is clear from the above model that basement-sediment contact is located at the spatial location approximately 700-750 m and basement depth is approximately 340 m and from south to north basement depth is increasing up to 370 m. At the contact between basement granite and limestone a thin layer of shale is also present and continuing with the increasing depth with the average susceptibility of 0.09 SI unit. Contact between granite and limestone is faulted in nature.

CHAPTER -3

INVESTIGATION BY INDUCED POLARISATION (IP)/RESISTIVITY METHOD

3.1 Introduction

The induced polarization method was developed in the middle of the twentieth century. It makes the use of the capacitive action of the subsurface to locate zones of conductive minerals which are disseminated in nature. This method aids the exploration of the conducting mineralization that may not be detected by any other method. With the depletion of marine ore bodies, particularly in the Indian context the IP method has become an indispensable tool in the search of base metals and gold mineralization. However it is general practice to try some reconnaissance gravity, magnetic techniques before applying IP survey. The most important advantage of IP method is that a couple of parameters viz. chargeability and resistivity can be measured simultaneously. The theory and practice of IP are well documented in (Sumner; Telford et al., 1976; Sharma., 1997).

The resistivity method is used in the study of layered structure in the form of horizontal and vertical discontinuities in the electrical properties of the ground, and also in the detection of three-dimensional bodies of anomalous electrical conductivity. Electrical methods utilize direct currents or low frequency alternating currents to investigate the electrical properties of the subsurface.

3.2 Theory of IP/Resistivity method:

3.2.1 Resistivity Method: In the resistivity method, artificially-generated electric currents are introduced into the ground and the resulting potential differences are measured at the surface.

Deviations from the pattern of potential differences expected from homogeneous ground provide information on the form and electrical properties of subsurface in rocks.

In actual field condition, the ground and subsurface never be homogeneous and the small variation due to moisture content or conductive minerals causes large variations in resistivity. This fact allows the successful application of finding resistivity distribution over an area and interpretation of the data in terms of geology and associated structural features in the subsurface.

(a) Apparent Resistivity

In practice one can measure the true resistivity of a formation by using any electrode array in a homogeneous and isotropic medium. However, in nature one encounters heterogeneity and anisotropy more often, and therefore, the resistivity measured under such conditions is not the true resistivity of the medium and is called the apparent resistivity.

The apparent resistivity is a formal concept and should not be considered to be some sort of average resistivity encountered in heterogeneous surface (Parasnis, 1973). Unlike the true resistivity, the apparent resistivity is not a constant physical property and the measured resistivity is dependent on factors such as (a) the resistivity contrast between the layers of different nature. (b) the geometric factor of the electrode configuration. (c) the thickness of geo-electrical layers and. (d) the position of the electrodes with respect to lateral inhomogenities.

(b) Methodology and measurements

In an investigation area, measurements are carried out by sending current into the ground through two electrodes (A and B) and measuring the potential difference at a different set of electrodes (M and N), and thereby getting an estimate of the resistivity of the ground called the apparent resistivity. The current pattern and equipotential surfaces for a homogenous and isotropic ground is shown in Figure 3.1

The potential at any observation point at the surface of a homogenous isotropic half space can be expressed as

$$V(r) = \frac{\rho I}{2\Pi r} \qquad (1)$$

Where I is the transmitted current, ρ is the resistivity of the ground and r is the distance from the observation point at the surface to the point source. With an electrode configuration like the one shown in Figure above, the potential difference in a homogenous halfspace can calculated from:

$$\Delta V = \frac{\rho I}{2\Pi}\left(\frac{1}{AM} - \frac{1}{BM} - \frac{1}{AN} + \frac{1}{BN}\right) \qquad (2)$$

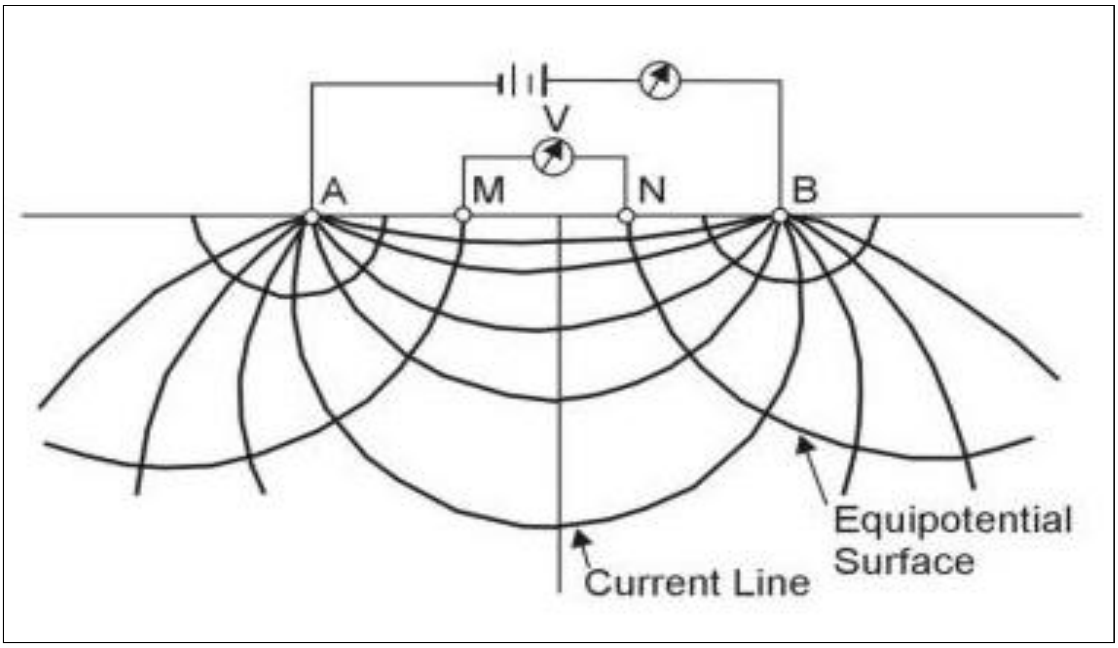

Figure 3.1 Schematic representation of equipotential lines and current lines for simple array

Where |AM|, |BM|, |AN| and |BN| denote the distance between current and potential electrodes. In reality the measured potential rarely comes from a homogenous half space and equation 2 is rewritten to give the apparent resistivity:

$$\rho_a = \frac{\Delta V}{I} 2\Pi\left(\frac{1}{AM} - \frac{1}{BM} - \frac{1}{AN} + \frac{1}{BN}\right)^{-1} = \frac{\Delta V}{I} K \qquad (3)$$

Where K is the geometrical factor, which depend on the geometry of the chosen electrode configuration. The apparent resistivity is the resistivity of a homogenous half space should have to give the actual measurement.

Different electrode configurations have different penetration depths, but generally when increasing the distance between current electrodes, information on deeper parts of the earth is obtained.

The concept of apparent resistivity is the foundation of the resistivity method. Though it is not directly related to the true resistivity of the layers, it can however be used to deduce the true resistivity of subsurface layered structure by making a series of measurements of the apparent resistivity for different electrode separations (Figure 3.2).

3.2.2 Induced Polarization Method:

Induced polarization is a method that uses similar electrodes set up with time-varying currents and voltages. The chargeability is measured at low frequencies. Induced polarization is observed when a steady current through two electrodes in the Earth is shut off, the voltage does not return to zero instantaneously, but rather decays slowly (Figure 3.3), indicating that charge has been stored in the rocks. This charge, which accumulates mainly at interfaces between clay minerals, is responsible for the IP effect.

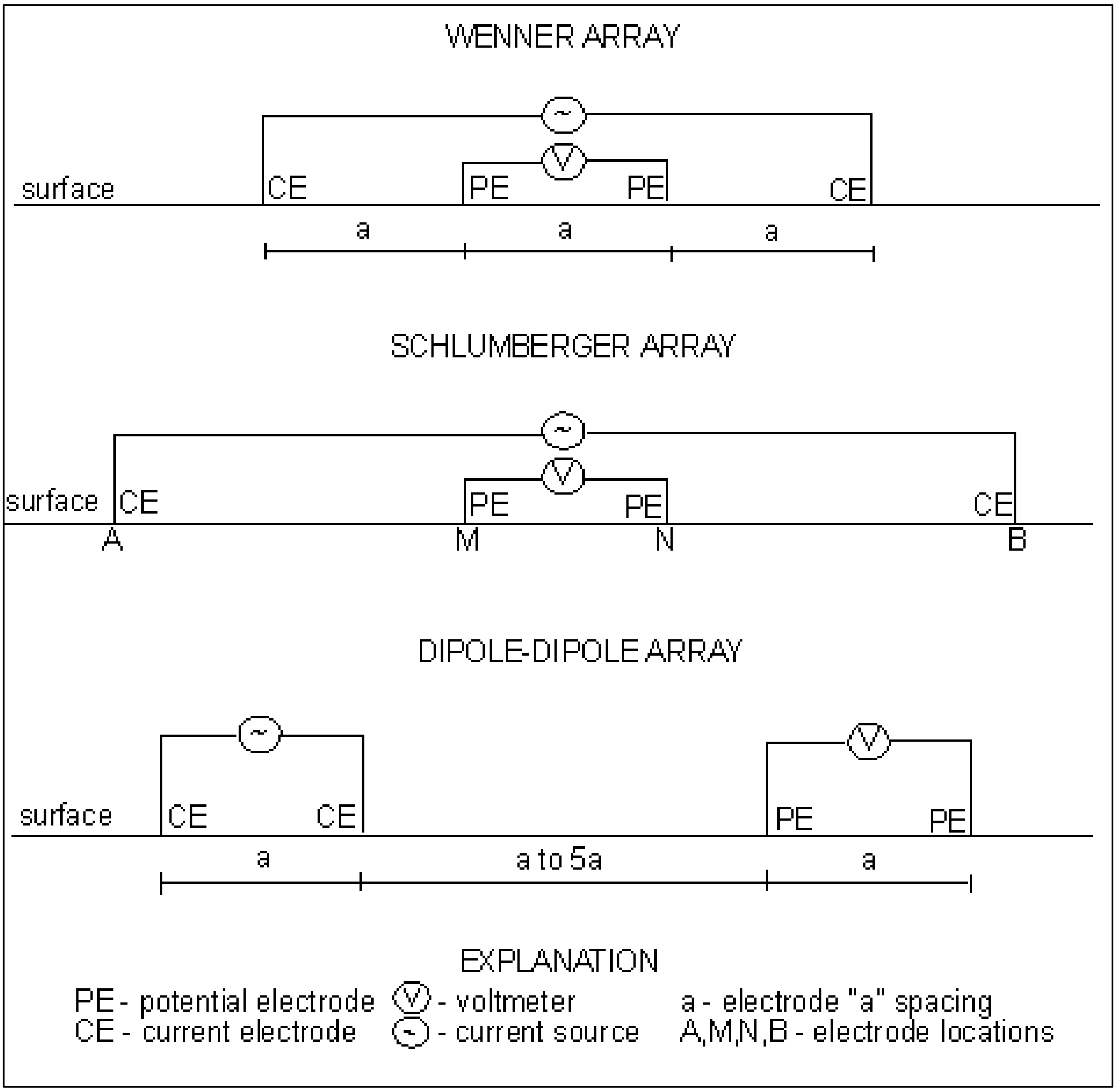

Figure 3.2 Different electrode configurations used in IP/Resistivity survey

This effect can be measured in either the time domain by observing the rate of decay of voltage, or in the frequency domain by measuring phase shifts between sinusoidal currents and voltages.

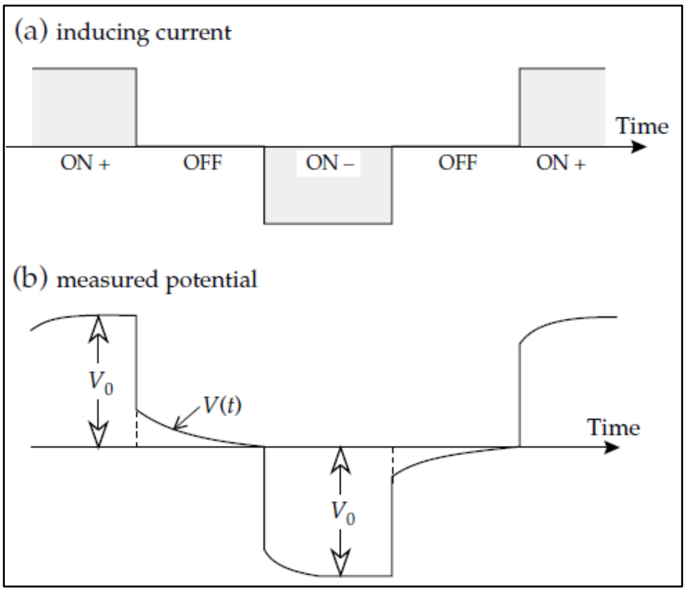

Figure 3.3 (a) Illustration of the IP-related decay of potential after interruption of the primary current. (b) Effect of the IP decay time on the potential waveform for a square wave input current.

In nature, the induced polarization (IP) effect is seen primarily with metallic sulphides, graphite, and clays. For this reason, IP surveys have been used extensively in mineral exploration. Recently, IP has been applied to hazardous waste landfill and groundwater investigations to identify clay zones. As with electrical resistivity surveys, vertical or horizontal profiles can be generated using IP.

Induced polarization is the capacitance effect, or chargeability, exhibited by electrically conductive materials. Time-domain IP is done by pulsing an electric current into the earth at one or two second intervals through metal electrodes. Disseminated conductive minerals in the ground will discharge the stored electrical energy during the pulse cycle. The decay rate of the discharge is measured by the IP receiver. The decay voltage will be zero if there are no polarizable materials present.

Generally, both IP and resistivity measurements are taken simultaneously during the survey. Survey depth is determined by electrode spacing.

The measurement of decaying voltage over a certain time interval is known as time-domain IP survey. Measurement of apparent resistivity at two or more low specific frequencies is known as frequency-domain IP survey.

3.3 Origin of IP:

(a) Membrane polarization

Membrane polarization is caused by the presence of clay grains. The clay grains have a negative surface charge, and to restore electron neutrality, cations from the electrolyte are attracted to the clay grain surface. Membrane polarization (Figure 3.4) is thus closely related to the electrical double layer, and likewise there will be a fixed and diffuse layer. In areas where the diffusive layer is thick enough, membrane zones will develop. The membrane zones will extend into the pore space, and thereby selectively only passing ions of a certain size and polarity, which causes local charge builds-ups. The mechanism behind membrane polarization is shown in Figure below. Here cationic clouds, related to clays grains, acts as electronegative membranes between sand grains. During application of an electrical current, the membrane zones enhance the transport of cations relative to anions. Upon termination of the applied current, voltages resulting from the local charge concentration gradients will slowly decay with time as the ions redistribute back to an equilibrium position.

According to (Slater, and Lesmes, (2002)) there is a non-linear relationship between chargeability and clay content. The non-linear relationship is caused by a trade-off between increasing polarization and higher conductivity with increasing clay content.

The optimal clay content, with regards to membrane polarization and high chargeability, is most likely a few percent clay distributed in the soil, but also depends on clay type, because of varying ion exchange capacity for different clay types, The induced polarization response is relatively low for montmorillonite, but higher for kaolinite and illite.

Often minerals like sand and clay are coated with organic matter, which like clays, have a high ion exchange capacity. Likewise contaminants often form a thin surface coating on mineral grains, so it is believed that membrane polarization is the mechanism for the induced polarization response seen in peat and hydrocarbon contaminated areas.

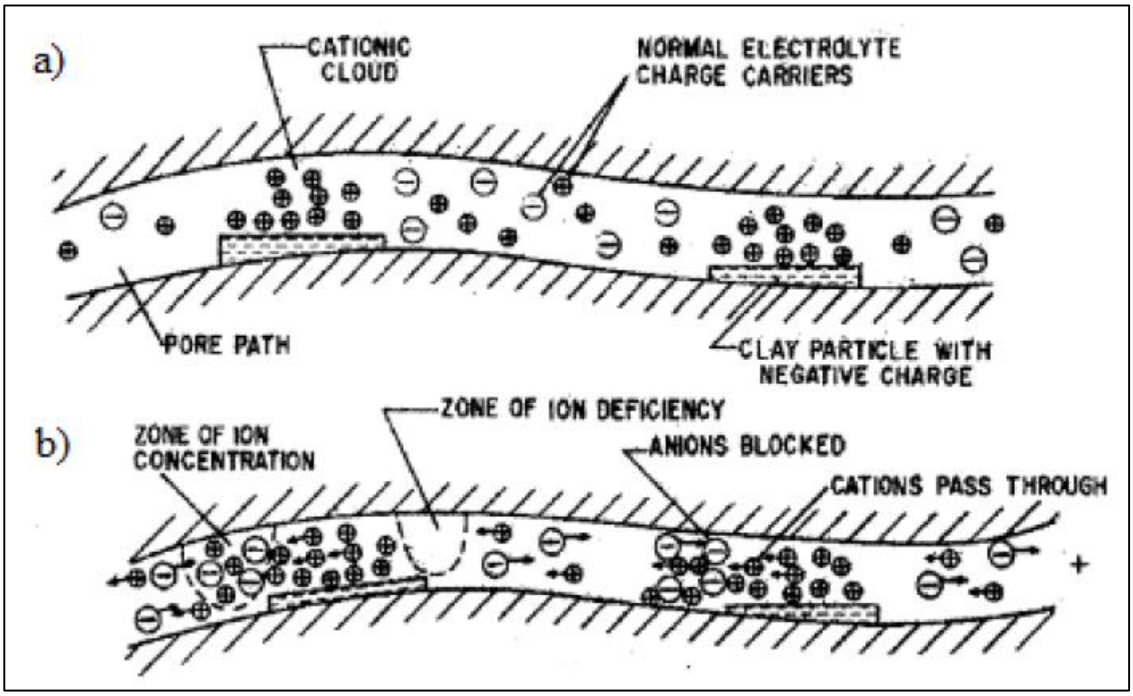

Figure 3.4 Schematic of membrane polarization.

a) Before application of an electrical current. Cationic clouds, related to clays, acts as electronegative membranes between sand grains. b) During application of an electrical current membrane zones locally enhance the transport of cations relative to anions, which give rise to local charge concentration gradients. The following redistribution of the ions to an equilibrium position when the current is shut off, will give an induced polarization response. Figure from Slater and Sandberg (2000).

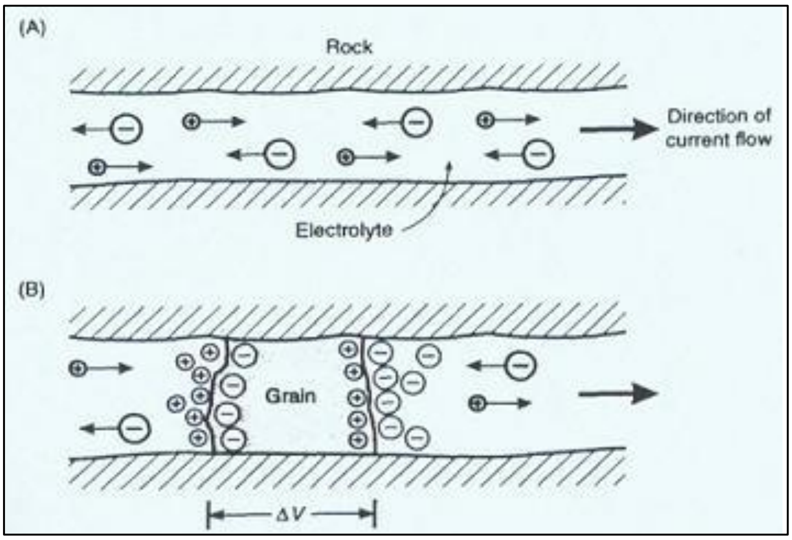

Figure 3.5 Schematic of electrode polarization effect (Slater and Sandberg, 2000).

(b) Electrode polarization

Electrode polarization is attributed to metal containing soils, where metallic minerals form a continuous conduction path (Figure 3.5), so the current conduction changes from ionic to metallic at the mineral grain – electrolyte surface. According to Slater et al, there are two mechanisms attributing to the polarization seen in metal containing soils; The first mechanism is an accumulation of inactive charge excess or deficits near the metal grain surface, due to flow of inactive ions in the diffuse layer of the electrical double layer. The flow of inactive ions is similar to the ion movement in the electrical double layer seen in non-metallic containing soils.

The second mechanism is caused by a minor concentration of redox active metal ions solution, which engages in electrochemical reactions, so charge-transfer reactions across the metal mineral grain – electrolyte surface occurs.

3.4 Methodology

When current is injected into the ground through the electrodes, the current will not reach its stationary value instantaneously, but rises from zero to a steady value. Likewise, the voltage will not disappear immediately after the current is shut off, but instead slowly decay over a time interval until it reaches a steady level. This is caused by the induced polarization effect and the magnitude of the induced polarization effect can be expressed in terms of the apparent chargeability. Chargeability is measured over a specific time interval shortly after the polarizing current is cut off. The apparent chargeability M in mV/V, can in the time domain be calculated as:

$$M = \frac{\int_{t1}^{t2} V_s dt}{V_{dc}} \frac{1}{\Delta t} \tag{4}$$

Where V_{dc} is the direct current voltage (also denoted the primary voltage) measured at a given time during application of the current and is used for calculating the resistivity. V_s is the secondary voltage integrated over a time interval delta t, defined between times t1 and t2 after the current is shut off as shown in Figure 3.6.

The relaxation time is the time taken by the voltage decays to reach a steady level and is characterized by the time constant denoted by Δt. The voltage decay is typically referred to as the induced polarization decay curve, and stems from a time varying potential originating from internal currents at the grain-fluid interface of polarisable materials. The internal currents originate from local charge gradients reaching equilibrium after the applied current is shut off.

Time-domain IP measurements involve the monitoring of the decaying voltage after the current is switched off. The most commonly measured parameter is the *chargeability M*, defined as the area A beneath the decay curve over a certain time interval (t_1–t_2) normalized by the steady-state potential difference. Chargeability is measured over a specific time interval shortly after the polarizing current is cut off.

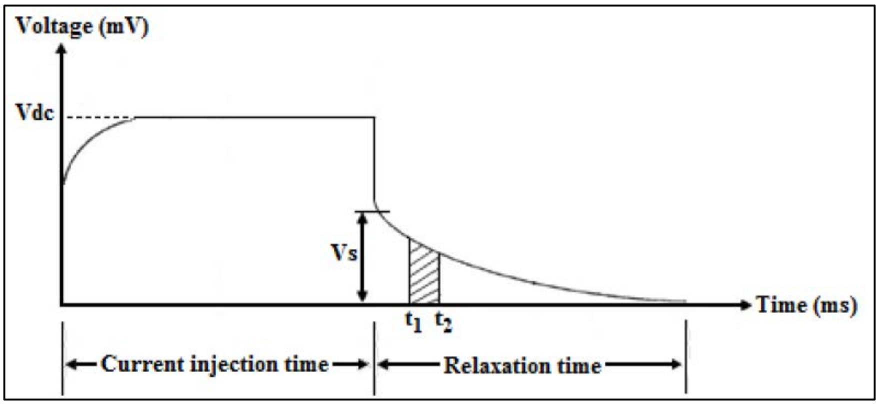

Figure 3.6 Schematics of the induced polarisation phenomena

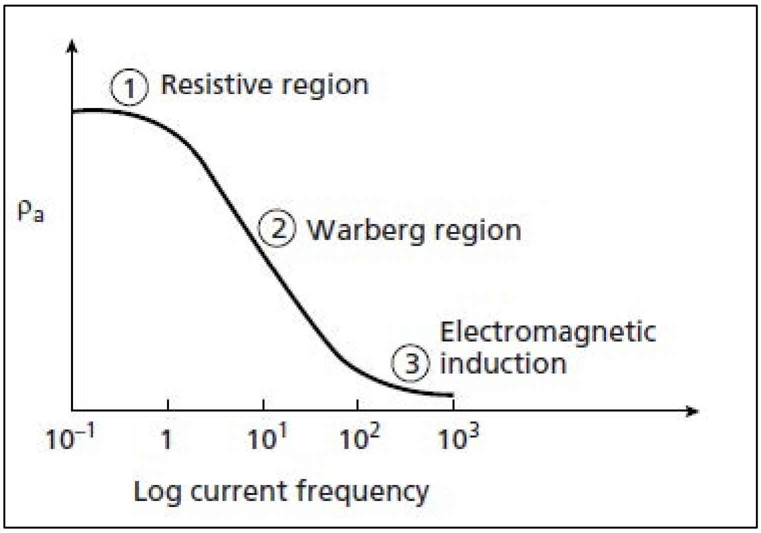

Figure 3.7 Plot of apparent resistivity and log current frequency

Frequency-domain techniques involve the measurement of apparent resistivity at two or more AC frequencies. Three distinct regions are apparent: region 1 is in low frequencies, where resistivity is independent of frequency; region 2 is the Warberg region where resistivity is a linear function of log frequency; region 3 is the region of electromagnetic induction where current flow is by induction rather than simple conduction. Since the relationship illustrated in Figure 3.7 varies with rock type and mineral concentration, IP measurements are usually made at frequencies at, or below, 10Hz to remain in the non-inductive regions. Two measurements are commonly made. The percentage frequency effect (PFE) is defined as

$$PFE = 100 \frac{(\rho_{a2} - \rho_{a1})}{\rho_{a2}} \quad (5)$$

Where ρ_{a1} and ρ_{a2} are apparent resistivity at measuring two frequencies.

ρ_{a1} - Resistivity at higher frequency.

ρ_{a2} - Resistivity at lower frequency.

The *metal factor* (MF) is defined as

$$MF = 2\pi 10^5 \frac{(\rho_{a2} - \rho_{a1})}{\rho_{a1}\rho_{a2}} \quad (6)$$

This factor normalizes the PFE with respect to the lower frequency resistivity and consequently removes, to a certain extent, the variation of the IP effect with the effective resistivity of the host rock.

3.5 Application of IP in Uranium Exploration:-

Uranium is mobile when it is in oxidized state (U^{+6}) and it gets deposited when it is reduced to U^{+4}state with the help of some ligands which creates the reducing environment. Sulphide is one of the ligand. So, finding of disseminated sulphide is an indirect clue for Uranium deposition. So, induced polarization method is a direct method for sulphide mineralization and an indirect method for uranium exploration.

3.6 Induced Polarisation survey in Bhima Basin:

Geophysical methods are more useful if a target of interest has a physical contrast with the surrounding rocks. Resistivity and Induced Polarization (IP) method is one of the important geophysical methods which measures the resistivity and chargeability of the earth subsurface. This method can be effectively utilized in mapping the basement-sediment contact and structural features like shear zones, faults and fractures (Telford et al., 1990). In uranium exploration, the Induced polarisation method is employed to map the zones rich in disseminated sulphides which may act as a reducing agents for the precipitation of uranium mineralisation (Dahlkamp, 1993).

Significant uranium deposit is known to occur at Gogi area, with the faulted contact of Bhima sediments with basement granitoids (Achar et al., 1997). The known mineralized zones are distributed mainly along the east-west trending Gogi-Kurlagere fault/shear and NE trending, cross-cutting faults and occur pre-dominantly in limestone and fractured granitoids (Dhana Raju et al., 2002). The mineralisation is intimately associated with sulphides, mainly pyrite, chalcopyrite, marcasite, aresenopyrite and galena. Association of uranium mineralisation with these metallic minerals along the faulted zone assumes the greater importance for locating the target areas using radioactive, magnetic, electromagnetic, resistivity and Induced Polarization (IP) methods (Dash et al., 2003). Heliborne geophysical surveys conducted over parts of the Bhima basin have revealed several target areas and electromagnetic (EM) conductors, vis-à-vis Uranium mineralisation (Chaturvedi, 2011). The uranium mineralization in Bhima basin does not produce a discernable EM or magnetic response, possibly due to cultural interference and the screening effect of more than one conductive shale formation, therefore the target areas with geological setting similar to Gogi, should be screened with Induced polarization method, prior to drilling (Geotech report for AMD, 2009). Subsequently, resistivity and Induced Polarisation (IP) method were conducted over one of the target areas at Hulkal east of Gogi-Kurlagere fault zone to understand the inferred EM conductor which is interpreted from the heliborne data and to delineate any structural features within the Bhima basin if any.

The present study addresses the delineation of the structural features near Hulkal area in Bhima basin by using IP/Resistivity method. Forward modeling is done by using RES2DMOD (Loke, 2004) and inversion is done by RES2DINV to understand the response from different formations present in the survey area.

Types of arrays

The choice of the best array for a field survey depends on the (i) type of structure to be mapped, (ii) the sensitivity of the resistivity meter and (iii) the background noise level (Loke, 2001). There are different types arrays that are used for electrical resistivity measurements surveys for profiling and sounding. Wenner, Dipole-dipole, Schlumberger, Pole-pole and Pole-dipole. The mean characteristic of an array that should be considered is its sensitivity to the vertical and horizontal changes in the subsurface resistivity, the depth of investigations, the horizontal data coverage and the signal strength. (Loke, 2001)

The typical methodology in conducting resistivity investigation begins by some pre-modeling to determine the type of array to be selected and electrode spacing. Choosing the type of array in investigations is not only an important factor to ensure success, it also determines the efficiency of the investigation. In resistivity profiling investigations, cables and electrodes are moved long distances and therefore the arrays chosen will be those which make movement simple and rapid as possible as well as efficient in delineating targets (Loke, 2001). The details of the arrays is given below briefly.

a. Wenner array: It is used for both resistivity profiling and depth sounding. This is a robust array that was popularized by the pioneering work carried out by the University of Birmingham research group (Griffiths and Turnbull 1985; Griffiths, Turnbull and Olayanka, 1990; Loke 2001). Early 2-D multi-electrode electrical resistivity surveys were carried out with this array (Loke, 2001).

The array is relatively sensitive to vertical changes in the subsurface resistivity below the centre of the array and less sensitive to horizontal changes in the subsurface resistivity. The array is best used for horizontal structures, but is relatively poor in detecting narrow vertical structures. The Wenner array has large signal strength.

This array is popular and widely used in ground water investigations. The arrays also require much smaller data than the others to construct a pseudo section (Barker, Rao and Thangarajan, 2001). However, all four electrodes are moved making more time consuming for sounding, whereas in profiling it is similar to Schlumberger. In this array near-surface conditions differ at all four electrodes for each reading, giving a rather high noise level. A disadvantage of this array for 2-D multi-electrode electrical resistivity survey is the relatively poor horizontal coverage as the electrode spacing is increased. This problem is normally observed in a system with relatively small number of electrodes.

b. Schlumberger array: This array is the most commonly used because of it speed in operation and convenience where only two electrodes are moved. The large availability of interpretation techniques for the Schlumberger array also makes it attractive for depth sounding. Site selection for sounding point is extremely important with the Schlumberger array because it is sensitive to conditions around the closely spaced inner electrodes.

c. Wenner-Schlumberger array: It is moderately sensitive to both horizontal and vertical structures. This array is a hybrid between Wenner-Schlumberger array (Pazdirck and Blaha, 1996 in Loke, 2001) arising out of a relatively recent work with electrical imagine surveys (Loke, 2001). This array is moderately sensitive to both horizontal and vertical structures. In arrears where both types of geological structures are expected this array may be a good compromise between the Wenner and the Dipole-dipole array. The signal strength of this array is smaller than that of the Wenner array but it is higher than that of the Dipole-dipole array. The median depth of investigation for this array is larger than that for the Wenner array for the same distance between the outer electrodes. The Wenner-Schlumberger array has a slightly better coverage compared with the Wenner array. The horizontal data coverage is slightly wider than the Wenner array but narrower than that obtained with the Dipole-dipole array.

d. Dipole-dipole array: It is suitable for vertical structures, vertical discontinuities and cavities, but less for identifying horizontal structures. The array is most sensitive to resistivity changes between the electrodes in each dipole pair. That means it is good in mapping vertical structures such as dykes and cavities but relatively poor in mapping horizontal structures such as sills or sedimentary layers. The depth of investigation is smaller than for the Wenner array. The array is mainly used in IP work where induction effects must be avoided at all costs; however it is also effective in resistivity profiling. It uses four moving electrodes and it is therefore less desirable and the observed voltages tend to be rather small. The array can also be used effectively for resistivity depth sounding.

To use this array effectively, the resistivity meter should have comparatively high sensitivity and very good noise rejection circuiting and a good contact between the electrodes and the ground is necessary.

e. Polar-dipole array: is asymmetrical and results in asymmetrical apparent resistivity anomalies in the pseudo section for surveys over symmetrical structures. This effect can be removed by repeating the measurements with the electrodes reversed. It has a higher signal strength compared with the dipole-dipole array. The array is not as sensitive to noise as the pole-pole array because the distance between the potential electrodes is not as large. The signal strength is lower compared with the Wenner and Wenner-Schlumberger arrays but higher than the Dipole-dipole array. The asymmetrical anomalies produced by this array is more difficult to interpret than those produced by symmetrical arrays.

A major problem with this array is that peaks are displaced from the centres of conductive bodies and there is no real agreement as to where the results should be plotted.

f. Pole-pole array: It is not as commonly used as the others arrays. In practice the ideal Pole-pole array with only one current and one potential electrode does not exist. To approximate the pole-pole array, the second current and potential electrodes must be placed at distances, which is more than 20 times the maximum separation between the first current and potential (C1P1) electrodes used in the survey.

In surveys where the electrode spacing along the line is more than a few meters there might be practical problems in finding suitable locations for the second current and potential (C2P2) electrodes to satisfy this requirement.

A disadvantage of this array is that because of the large distance between (P1P2) electrodes, it can pick up a large amount of telluric noise which can severely degrade the quality of the measurements and so it is mainly used in surveys where relatively small electrode spacing (less than 10 m) are used. This array has the widest horizontal coverage and the deepest depth of investigations.

Comparison

A summary of the various arrays and their effective use are illustrated below after (Loke, 2001) are as follows;

- If the survey is in a noisy area and a good vertical resolution is required with a limited survey the Werner array will be the best option.

- When a good horizontal resolution and data coverage is important with a resistivity meter sufficiently sensitive with a good ground contact, the dipole- dipole array will be the preferred choice.
- If there is uncertainty whether both reasonably good horizontal and vertical resolution are required, the Wenner-Schlumberger array with overlapping data levels is the best option.
- Survey with a system with a limited number of electrodes the Pole-dipole array with measurements in both the forward and reverse directions might be a viable choice.
- For surveys with small electrode spacing and where good horizontal coverage is required, the Pole-pole array might be a suitable choice.

2D Modelling:

Modeling is a very useful tool in applied geophysics for comparing the resolution power of different dc resistivity electrode arrays. Classical arrays, such as pole–pole, Wenner, and dipole–dipole, are frequently employed in 2D or 3D resistivity imaging applications (Dahlin., 1996 and Storz et al., 2000). The 2D resistivity model of the Gogi-Kurlagere fault and the Bhima basin was simulated in RES2DMOD software (Loke., 2004) after studying the local geology.

Method for selection of resistivity array using RES2DMOD

RES2DMOD is a 2D forward modelling program that calculates the apparent resistivity pseudo section for a user defined 2D subsurface model. The arrays supported by this program are the Wenner (Alpha, Beta and Gamma configurations), pole-pole, gradient, inline dipole-dipole, pole-dipole and equatorial dipole-dipole (Edwards., 1977). This program helps in choosing the "best" array for a particular survey area after carefully balancing such factors as the cost, depth of investigation (or equivalent depth), resolution and practicality

The 2-D model used by the finite-difference or finite-element method divides the subsurface into a number of blocks using a rectangular mesh (Figure 3.8). Some improvements were made to the (Dey., Morrison., 1979) finite-difference formulation to improve the accuracy of the calculated apparent resistivity values (Loke., 1994). The finite-difference method basically determines the potential at the nodes of the rectangular mesh that consists of N nodes in the horizontal direction and M nodes in the vertical direction. The grid model has L-1 columns and M-1 rows of rectangular blocks. The blocks can have different resistivity values. By using a sufficiently fine mesh, complex geological structures can be modelled.

The synthetic apparent resistivity pseudo section data for different array system with 24 electrodes and 50m unit electrode spacing were calculated for 2D resistivity Gogi-Kurlagere fault model in RES2DMOD software (Figure 3.9). In wenner array the fault response was not significant while the pole-pole array and dipole-dipole array give a better response of fault, but the resolution of the dipole-dipole array is much better than the pole-pole array. So, dipole-dipole array system was selected to carry out the IP/Resistivity survey in the study area.

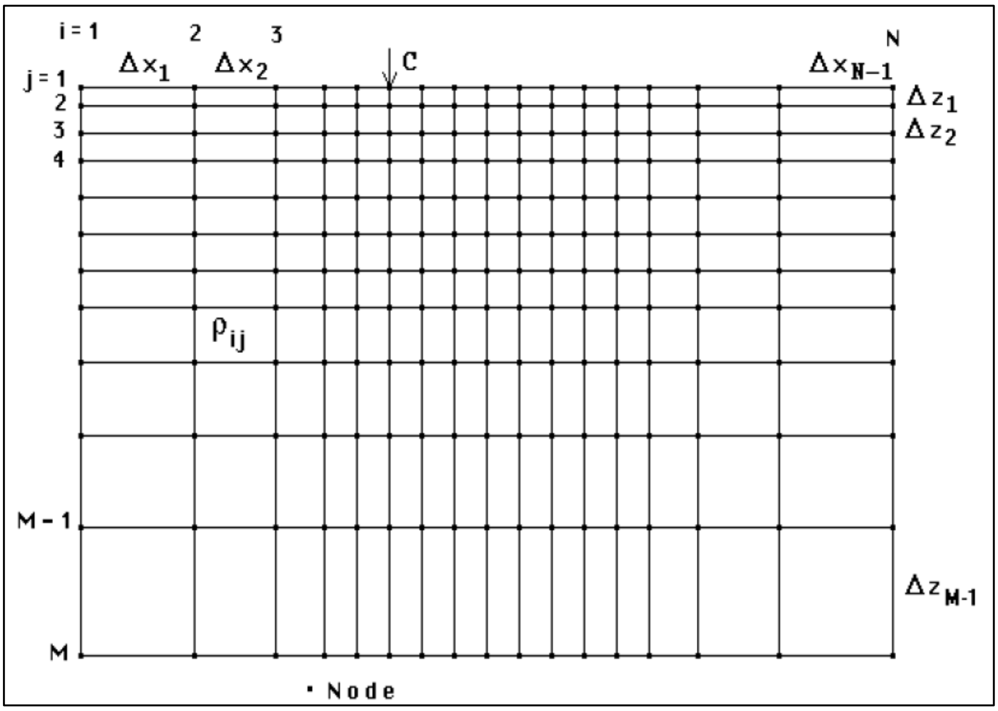

Figure 3.8 The finite-difference or finite-element mesh used by the RES2DMOD.

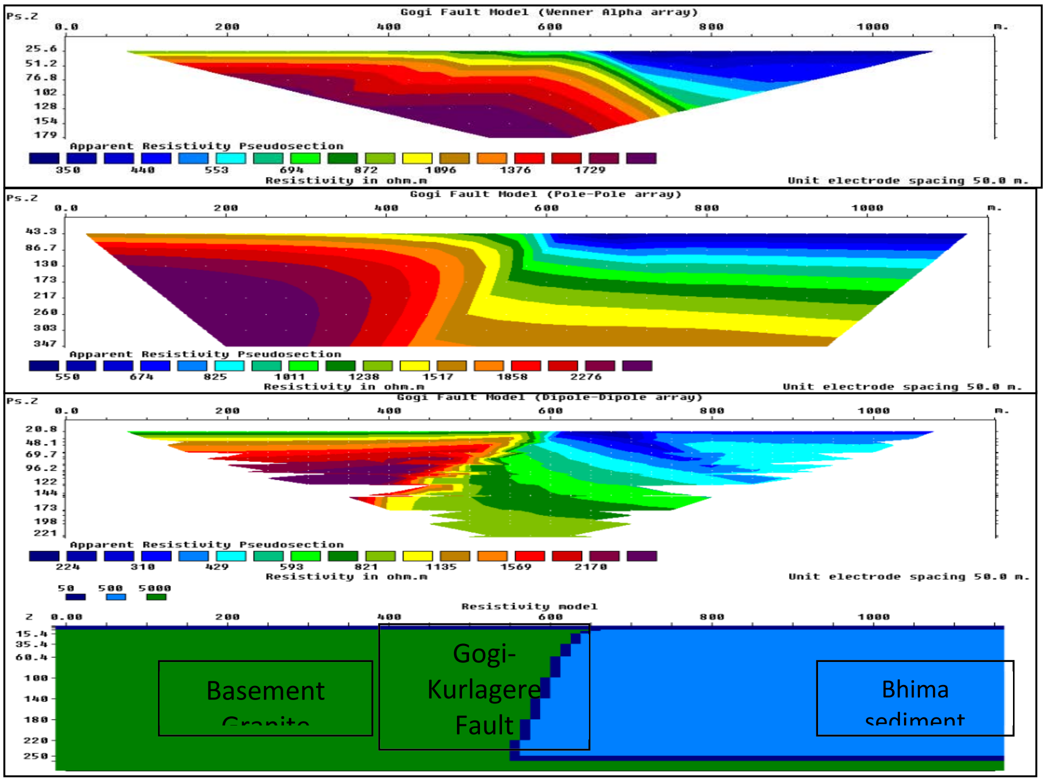

Figure 3.9 2D Resistvity modelling of Gogi-Kulagere fault in Bhima Basin.

3.7 Data Acquisition:

A survey block having dimension of 2500m N-S and 1100m E-W was designed in Hulkal area. Data was acquired in N-S direction at every 50 m station interval along 6 traverses separated by 200 m using dipole-dipole array having a dipole length of 150 m and a dipole separation of 150 m. High power and reliable constant current are the primary requirements for the transmitter, so a power generator of 14.4HP was utilised for injecting current into the ground. Time domain IP equipment comprising of IRIS VIP 5000 transmitter (Figure 3.10) powered by 5000 watt.

Current is usually injected as a 50% duty cycle reversing square wave; in this instrument the current is on for two seconds and off for two seconds. During on-time the current values are recorded from the transmitter and the resistivity values are recorded from IRIS ELEREC PRO-10 receiver. The chargeability values are recorded during the off-time by the same receiver.

Figure 3.10 IRIS IP Instrument (Left: VIP 5000 Transmitter, Right: IRIS ELEREC PRO-10 Receiver)

3.8 Data presentation:

Apparent resistivity and chargeability observations were gathered in the field along six profiles in the form of pseudo sections to understand the depth persistence of the structural features and different lithological units present there. To find out the true resistivity and chargeability distribution in the subsurface, pseudo-section data sets (resistivity and chargeability) have been inverted using RES2DINV software.

After applying the inversion, true resistivity and chargeability maps of the study area for each level with corresponding depths were prepared using Oasis Montaj software (Geosoft). It was observed that the subsurface fracture zone was very well delineated at the depth of 192 m. Hence, inverted resistivity and chargeability data of this depth level (n=5) with dipole length of 750 m and unit electrode spacing of 50 m was sliced.

3.9 Theoretical background of inversion:

The raw data from induced polarization survey is processed using RES2DINV software (Loke., 2015). The models of resistivity and chargeability values are applied with the smoothness-constrained inversion (de Groot-Hedlin and Constable 1990, Sasaki 1992). The smoothness-constrained least-squares method is based on the following equation (1)

$$(J^T J + u F)\, d = J^T g \qquad (7)$$

Where $F = f_X f_X^T + f_Z f_Z^T$

f_X = horizontal flatness filter , f_Z = vertical flatness filter, J = matrix of partial derivatives

u = damping factor, d = model perturbation vector and g = discrepancy vector

This program provides editing options to remove noisy or unwanted data points before inverting the 2D apparent resistivity data. The RES2DINV two-dimensional inversion software computes the best fit 2D electrical model of the subsurface to the apparent resistivity data using an iterative process for a given trial. Each trial allows the user to remove a certain amount of noisy data from the resistivity and/or chargeability data. The root mean square (RMS) error is computed after each iteration and the iterations continues until the maximum number of iterations selected is reached or the RMS error is less than the value set by the user. Once the best fit resistivity model has been computed, the inversion of the apparent IP data is carried out to produce a best fit two-dimensional IP model of the subsurface.

3.10 Results and Interpretation

A. The Resistivity map

IP/Resistivity pseudo-section profiles are plotted on geological map of the area and shown in Figure 3.11. Along these lines IP/Resistivity data has been observed. The resistivity map of the study area (Figure 3.12) at different levels have revealed the wide variation in resistivity values ranging from 20 Ωm to 9602 Ωm for different lithological formations. Four formations are differentiated based on the interpretation of the resistivity map. Resistivity values of the formations are classified in table 3.

Table 3: Lithological formation and their corresponding resistivity values

SI. No.	Geological formation	Resistivity in ohm-m
1	Basement Granite	400 Ωm - 800 Ωm
2	Limestone	100Ωm - 300 Ωm
3	Arenite	200 Ωm -400 Ωm
4	Purple shale	50 Ωm - 100 Ωm

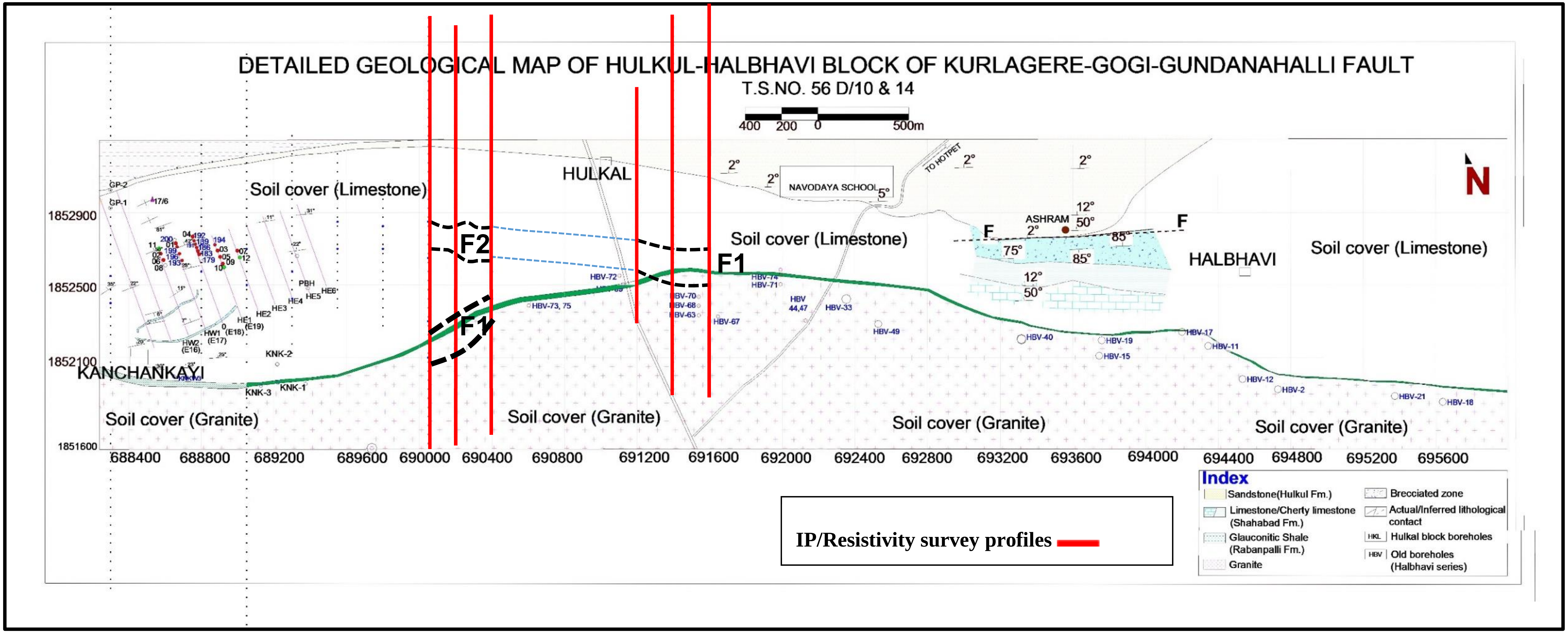

Figure 3.11 Layout of IP/Resistivity Survey, Hulkal area

Apparent resistivity values at different levels (n= 1, 2, 3, 4, 5, 6,) is observed. Inversion of this data gives true resistivity values at different depths shown in figure 3.12.

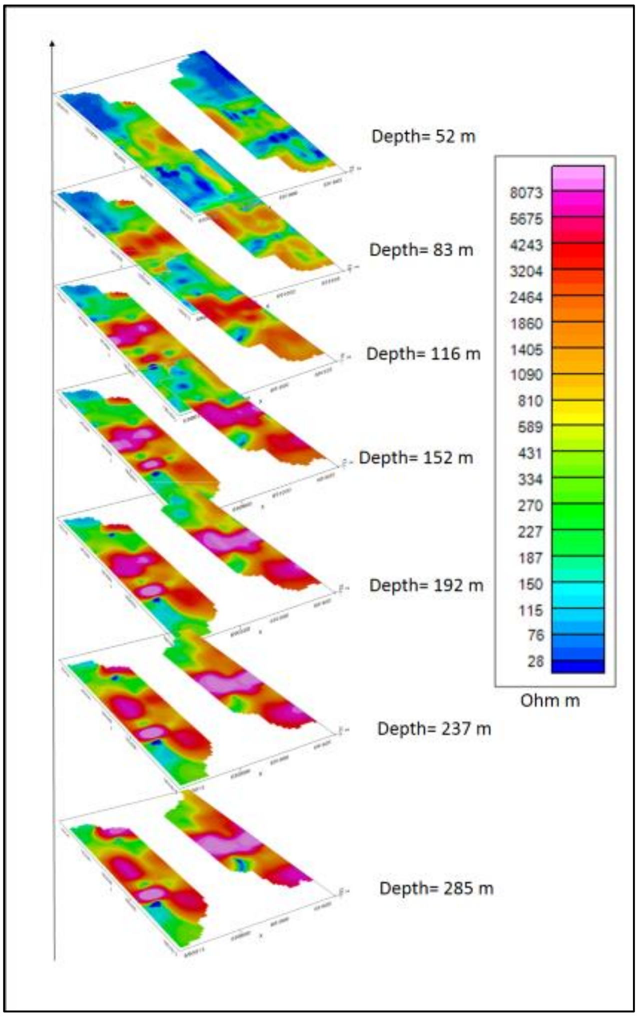

Figure 3.12 True resistivity map of the Hulkal area at different depths

Resistivity maps at the depth 0f 192 m (Figure no. 3.13) clearly shows the low resistivity zone which is interpreted as fracture zone. Therefore resistivity map of this depth is chosen for further analysis. Data is missing in the area, because of lockdown it can't be observed, so interpolation is done to cover the area and an interpolated map of true resistivity data is shown in (Figure 3.14). Based on the gradient in the resistivity map (Figure no. 3.14), a linear E-W trending low resistive zone (90 to 2000 Ωm) is demarcated at the depth of 192 m.

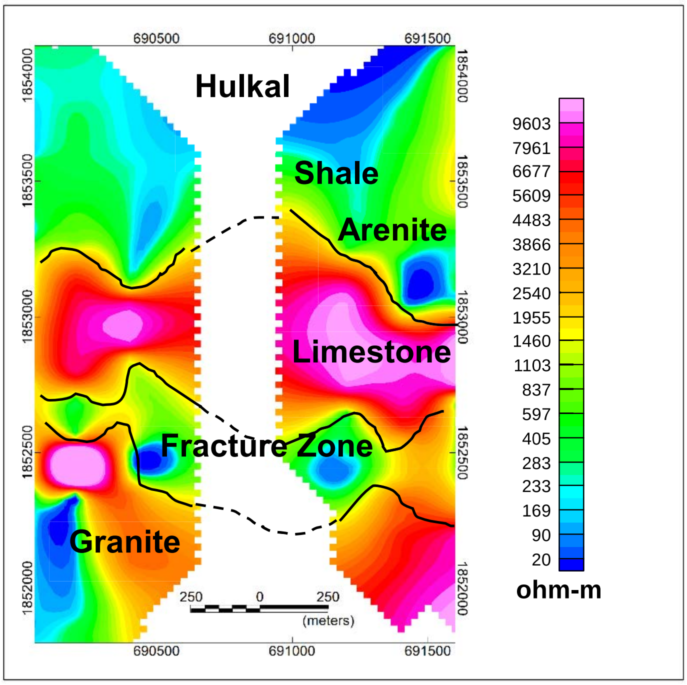

Figure 3.13 Resistivity map at depth of 192 m of the Hulkal area

In the western most part low resistivity zone is attributed to fracture within the sediments (i.e. limestone) and in the eastern most part same is attributed to fractured contact between granite and limestone i.e. Gogi-Kurlagere fault.

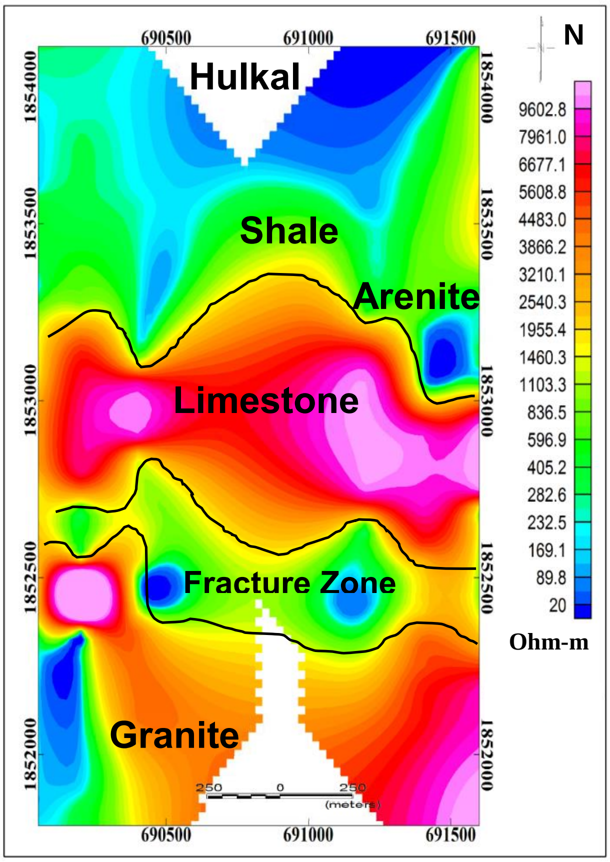

Figure3.14 Interpolated resistivity map of the Hulkal area

So it can be inferred that as we move from west to east, fault within the sediment is trending toward the faulted basement-sediment contact. The arenite as the small patch, with moderate resistivity value (350 Ωm) in the eastern part and purple shale (50-100 Ωm) in the northern most part of the study area were observed. Resistivity amplitude of the identified fracture zones are of similar nature as noticed in mineralised zone of Kanchankayi.

B. The Chargeability map

After the inversion of apparent chargeability data true chargeability data is observed at different depths shown in (figure 3.15), here the chargeability map (figure no. 3.16) of study area at the depth of 192 m shows variation in chargeability amplitude from 3.2 mV/V to 10.3 mV/V. Data is missing in between the study area because of the pandemic. Therefore an interpolated map of true chargeability, shown in (figure 3.17) is prepared which shows high chargeability vales in the western part within the sediments and in the eastern part shifted towards faulted basement-sediment contact i.e. K-G fault. From the chargeability map shown in (figure 3.17), it was inferred that, the southern most part has low chargeability within undisturbed basement granite. North of this a high chargeability (5.8 mV/V - 9.6 mV/V) was observed along fractured part of limestone. Most of the high chargeability values are concentrated towards the massive limestone. Chargeability maps of different depth same as resistivity maps, are analyzed and it is found that high chargeability variation is well correlated with the low resistivity variation at the depth of 192 m.

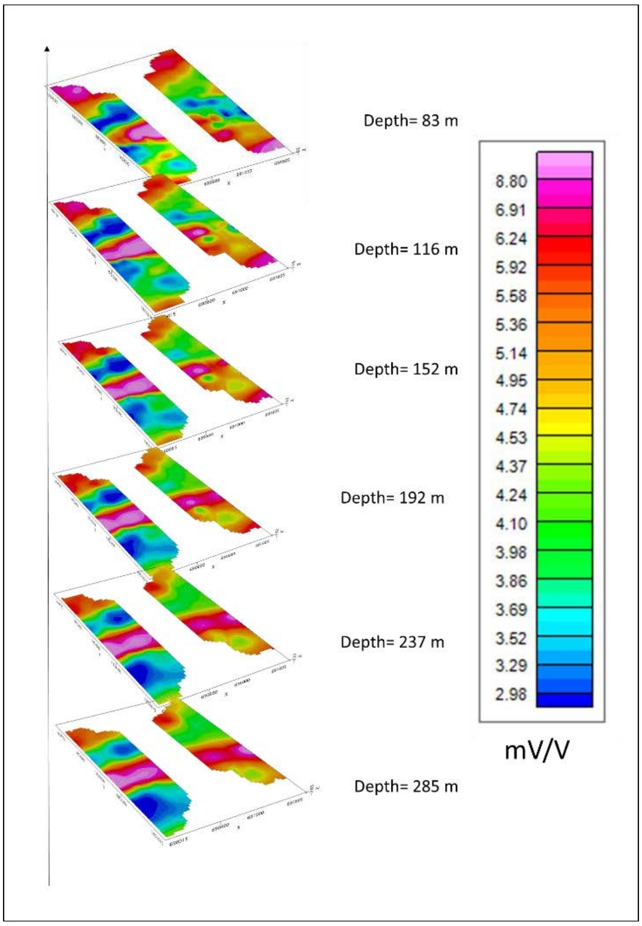

Figure 3.15 Chargeability maps at different depths of Hulkal area

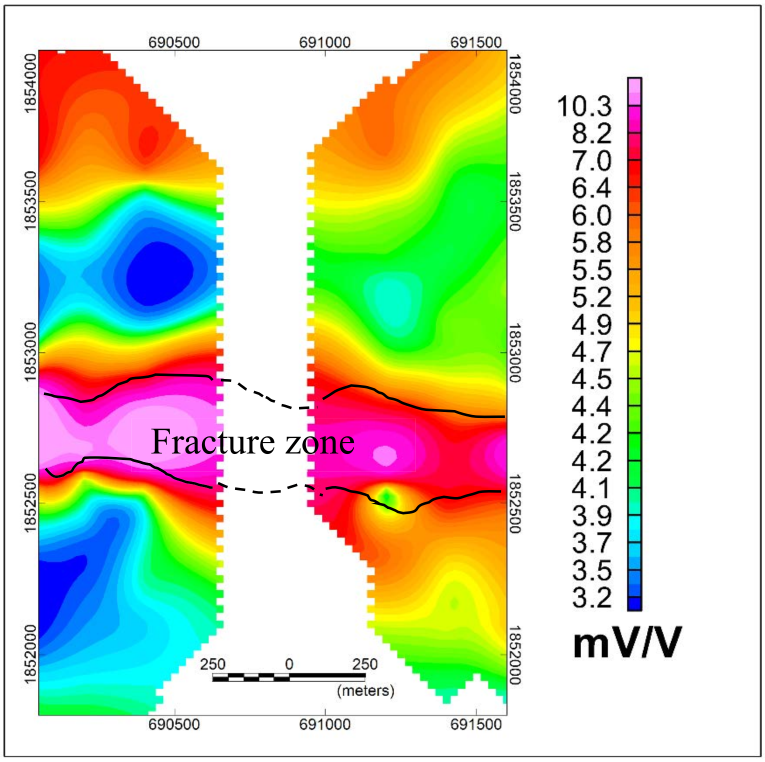

Figure 3.16 Chargeability map at 192 m depth of Hulkal area

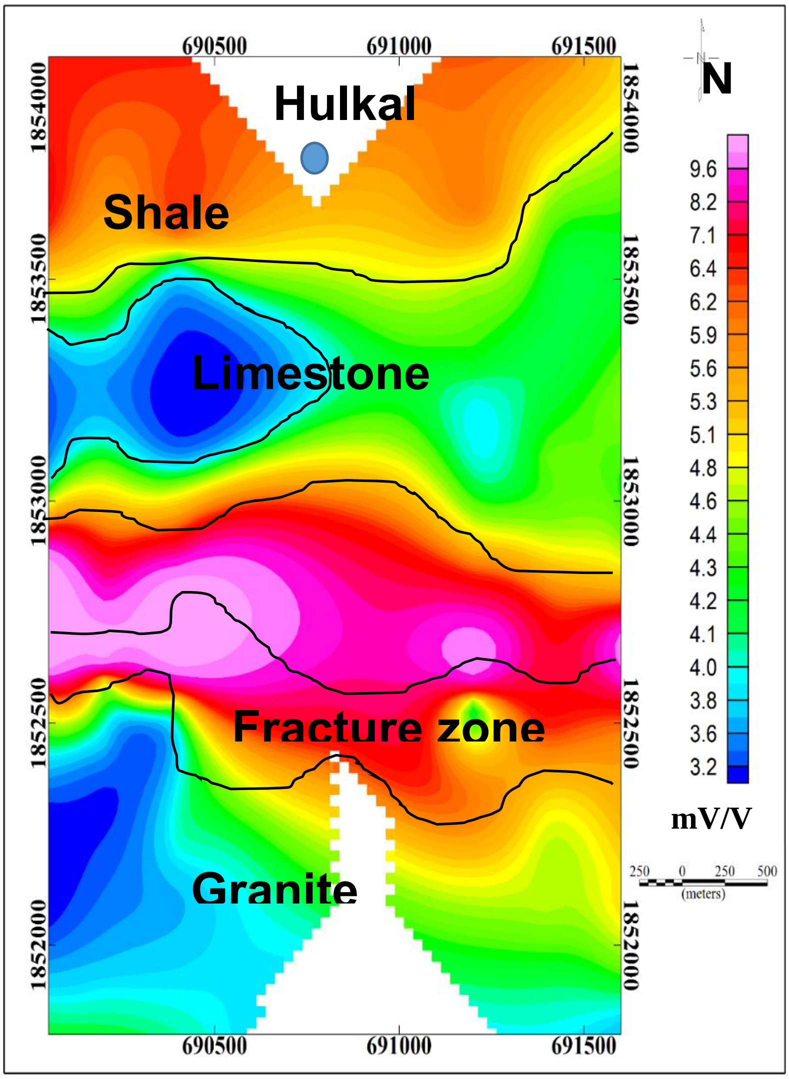

Figure 3.17 Interpolated Chargeability map at 192 m depth of Hulkal area

C. The Inverted Resistivity and Chargeability pseudo-section model using RES2DINV

In the continuation of Kanchankayi exploration block, total 6 IP/Resistivity pseudo-sections were conducted over an area of 3.5 sq km in the eastern and western part of Hulkal village, along Gogi-Kurlagere fault. To study the subsurface in detail, data was acquired following the grid of 200m x 50m in N-S profile direction. Average length of pseudo-section profile is about 1.3km. In order to investigate the depth wise information, IP/Resistivity data at different depth levels is collected using dipole-dipole array with different dipole separation (a=150, n=1, 2, 3, 4, 5 & 6). This data is plotted as pseudo depth section and is inverted to obtain the true resistivity and chargeability depth model of the subsurface.

Inverted depth section along the line- 690050

Total 2.4 line km covered along this line. The inverted depth section has given the subsurface information up to 312m depth along this traverse (Figure 3.14). Resistivity values are ranging from 19ohm-m to 6500ohm-m. Toward southern part, a broad zone (F1) of about 300m width, with very low resistivity (60 – 150 ohm-m) is noticed. Resistivity values indicates the intense deformation in this part and demarcated as faulted basement-sediment contact i.e. K-G fault zone. Low resistivity (< 50 ohm-m) up to the depth of 60m in upper layer is due to the overburden effect. Further north of faulted contact very high resistivity (> 3000 Ohm-m) is attributed to the massive limestone. In the central portion between two massive limestone bodies, low resistivity (Zone F2) (600-3000 Ohm-m) has been recorded and interpreted as fracture with in limestone. In this zone (F2) resistivity is low in upper part and increased at deeper level. The increase in resistivity in the deeper part is because of the chertification with in fractured limestone. Towards northern part of pseudo-section very low resistivity zone (10-100 Ohm-m) in the shallow portion up to the depth of ~100m is the response from shale formation whereas the moderate to high resistivity (300–700 ohm-m) below the shale is attributed to the limestone.

Chargeability along the line is ranging from 1mV/V to 16mV/V. Low chargeability values (< 3mV/V)) have been recorded along faulted basement-sediment contact and devoid of any metallic minerals like sulphides. Highest chargeability pocket (> 15 mV/V) (Zone C) has been recorded at deeper level with in fractured part of limestone. This high chargeability is due to presence of sulphide minerals. Moderate resistivity associated with very high chargeability with in fractured limestone is the potential target for uranium mineralization as in Kanchankayi area mineralisation intercepted with in fractured limestone.

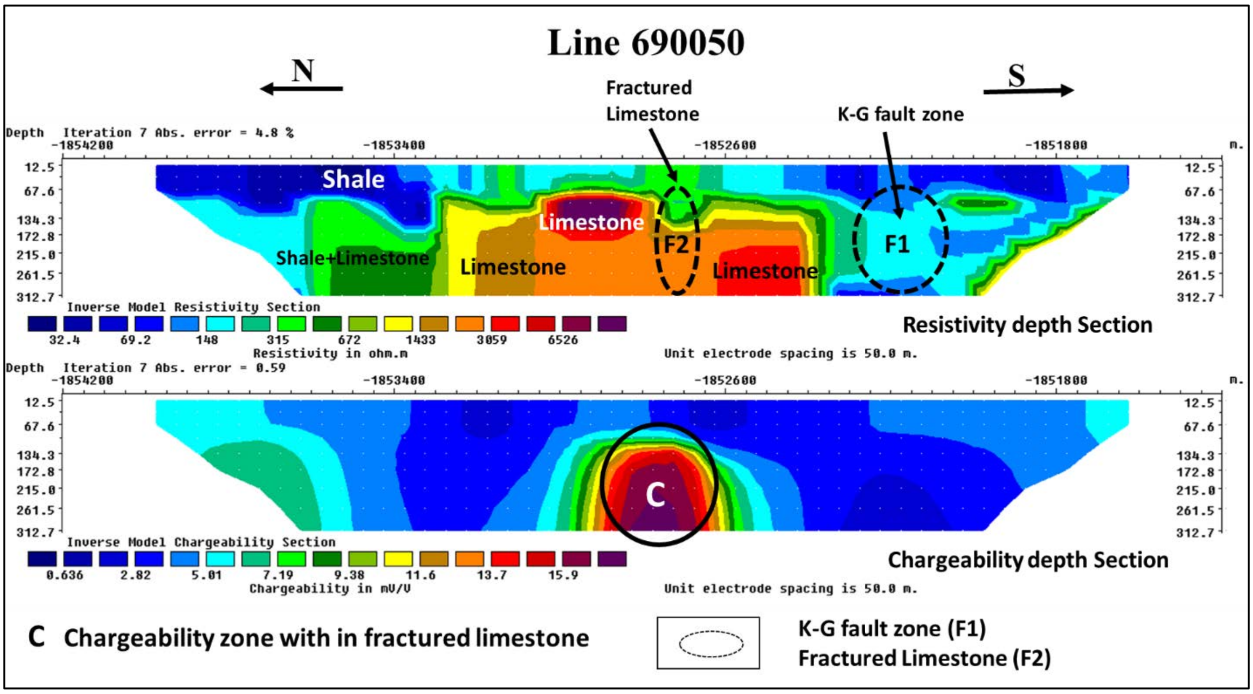

Figure 3.18 Inverted Resistivity and Chargeability depth section along traverse no. 690050, Hulkal area

Inverted depth section along the line- 690200

Resistivity values are ranging from 19ohm-m to 6500ohm-m. Toward southern part, a broad zone (F1) of about 300m width, with very low resistivity (60 – 150 ohm-m) is noticed. Resistivity values indicates the intense deformation in this part and demarcated as faulted basement-sediment contact i.e. K-G fault zone. Low resistivity (< 50 ohm-m) up to the depth of 60m in upper layer is due to the overburden effect. Further north of faulted contact very high resistivity (> 3000 Ohm-m) is attributed to the massive limestone. In the central part a very high resistivity zone (>8000 ohm-m) is attributed to massive limestone. Resistivity of limestone is abruptly decreased from 8000ohm-m to 600ohm-m as moving further north. But further adjacent to this low resistivity zone again high resistivity value is observed in limestone.

So between two high resistive parts of limestone, a prominent low resistivity zone has been demarcated with black dotted line (zone F2) and interpreted as fracture with in limestone. It is the eastern side continuation of fracture zone in limestone, which was revealed in previous depth section (line 690050). Towards northern part of depth-section very low resistivity (10-100 Ohm-m) up to the depth of ~100m, is the response from shale formation whereas the moderate to high resistivity (400–700 ohm-m) below the shale is attributed to the limestone.

Chargeability along the line is ranging from 1mV/V to 16mV/V. Within the K-G fault zone chargeability values are less than 3 mV/V, which is lowest along this depth section and clearly indicates the absence of sulphides or any other metallic minerals in this disturbed zone. However high chargeability pocket (> 12 mV/V) is associated with fractured limestone at deeper level. As resistivity data shows that intensity of fracturing with in limestone is high and also associated with high chargeability, therefore it is the potential zone for uranium mineralization.

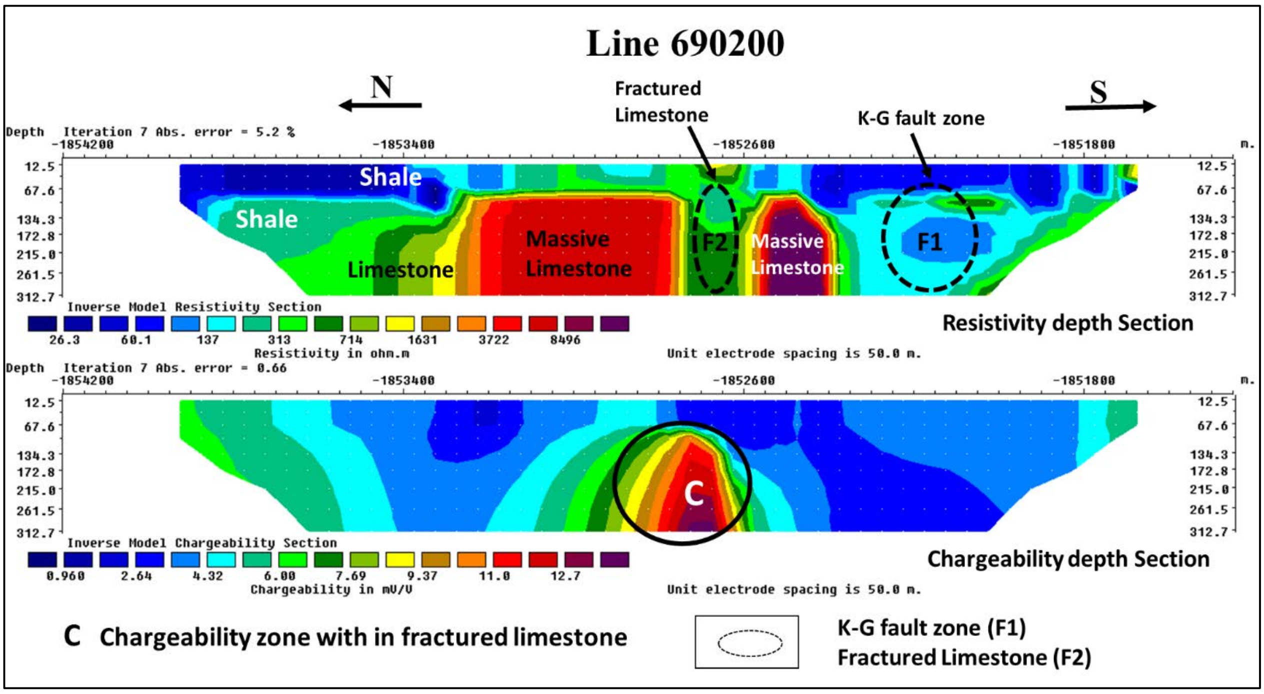

Figure 3.19 Inverted Resistivity and Chargeability depth section along traverse no. 690200, Hulkal area

Inverted depth section along the line- 690400

High resistivity value of range more than 3000 ohm-m in the southern part is the response over basement granite. Further north of this basement granite resistivity values decreased from 3000ohm-m to 600ohm-m and attributed to faulted basemen-sediment contact zone (F1) K-G fault. Close to faulted contact zone low resistivity value (10- 50 ohm-m) at the top is due of fractured granite and high resistivity formation below granite is the response from massive limestone. Here geophysical signature is showing that granite override the limestone, which is the indication of being reveres fault along the basement-sediment contact. Over the limestone itself resistivity is varying from south to north. Between two high resistive parts of limestone a moderate resistivity is noticed. This moderate resistivity is interpreted as fracture with in limestone (zone F2). Chertification of limestone with in fracture zone is mainly responsible for moderate resistivity in this part. Towards northern part very low resistivity (10-50 ohm-m) is observed over shale formation and below this, at deeper level high resistivity is due to limestone.

Chargeability along the line is varying from 1mV/V to 14mV/V. Highest chargeability pocket (> 13 mV/V) has been recorded at deeper level with in fractured part of limestone. This high chargeability is due to presence of sulphide minerals. Association of low resistivity with very high chargeability with in fractured limestone has got importance from uranium mineralization point of view.

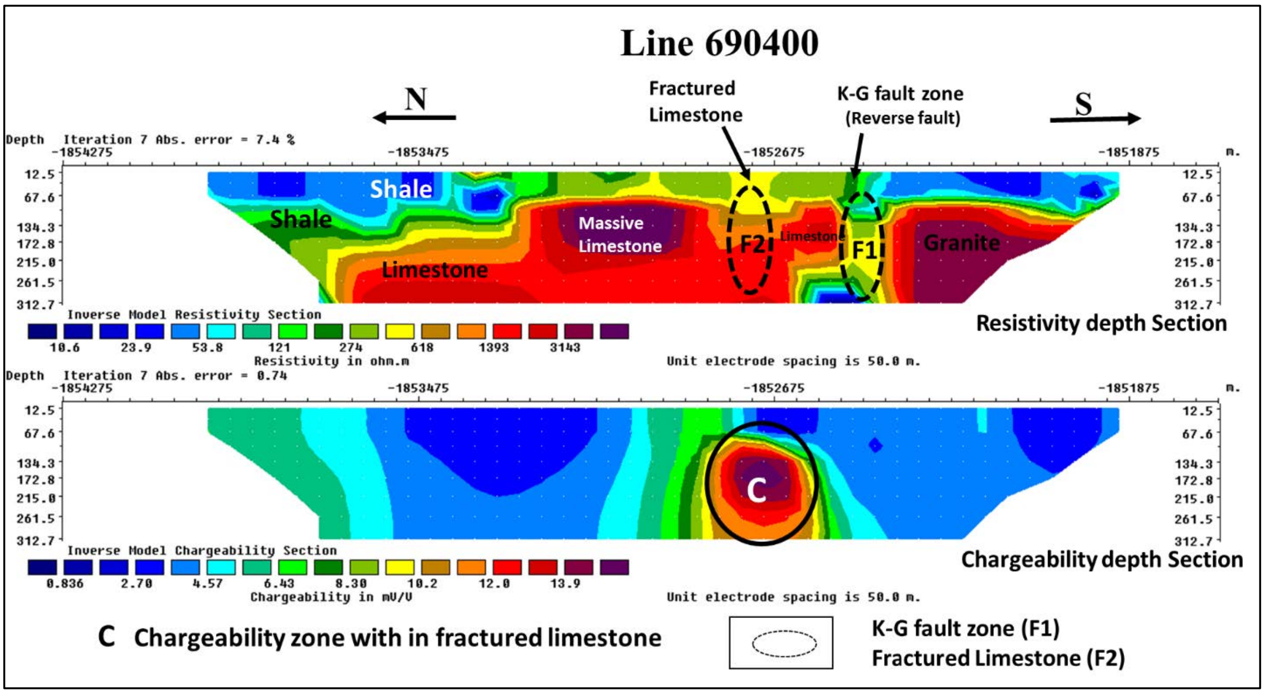

Figure 3.20 Inverted Resistivity and Chargeability depth section along traverse no. 690400, Hulkal area

Inverted depth section along the line- 691200

Length of this inverted section is 1.2 km (Figure 3.17). Resistivity values are varying from 7 ohm-m to 4000 ohm-m. This depth section is located east of Hulkal village. In the extreme south of inverted depth section low resistivity up to the depth of about 130m is the combined effect overburden and fractured granite below. Close to this fractured granite, vertically low resistivity is demarcated. It is interpreted as faulted basement-sediment contact (K-G fault zone (F1)). Further north to this vertical low resistive zone, very high resistivity in bedded form is attributed to massive limestone. From UTM 1853000N to 1853200N, massive limestone is overlain by very low resistive bed (50 ohm-m – 80 ohm-m). This low resistivity layer is due to arenite over there. Below arenite resistivity less than 50 ohm-m is contributed from shale. Resistivity value less than 100 ohm-m in the extreme north is the response over shale. Below shale, limestone presence is showing moderate resistivity.

Chargeability along the line is ranging from (0.5mV/V to 10mV/V). Highest chargeability (8-10mV/V) is recorded with in K-G fault zone. This high chargeability associated with low resistivity along the inferred K-G fault zone is indicating the presence of sulphide and favourable zone for uranium mineralisation.

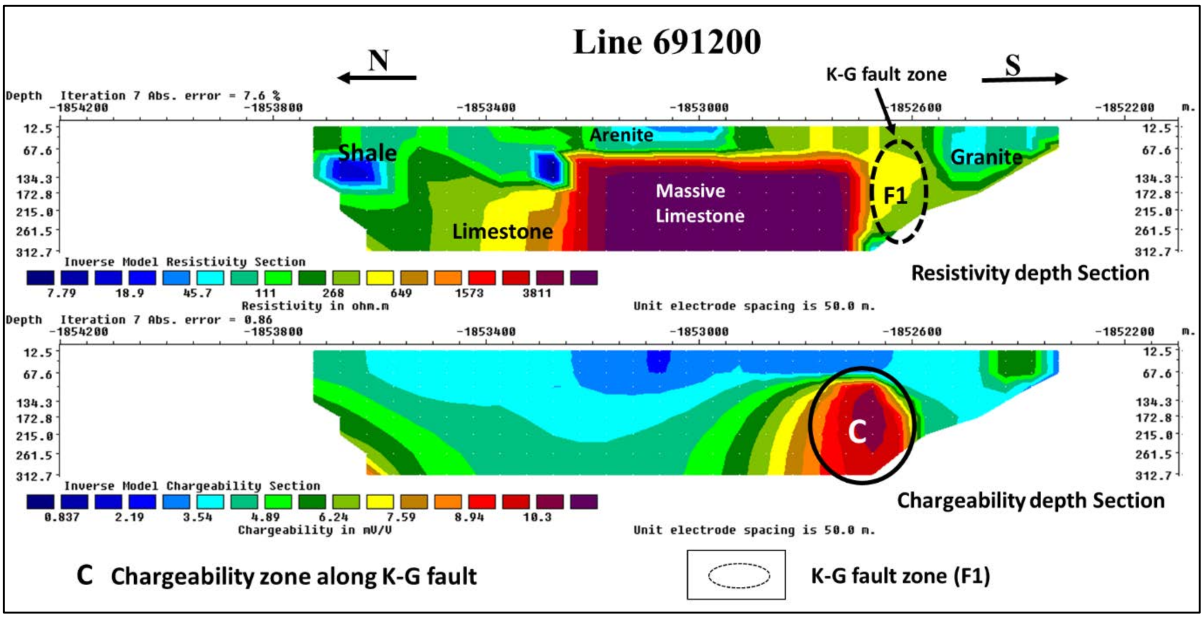

Figure 3.21 Inverted Resistivity and Chargeability depth section along traverse no. 691200, Hulkal area

Inverted depth section along the line- 691400

Total 2 km traverse length has been covered for each level (Level 1, 2,3,4,5 & 6). Subsurface information upto the depth of 312m was achieved (Figure 3.18). Resistivity values are ranging from 15ohm-m to 3700 ohm-m. High resistivity (> 3700 ohm-m) in the southern part, is attributed to basement granite. In the vicinity of basement-sediment contact resistivity values decreased from 3700 ohm-m to 1500ohm-m and indicating deformational contact. In this fracture zone resistivity is decreasing much below 260m depth and is part of K-G fault. Close to UTM 1852600N, low resistivity value (10- 80 ohm-m) up to 70m depth is related to fractured granite at the top and highly resistive layer (1000- 4000 ohm-m) below granite is attributed to massive limestone. Therefore, It is well explained by resistivity signatures that granite override the limestone in this narrow zone indicating the reveres nature of fault at this location. In the central part, very high resistivity in bedded form is due to massive limestone. Low resistivity layer, above the massive limestone, near to UTM 1852950N is attributed to combined effect of arenite and shale. Further towards north low resistivity layer up to the depth of about 80 to 100m is contributed from shale formation and depth greater than 100 m moderate to high resistivity is observed in limestone.

Chargeability along the line is ranging from 0.6mV/V to 8.5mV/V. Along the K-G fault zone moderate resistivity and its association with high chargeability (7 mV/V- 8mV/V) is due to disseminated sulphide minerals and also a potential target for uranium mineralisation.

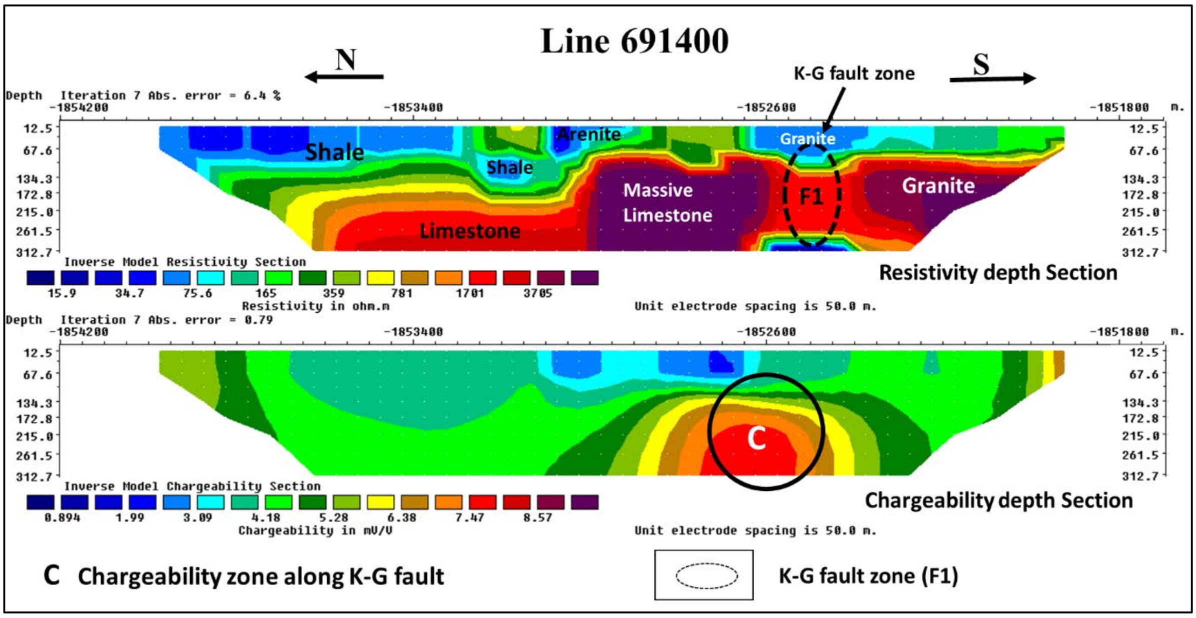

Figure 3.22 Inverted Resistivity and Chargeability depth section along traverse no. 691400, Hulkal area.

Inverted depth section along the line- 691600

Total 2.6 km length was covered along this line (Figure 3.19). High resistivity greater than 5000ohm-m amplitude in the southern part is attributed to basement granite. Adjacent to compact basement granite a vertical moderate resistivity zone (F1) of 120-150 m is demarcated and interpreted as the response from faulted basement-sediment contact. Within this zone low resistivity value (10-50 ohm-m) up to ~60m depth is because of fractured granite at the top and highly resistive layer (1000-4000 ohm-m) below granite is massive limestone response. Therefore, resistivity signatures shows that granite override the limestone in this narrow zone. It indicates that K-G fault is reverse fault over here. In the central part very high resistivity (>500ohm-m) starting from depth of 60m and continuing at deeper depth is due to massive nature of limestone formation. From UTM 1852900N to 1853250N low resistivity layer, above the massive limestone is attributed to combined effect of arenite and shale. Towards northern part of depth-section very low resistivity (10-100 Ohm-m) up to the depth of ~60m, is the response from shale formation whereas the moderate to high resistivity (1000–2000 ohm-m) below the shale is observed in limestone

Chargeability along the line is ranging from 1mV/V to 14mV/V. High chargeability (10 - 14mV/V) is recorded within K-G fault zone. This high chargeability associated with moderate resistivity along the inferred K-G fault zone is indicating the sulphide presence over there and favourable zone for uranium mineralisation.

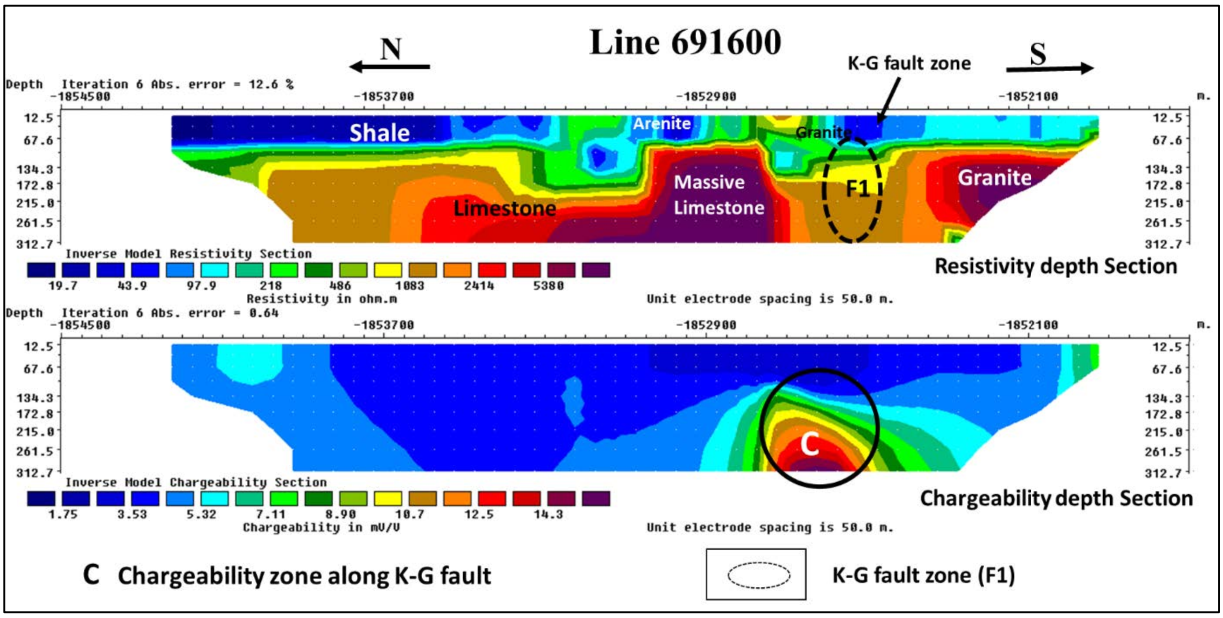

Figure 3.23 Inverted Resistivity and Chargeability depth section along traverse no. 691600, Hulkal area

The spatial distribution of the high chargeability zone is continuing downward and can be associated with the sulphide mineral which in turn helps in the precipitation of the uranium mineral.

3.11 3D stack of vertical depth slices of resistivity:

All inverted sections are stacked to view the trend of fracture and contact between different lithologies. In the western part resistivity contrast shows fracture zone within the sediment, and in the eastern part this resistivity contrast show the presence of K-G fault zone. From west to east, fracture zone within the sediment is trending towards basement-sediment contact (Gogi-Kurlagere fault zone). In the north direction contact between limestone and shale is also demarcated.

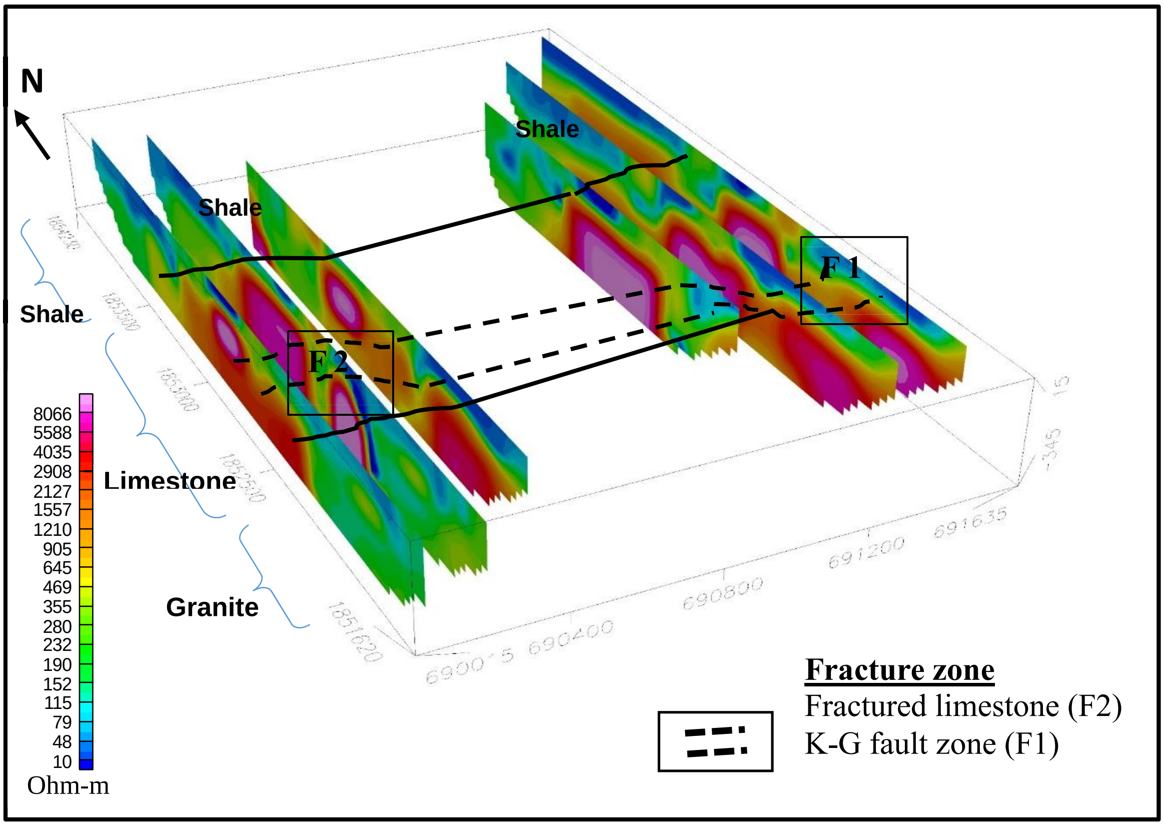

Figure 3.24 Stacked inverted resistivity depth sections

After the inversion of apparent resistivity data, true resistivity data is gridded in three dimension to obtain resistivity map at different depths. Similarly true chargeability data is also gridded in three dimension and it is observed that, at the depth of 192 m, low resistivity fracture zone which is attributed to K-G fault zone (F1) (Figure no. 3.24) and fracture zones within sediment (F2) (Figure no. 3.24) are well incorporated with high chargeability zone (6 mV/V) (Figure no. 3.25). This observation shows that, from west to east, fracture zone is trending from sediments to basement-sediment contact (K-G fault zone).

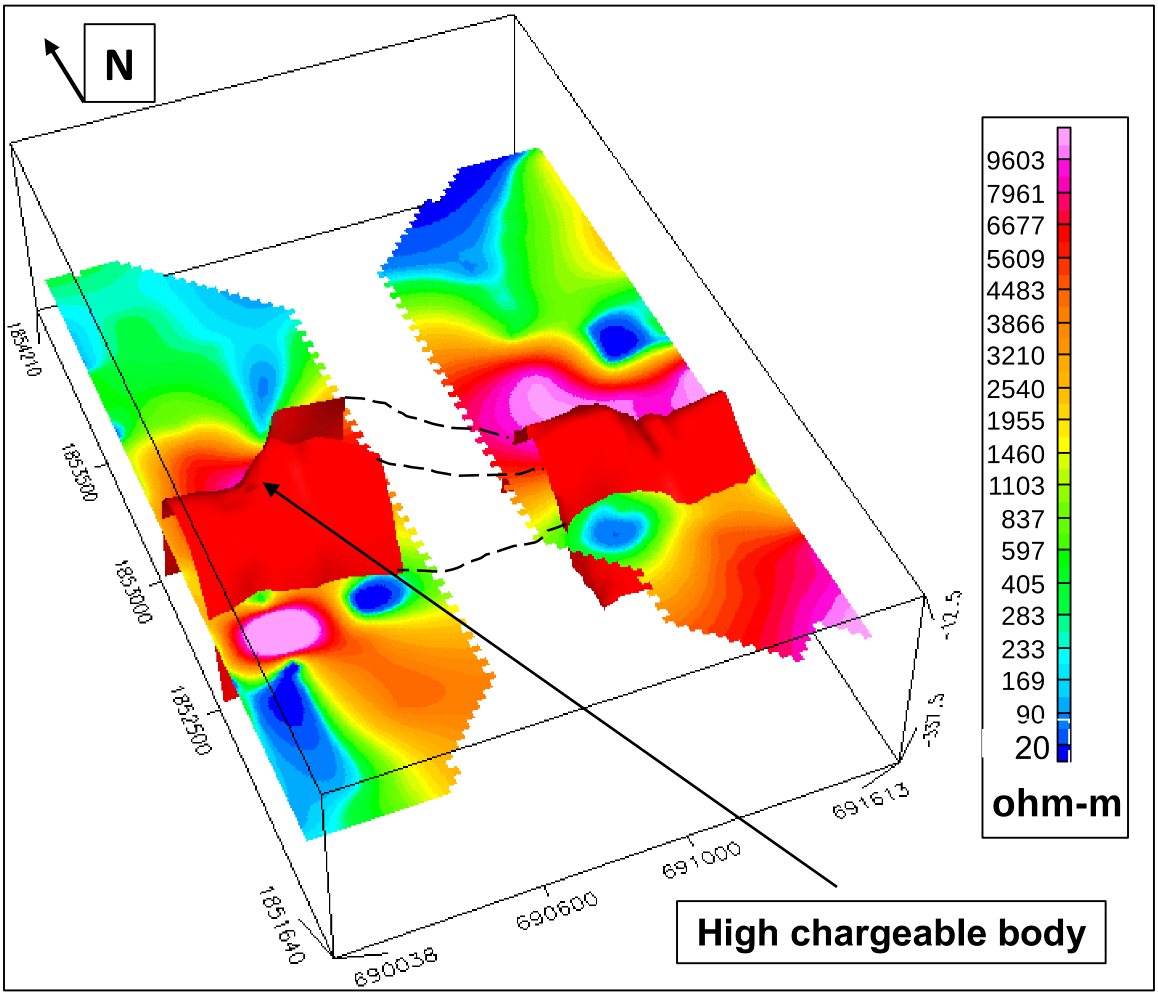

Figure 3.25 3D view of high chargeable (6mV/V) body passing through low resistivity fracture zone

CHAPTER- 4

CORRELATION BETWEEN RESULTS OF MAGNETIC AND IP/RESISTIVITY SURVEY

4.1 Introduction

The current strategy for most uranium exploration in a broad sense is based on the application of integration of several disciplines - geology, radiometry, geochemistry and geophysics including airborne surveys. An expanded but viable and carefully selected integrated approach and their analysis would no doubt speeds up the discovery and development of potential resource. .

To solve a particular geological problem by integrated study of geophysics is not new in the history of uranium exploration. In fact, integration of geophysical methods is effectively carried out without any appreciable enhancement in the operational costs, and thus integrated geophysical surveys continue to receive considerable attention of geoscientists. In mineral exploration, gravity and magnetic (both ground and airborne) methods are used in reconnaissance and electrical (self-potential and induced polarization) and electromagnetic (Turam, TEM) for detailed surveys. Although radiometric methods are traditionally used as a direct method for uranium exploration, magnetic method is mostly complemented with IP & resistivity method. Therefore, an integrated strategy of geophysical exploration for uranium exploration has become a common practice in mineral exploration.

. Thus, in an ideal situation the geophysical survey work should be carried out in a well ordered sequence, proceeding from reconnaissance to detail extracting all possible information from each survey before going for the next one. Also, an integrated approach is required both for measuring and processing of geophysical data.

In view of the present study, the integration of magnetic and IP/resistivity is not only more effective if used in close conjunction with the knowledge of geology but also the geophysical methods, themselves are often much more effective if used to complement each other, each method provide some additional information /confirmation of the results of other methods in deducing the complete subsurface picture of the area. In view of the availability of great variety of targets and detection methods in order to arrive at definite and comprehensive outcome, the interpreted results of each method are correlated for enhancing the quality, accuracy and reliability.

4.2 Correlative Study and integrated analysis

Delineation of geological structures which are favorable to uranium is one of the most important aspects to be studied. Accordingly, it is meaningful to treat the problem with the results of integrated approach than depending on the outcome of a single geophysical method. Therefore, a correlative study of magnetic and electrical signatures was made and found to be fruitful to identify the structural features such as geological contact and other weak zones, which can control and host the uranium mineralization. Although, the results of each method is presented in the respective chapter, here they are compared and correlated in order to resolve the suitability of the integrated approach to delineate the geological boundaries and estimate the width and geometry of the different formations.

4.3 Integrated interpretation

In this section combined results of inverted chargeability, true resistivity and RTP are discussed, which focuses on the lithological and structural interpretation.

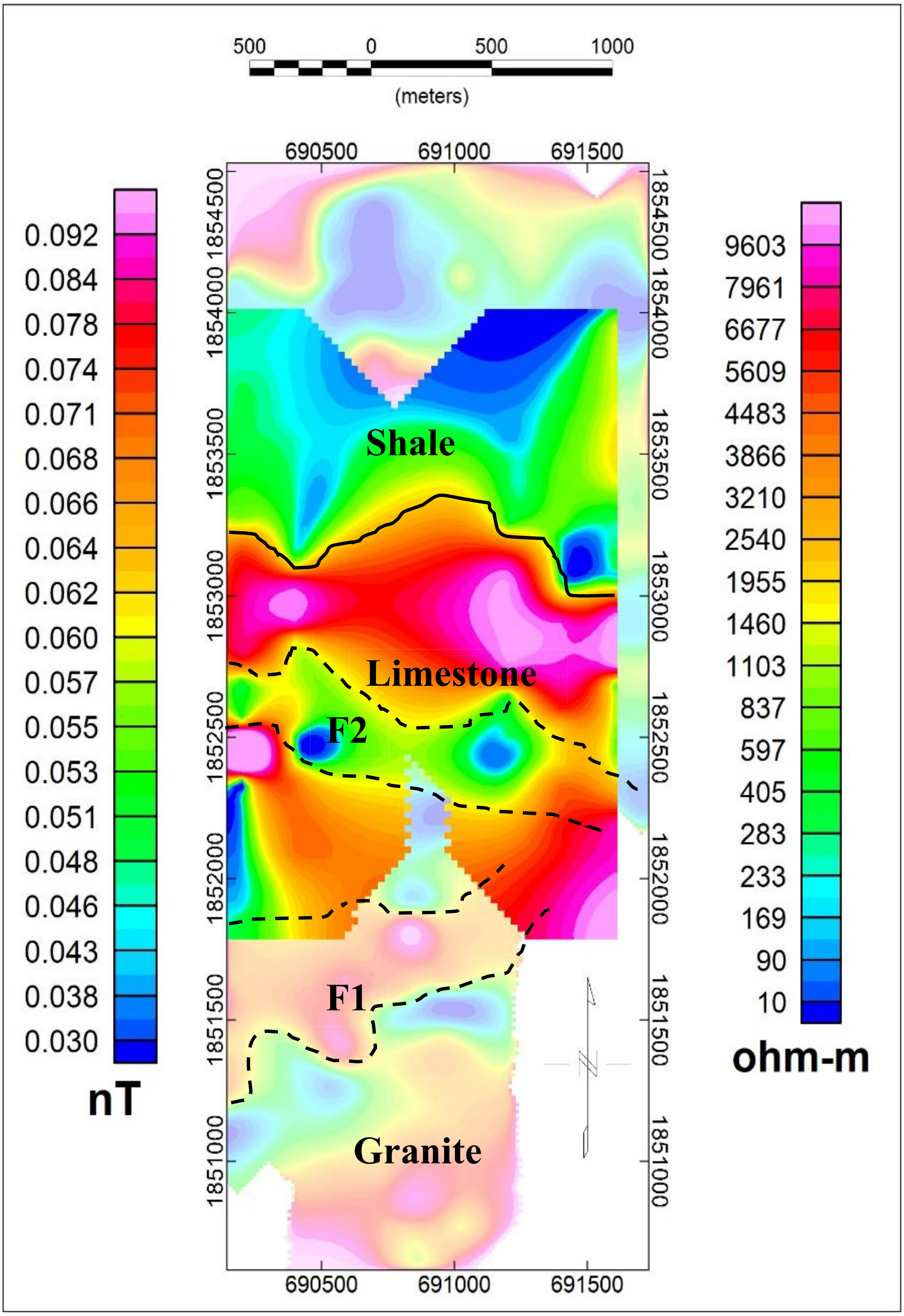

Figure 4.1 True Resistivity map superimposed over magnetic analytical signal map

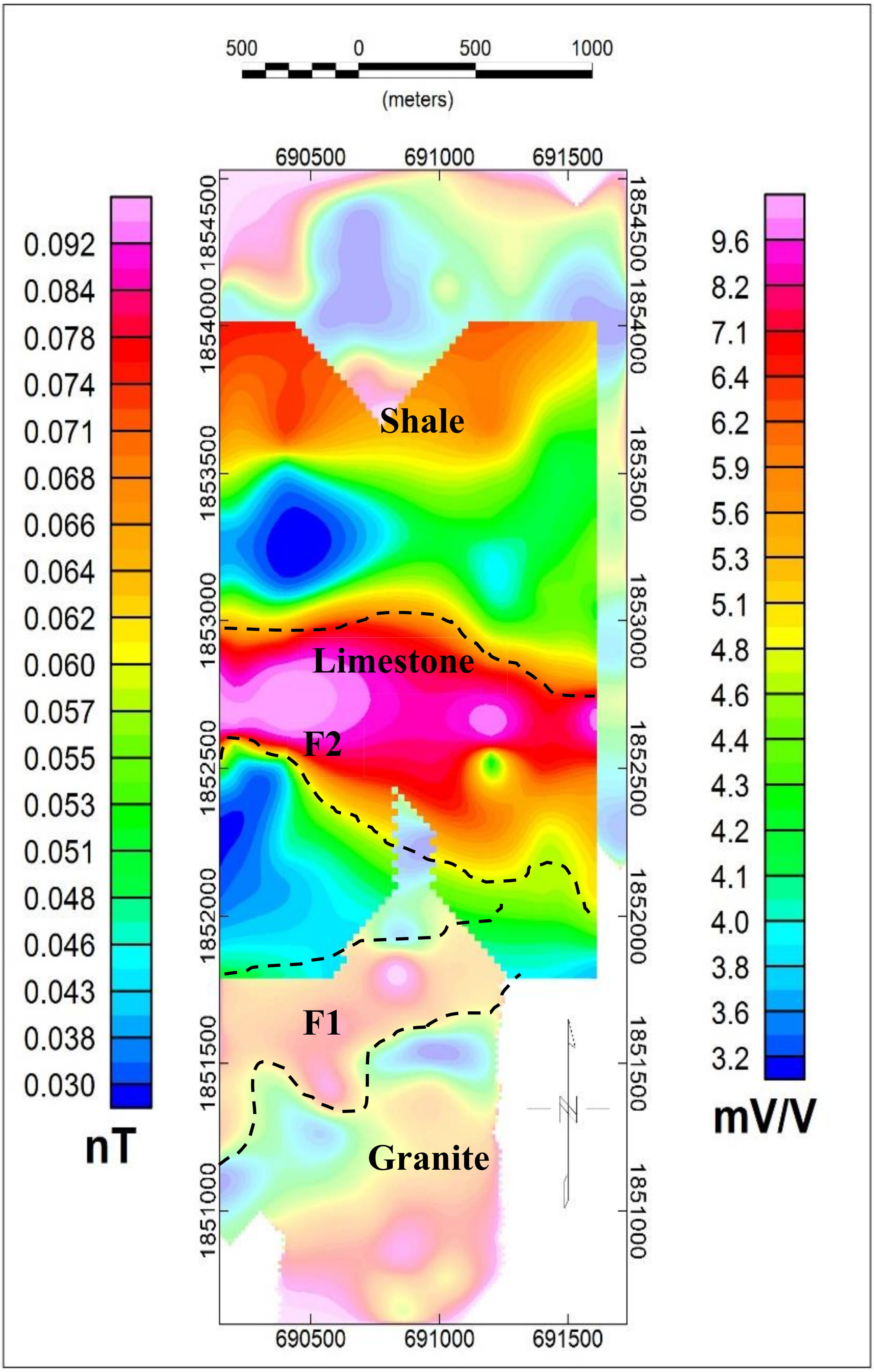

Figure 4.2 True Chargeability map superimposed over magnetic analytical signal map

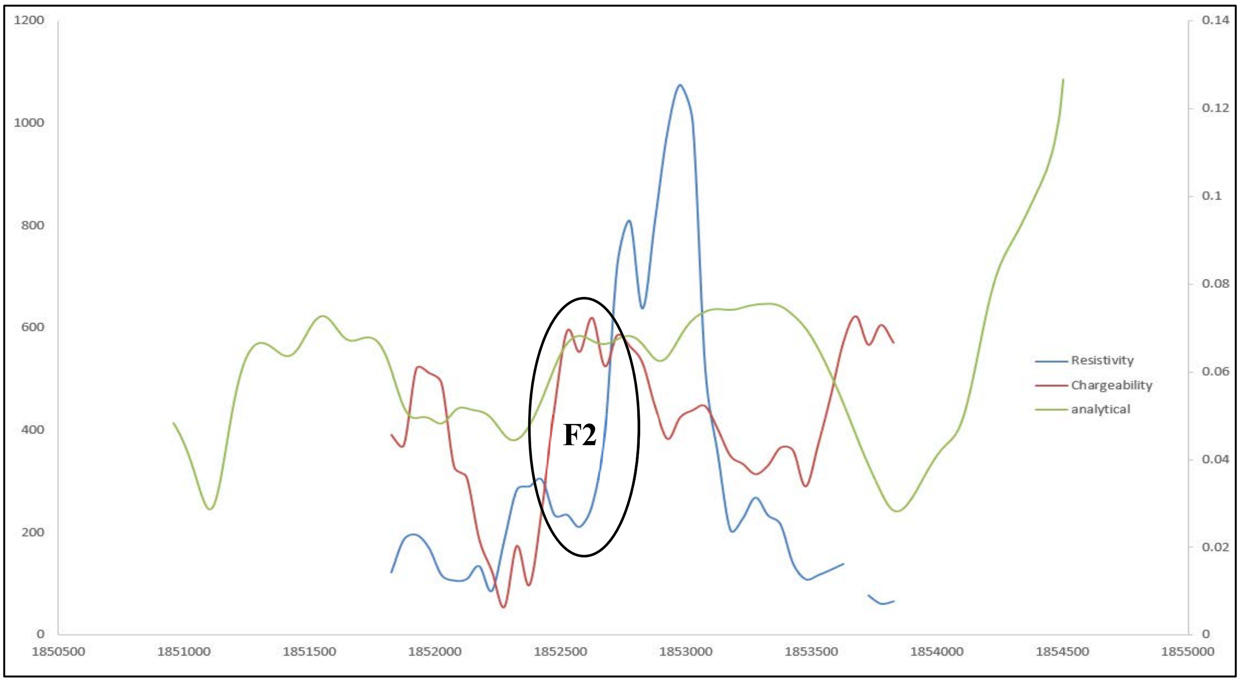

Figure 4.3 Cross plot of resistivity, chargeability and magnetic analytical signal anomaly along the line number 690200E

After the inversion of resistivity and chargeability data, true resistivity data is gridded with the cell size of 25 using Geosoft and superimposed on analytical signal map to cross verify the fracture zones and to delineate the trend (Figure no. 4.1). Here, low resistivity zone is attributed to fracture zone (F2) with the trend of NW-SE and it converges to basement-sediment contact. Basement-sediment contact (F1) is demarcated in analytical signal map of magnetic data and its trend is NE-SW. From the above Figure it is clear that fracture zone F2 which is within sediment is trending towards the basement sediment contact (K-G Fault (F1)). Chargeability map is also superimposed on analytical signal map and both fracture zones are well demarcated (Figure no. 4.2). Trend of both the zones are also same as derived from resistivity and analytical signal map. Contact between limestone and shale is very well demarcated in chargeability and analytical signal map. A profile on line number 690200 is extracted from resistivity, chargeability and analytical signal map and shown in the figure 4.3. Here the zone of low resistivity and high chargeability lies together with the gradient in analytical signal profile. This zone is attributed to fracture within the sediment (Limestone).

CHAPTER 5

SUMMARY AND CONCLUSIONS

The high grade uranium deposit in Bhima basin was well established in Gogi, Yadgir district, Karnataka along the Gogi-Kurlagere fault in association with sulphide. Heliborne and several ground geophysical surveys were carried out over this fault zone to understand the structural features in this area and to demarcate the high chargeability and low resistivity zone, which is the potential zone for uranium exploration. The main objective of the present investigation was to carry out the Magnetic and IP/Resistivity survey in Hulkal area to understand the structural features within the Bhima sediments. The current studies have resulted in the demarcation of a different anomalous zone with low resistivity and high chargeability in comparison with the previous geophysical surveys. The results were integrated with geological information of this area and conclusions are listed below:

- Chargeability and resistivity depth sections has brought out the subsurface information up to depth of 312m.
- Resistivity signatures revealed fracture within the limestone trending in E-W direction. Fracture marked on the basis of low resistivity zone within highly resistive massive limestone.
- Faulted basement-sediment contact (K-G fault) has also been delineated and showing directional change from NE-SW to E-W.
- Resistivity amplitude of the identified fracture zones are of similar nature as noticed in mineralised zone in Kanchankayi.
- Chargeability is of higher order (8mV/V - 16mV/V) in both the fracture zones compare to the chargeability (4.5mV/V-5.5mV/V) of mineralised zone in Kanchankayi.

- Limestone-Arenite and limestone-shale contacts are also delineated.
- 3D model with vertical depth slices of resistivity shows that fracture (F2) within the sediment is trending towards the faulted basement-sediment contact (K-G fault) (F1) as traversed from west to east.
- 3D gridding of true resistivity and changeability data show that low resistivity fracture zone is well incorporated with high chargeability zone showing the trend of fracture zone. This high chargeability zone may be favourable for uranium mineralisation.
- Analytical signal anomaly map of magnetic data clearly indicate presence of K-G fault zone in the southern part of the study area.
- 2D forward modelling of magnetic data shows possible subsurface geology of the study area.
- Continuous wavelet transform and radially averaged power spectrum both methods give very similar results for basement depths.

Future Work

- In each chargeability section it is observed that, high chargeability zone is extending more than 300 m in depth so further subsurface exploration is possible in future.
- The eastern part of the study area has to be explored to get the further extension of the high chargeability zone.
- Continuous wavelet transform will be applied in 2 dimension on magnetic and electrical gridded data to demarcate geological features.

REFERENCES

Bhattacharya, P.K., and Patra, H.P., 1968, Direct current geo-electric sounding, principles and interpretation: Elsevier Publishing Co. Amsterdam.

Baranov, V. (1957). A New Method for Interpretation of Aeromagnetic Maps, Pseudo-Gravimetric Anomalies. Geophysics, v. 22, pp. 359-363.

Baranov, V. and Naudy, H. (1964). Numerical Calculation of the Formula of Reduction to the Magnetic Pole. Geophysics, v. 29, pp. 67-79.

Briggs, C.I. (1974). Machine contouring using minimum curvature. Geophysics, v.39, No.1, pp. 39-48.

Blakely, R.J. (1995). Potential Theory in Gravity & Magnetic Applications. Cambridge University Press, Cambridge.

Boukerbout, H., Gibert, D. and Sailhac, P. (2003). Identification of sources of potential fields with the continuous wavelet transform: Application to VLF data. Geophysical Research Letter, v.30, No.8, 1427.

Barker, R., Rao, T.V. and Thangarajn, M. (2001). Delineation of contaminant zone through electrical imaging technique. Current Science, v.81, No.3, pp. 277-283.

Dimri, V. (1992). Deconvolution and Inverse Theory application to geophysical problem, Elsevier, v. 29, 1st edition.

Dey, A. and Morrision, H. F. (1979). Resistivity modelling for arbitrarily shaped two-dimensional structures. EAGE, v.27, pp. 106-136.

Edwards, L. S. (1977). A modified pseudosection for resistivity and IP. Geophysics, v.42, No.5, pp. 1020-1036.

Gabor, D. (1946). Theory of communication. Part 1. The analysis of information. Journal of the Institution of Electrical Engineers, v.93, p.429-441

Griffiths, D. H. and Turnbull, J. (1985). A multi-electrode array for resistivity surveying. First break, v. 3.

Griffiths, D. H., Turnbull, J. and Olayinka, A, I. (1990). Two dimensional resistivity mapping with a computer-controlled array. First break, v. 8.

Hinze, W.J., Ralph, R.B.V.F. and Saad, A.H. (2013). Gravity and Magnetic Exploration, Principles, Practices, and Applications, Cambridge university press.

Jayaprakash A.V. (1999) Evolutionary history of Bhima basin. In Field Workshop on integrated evaluation of Kaladgi and Bhima basin. Geol. Soc. India, abstract volume pp22-28.

Kearey, P., Brooks, M. and Hill, I. (2002). An Introduction to Geophysical Exploration. Blackwell science, Third edition.

Lowrie, W. (2007). Fundamental of Geophysics. Cambridge university press, second edition.

Loke, M.H. (2001). Tutorial: 2-D and 3-D Electrical Imaging Surveys, RES2DINV Manual. IRIS Instruments.

Loke, M.H. (1994). The Inversion of Two Dimensional Resistivity Data. PhD Thesis, University of Birmingham, Birmingham.

Macleod, I., Jones, K. and Dai, T.F. (1993). 3D Analytic Signal in the Interpretation of Total Magnetic Field Data at Low Magnetic Latitudes. Exploration Geophysics, v.24, pp. 679-688.

Moreau, F., Gibert, D., Holschneider, M. and Saracco, G.(1997). Wavelet analysis of potential fields. Inverse problem, v. 13, pp. 165-178.

Moreau, F., Gibert, D., Holschneider, M. and Saracco, G. (1999). Identification of sources of potential fields with the continuous wavelet transform: Basic theory. Journal of geophysical research atmosphere, v. 104, pp. 5003-5014

Martelet, G., Sailhac, P., Moreau, F. and Diament, M. Characterization of geological boundaries using 1-D wavelet transform on gravity data: Theory and application to the Himalayas. Geophysics, v. 66, No.4, pp. 1116-1129.

Nabighian, M.N. (1972). The Analytic Signal of Two-Dimensional Magnetic Bodies with Polygonal Cross-Section: Its Properties and Use for Automated Anomaly Interpretation. Geophysics, v. 37, pp.507-517.

Pazdirek, O. and Blaha, V. (1996). Examples of resistivity imaging using ME-100 resistivity field acquisition system. EAGE, 58th conference.

Sarma, V. V. Jagannadha , Bhaskara Rao, V., 1962 'Variation of electrical resistivity of river sands, calcite, and quartz powders with water content'. Geophysics, 27. 470-479.

Siegel, H. O., 1959, Mathematical formulation and type curves for induced polarization: Geophysics, 24, 547-565.

Summer, J.S., 1976, Principles of induced polarization for geophysical exploration, Elsevier Scientific Publishing Company.

Spector, A. and Grat, F.S.(1970). Statistical Models for Interpreting Aeromagnetic Data. Geophysics, v.35, pp. 293-302.

Sailhac, P., Galdeano, A., Gilbert, D., Moreau, F. and Delor, C. (2000). Identification of sources of potential fields with the continuous wavelet transform' Complex wavelets and application to aeromagnetic profiles in French Guiana. Journal of geophysical research, v. 105, No. 105, pp. 19455-19475.

Slater, L.D. and Sandberg, S.K. (2000). Resistivity and induced polarization monitoring of salt transport under natural hydraulic gradients. Geophysics, v. 65, pp. 340-687.

Storz, H., Storz, W. and Jacobs, F. (2000). Electrical resistivity tomography to investigate geological structures of the earth's upper crust. Geophysical prospecting, v. 48, pp. 455-471.

Telford, W.M., Geldart, L.P. and Sheriff, R.E. (1990). Applied Geophysics, Cambridge university press, Second edition.

Thurston, J.B. and Smith, R.S. (1997). Automatic Conversion of Magnetic Data to Depth, Dip, and Susceptibility Contrast Using the SPITM Method. Geophysics, v. 62, pp. 807-813.